BACTERIOPHAGE DISPLAY SELECTIONS OF OVARIAN CANCER AVID PEPTIDES

A Dissertation Presented to
The Faculty of the Graduate School
University of Missouri-Columbia

In Partial Fulfillment of the Requirements for the Degree
Doctor of Philosophy

By

METTE SOENDERGAARD

Dr. Susan L. Deutscher, Dissertation Supervisor

MAY 2014

The undersigned, appointed by the dean of the Graduate School, have examined the dissertation entitled

BACTERIOPHAGE DISPLAY SELECTION OF OVARIAN CANCER AVID PEPTIDES FOR SPECT AND OPTICAL IMAGING.

Presented by Mette Soendergaard, a candidate for the degree of doctor of philosophy, and herby certify that, in their opinion, it is worthy of acceptance.

_____

Dr. Susan Deutscher

_____

Dr. Thomas Quinn

_____

Dr. Frank Schmidt

_____

Dr. Scott Peck

_____

Dr. Silvia Jurisson

ACKNOWLEDGEMENTS

I would like to thank my advisor Dr. Susan L. Deutscher for her guidance and encouragement throughout my graduate studies. I would also like to thank my committee members, Dr. Thomas Quinn, Dr. Scott Peck, Dr. Frank Schmidt and Dr. Silvia Jurisson for always being helpful and for providing useful and interesting discussions.

Also, thank you to all the members of Dr. Deutscher's lab, without whom this dissertation would not have been a reality. A special thanks to Jessica Newton-Northup for excellent mentorship and for being a great friend. Also, thank you to Marie Dickerson for always being helpful and making everything run more smoothly in the lab, and to fellow graduate student Benjamin Larimer for support and many long discussions throughout the years.

Also, I must thank my parents for always supporting me, not just throughout my graduate studies, but throughout my entire life. Most importantly, I need to thank my husband Jason for endless love and encouragement. Without him I would neither have been at the University of Missouri, nor been able to complete my Ph.D.

TABLE OF CONTENTS

Acknowledgement ii

List of Table and Figures vi

List of Abbreviations viii

Abstract xii

Chapter 1

Introduction 1

Ovarian Cancer 5

Ovarian Cancer Diagnosis and Imaging 9

Ovarian Cancer Therapy 13

Phage Display 17

Peptide Based Cancer Targeting 19

Chapter 2

In Vivo Phage Display Selection of an Ovarian Cancer Targeting Peptide for SPECT/CT Imaging 22

Introduction 23

Materials and Methods 26

Results 36

Discussion 58

Conclusion.....70

Acknowledgements 71

Chapter 3

In Vitro High-Throughput Phage Display Selection of Ovarian Cancer Avid Phage Clones for In Vivo Near-Infrared Optical Imaging 72

Introduction 73

Materials and Methods 76

Results 82

Discussion 93

Conclusion.....98

Acknowledgements 99

Chapter 4

Peptide Phage Display for Discovery of Novel Biomarkers for Imaging and Therapy of Cell Subpopulations in Ovarian Cancer.....100

Introduction 101

Materials and Methods 117

Results 119

Discussion 126

Conclusion.....129

Acknowledgements.....130

References.....131

Addendum.....163

Vita.....164

LIST OF TABLES AND FIGURES

Table

2.1 Micropanning assay of phage clones pJ1-pJ31 37

2.2 Alanine scanning peptides.....51

2.3 Biodistribution of ^{111}In-DOTA-GSG-J18 54

3.1 Micropanning assay of phage clones pM1-pM9 83

4.1 Negative phage display selection against SKOV-3 cells 124

4.2 Positive phage display selection against SKOV-3 spheroid cells 125

Figure

2.1 Cell binding properties of biotinylated peptides J18, J24 and J30.....39

2.2 Fluorescent microscopy of peptide binding 40

2.3 Biodistribution of AF680-labeled phage clones pJ18 and pJ24.....41

2.4 *In vivo* optical imaging of AF680-labeled phage clones pJ18 and pJ24.....44

2.5 Stability of ^{111}In-DOTA-GSG-J18 under physiological conditions.....46

2.6 Cell binding properties of ^{111}In-DOTA-GSG-J18.....48

2.7 Cell binding competition study of ^{111}In-DOTA-GSG-J18 49

2.8 Alanine scanning experiment of peptide bio-GSG-J18.....52

2.9 *In vivo* SPECT/CT imaging study using ^{111}In-DOTA-GSG-J18 56

3.1 Fluorescent microscopy of phage binding 84

3.2 Cell binding of phage clones pM6 and pM9 85

3.3 Biodistribution of AF680-labeled phage clones pM6 and pM9.....89

3.*4 In vivo* optical imaging of AF680-labeled phage clones pM6 and pM9 92

4.1 Traditional and CSC targeted therapies in ovarian cancer 103

4.2 SPECT/CT imaging of ^{111}In-DOTA-GSG-KCCYSL 113

4.3 Isolation of bacteriophage using thioredoxin fusion proteins 116

4.4 Growth of SKOV-3 spheroid cells 120

4.5 Growth of SKOV-3 spheroid cells under differentiating conditions 121

4.6 Expression of CD44 and CD117 in SKOV-3 and SKOV-3 spheroid cells 122

LIST OF ABBREVIATIONS

^{18}F-FDG: ^{18}F-fluoro-deoxyglucose

%ID/g: injected dose per gram of tissue

α-MHS: α-melanocyte stimulating hormone

ABTS: substrate [2,2-azino-bis(3-ethylbenzothiazoline-6-sulfonic acid]

AF680: Alexa Fluor-680

ALDH: aldehyde dehydrogenase

bFGF: basic fibroblast growth factor

BRCA1: breast cancer antigen-1

BRCA2: breast cancer antigen-2

CA-125: carbohydrate antigen

CD44: hyaluronic acid receptor

CD117: tyrosine-protein kinase kit

CD133: prominin-1

CHAPS: 3-[3-(cholamidopropyl) dimethylammonio]-1-proanesulfonate

CIC: cancer initiating cells

cpIII: coat protein III

cpVIII: coat protein VIII

CRIP1: cysteine rich protein 1

CSC: cancer stem cells

DMEM: Dulbecco's modified Eagle's medium

DMSO: dimethyl sulfoxide

DOTA: 1,4,7,10-tetraazacyclodecane-1,4,7,10-tetraacetic acid

DTPA: diethylenetriaminepentaacetic acid

EC_{50}: half maximal effective concentration

E. coli: Escherichia coli

EGF: epidermal growth factor

ELISA: enzyme-linked immunosorbent assay

EpCAM: cellular adhesion molecule

ephA2: ephrin type-A receptor 2

eV: electronvolt

FBS: fetal bovine serum

FGF: fibroblast growth factor

FITC: fluorescein isothiocyanate

HE4: human epididymis protein 4

HEK293: human embryonic kidney cell line

HEPES: 2-[4-(2-hydroxyethyl)piperazin-1-yl] ethanesulfonic acid

HER2: human epidermal growth factor 2

HPLC: high-pressure liquid chromatography

HRP: horseradish peroxidase

HS-832: human normal ovarian cell line

IC_{50}: half maximal inhibitory concentration

IL-6: interleukin 6

IL-8: interleukin 8

keV: kilo electronvolt

MCP-1: monocyte chemoattractant protein-1

MRI: magnetic resonance imaging

PARP: poly-ADP-ribose polymerase

PBS: phosphate buffered saline

PC3: prostate carcinoma cell line

PDGF: platelet derived growth factor

PET: positron emission tomography

pfu: plaque forming units

PSA: prostate specific antigen

PTEN: phosphatase and tensin homolog

ROI: region of interest

RP-HPLC: reverse-phase high-pressure liquid chromatography

SDS-PAGE: sodium dodecyl sulfate polyacrylamide gel electrophoresis

sEGFR: soluble epidermal growth factor receptor

SKOV-3: human ovarian adenocarcinoma cell line

SPARC: secreted protein acidic and rich in cysteine

SPECT: single photon emission computed tomography

TBS: tris buffered saline

TF antigen: Thomsen-Friedenreich antigen

TGFβ: transforming growth factor β

TU: transducing units

uPA: urokinase plasminogen activator

VEGF: vascular endothelial growth factor

VCAM1: vascular cell adhesion protein 1

V/mL: virions per mL

BACTERIOPHAGE DISPLAY SELECTIONS OF OVARIAN CANCER AVID PEPTIDES

By Mette Soendergaard

Dr. Susan L. Deutscher, Dissertation Supervisor

ABSTRACT

Ovarian cancer is among the leading causes of cancer deaths in women, and is the most fatal gynecological malignancy. The disease has been termed the silent killer due to asymptomatic disease progression and quick dissemination of aggressive metastatic cells. The poor outcomes of ovarian cancer are a direct result of inadequate detection methods and development of drug resistant disease. Currently, standard detection methods include measurement of the ovarian cancer biomarker CA-125 and ultrasonography; however, both methods are mostly limited to late-stage disease and are associated with false positive results. As a consequence, approximately 80% of ovarian cancer patients are diagnosed at regional or distant stages, at which point five-year survival rates are merely 44%. Comparatively, five-year survival rates for women diagnosed at local disease are above 90%, which emphasizes the significance of diagnosis at early onset, and the need for development of novel detection methods. This may be achieved by discovery of new ovarian cancer targeting agents that can be labeled with radionuclides and utilized to detect and image tumors. Whereas, antibodies are by far the most used targeting agents of

cancer biomarkers due to superior specificity and affinity, peptides offer advantages in respect to low immunogenicity and rapid biodistribution. Cancer targeting peptides may be developed by bacteriophage (phage) display technology, which is a high-throughput method that allows identification of ligands by screening of large peptide libraries against cellular antigens. Most cancer targeting peptides that have been identified by this method have been selected against *in vitro* antigens; however, these ligands frequently display poor biodistribution and stability, and fail to bind tumors *in vivo*. To the contrary, phage display selections against *in vivo* tumor targets have identified peptides with superior properties. Nonetheless, the majority of these ligands bind tumor vasculature instead of cancer cells. This problem may be overcome by employing a two-tier selection strategy that combines *in vivo* and *in vitro* selections.

Phage display technology may additionally be used to identify phage clones that can be utilized as detection and imaging agents. These clones can display multiple copies of peptides, which afford an avidity effect, and their large size allows labeling with up to hundreds of tags, providing significant signal amplification compared to peptides and antibodies. However, the large size of phage leads to long biodistribution times, which may complicate use of radionuclides due to increased toxicity to surrounding tissues. Instead, near-infrared fluorophores are minimally toxic, can easily be conjugated to phage and may be utilized in optical imaging. Further, the development of phage particles as imaging agents is time efficient and cost effective compared to peptides, in that many of the challenges involved in translating targeting agents from *in vitro* to *in vivo* use may be eliminated.

Standard treatment of ovarian cancer involves chemotherapy, which the majority of patients initially respond to; nevertheless, most succumb to the disease after presenting with recurrent and drug resistant malignancy. Such dire prognosis is associated with a subpopulation of cancer cells, known as cancer stem cells (CSC). Traditional chemotherapy fails to kill CSC, due to the ability of these cells to efflux drugs, undergo senescence and repopulate tumors. While most chemotherapeutic drugs work by altering cell signaling, radionuclides offer cytotoxicity that is independent of cellular pathways, which may overcome drug resistance. Radionuclide labeled peptides may be used to specifically target and kill the CSC subpopulation, potentially leading to better prognosis and overall survival rates for ovarian cancer patients.

Taking the lack of adequate ovarian cancer detection and therapeutic strategies together, it is evident that there is a great need to discover and develop novel methods of both. Here it is hypothesized that phage display technology may be utilized to identify new ovarian cancer targeting agents, in the form of peptides and phage particles, for use in radionuclide mediated imaging and therapy. This thesis reports the discovery and development of a novel ovarian cancer targeting peptide (J18; RSLWSDFYASASRGP) that was selected by a two-tier phage display selection strategy from a fUSE5 15-mer peptide library. The first tier of selection was carried out against xenografted human ovarian carcinoma (SKOV-3) tumors in nude female mice, which was followed by a second tier against enriched SKOV-3 tumor cells, which indentified 31 individual phage clones. In order to evaluate their ovarian cancer specificity, the phage were employed in micropanning experiments, by incubating the clones with either SKOV-3 or normal ovarian (HS-832) cells. The results revealed that phage clone pJ18 exhibited the highest

SKOV-3 to HS-832 ratio and was, therefore, selected for further studies, for which the phage displayed peptide was synthesized with a gly-ser-gly (GSG)-spacer and a biotin group (biotin-GSG-J18). Fluorescent microscopy studies showed that biotin-GSG-J18 bound specifically to ovarian carcinoma cells; while a modified ELISA revealed a half maximal effective concentration (EC_{50}) value of 22.2 ± 10.6 μM (mean ± SE). To evaluate the biodistribution and imaging properties, the peptide was synthesized with a GSG-spacer and a 1,4,7,10-tetraazacyclodecane-1,4,7,10-tetraacetic acid (DOTA) chelator and radiolabeled with ^{111}In (^{111}In-DOTA-GSG-J18). The radiolabeled peptide was stable under physiological conditions and displayed half-lives of 14.0 h and 5.2 h in 2-[4-(2-hydroxyethyl)piperazin-1-yl] ethanesulfonic acid (HEPES) buffer and mouse serum, respectively. Additional cell studies confirmed specificity of the peptide for ovarian carcinoma cells, and competitive binding experiments revealed a half maximal inhibitory concentration (IC_{50}) value of 10.5 ± 1.1 μM. *In vivo* biodistribution studies in SKOV-3 xenografted mice showed good tumor uptake and retention of the radiolabeled peptide, as well as rapid clearance and renal excretion. Finally, SPECT/CT imaging demonstrated good tumor uptake and minimal background binding, and tumor specificity was further validated by blocking of radiolabeled peptide uptake using the non-radioactive peptide counterpart. This study demonstrated successful identification and development of a novel peptide with excellent stability and biodistribution properties as well as SPECT/CT imaging capabilities; rendering peptide J18 a possible ovarian cancer imaging agent that may be utilized in detection and diagnosis of the disease.

Utilization of phage display technology to identify ovarian cancer avid phage clones can lead to the discovery of peptide ligands with excellent tumor targeting

properties. However, the validation process that is involved in translating a phage clone to use as a peptide imaging agent is often long and costly. Instead, phage clones may be selected in a rapid manner against cultured cells and employed as imaging agents by labeling with near-infrared fluorophores, which is both cost effective and time efficient. This thesis also describes the selection of two such ovarian cancer avid phage clones, pM6 and pM9, that were successfully employed in optical imaging of SKOV-3 tumors in xenografted mice. The phage clones were identified by a rapid and cost effective phage display selection strategy against cultured SKOV-3 cells from a fUSE5 15-amino acid peptide library. This method is more time efficient compared to the *in vivo* selections employed in the previous study, in that cultured cells can easily be propagated, and there is no need to establish tumors in mice. Micropanning, cell binding and fluorescent microscopy studies revealed that pM6 and pM9 exhibited specific binding to ovarian cancer cells, as well as increased affinity to these cells compared to WT phage. To validate that the binding was mediated by the phage-displayed peptides, M6 and M9, these were synthesized with a GSG-spacer and a biotin group and employed in cell studies. Results showed that M6 and M9 bound to SKOV-3 cells in a dose-response manner and exhibited EC_{50} values of 22.9 ± 2.0 μM and 12.2 ± 2.1μM (mean ± STD), respectively. To analyze the pharmacokinetic properties and tumor imaging capabilities of pM6 and pM9, the selected the phage clones were labeled with the near-infrared fluorophore AF680, and examined in SKOV-3 xenografted mice. Both pM6 and pM9 successfully targeted and imaged SKOV-3 tumors, which demonstrated the potential us of these phage clones as ovarian carcinoma detection and imaging agents.

Further, this thesis discusses how phage display technology can be utilized to discover peptides with high binding affinity for ovarian CSC. Such peptides may be radiolabeled and employed in therapeutic settings to directly target and eliminate CSC subpopulations. Previous research groups have reported isolation of CSC spheroids from ovarian tumors and cell lines by growing these under stem-like conditions. Here we describe the establishment of CSC-like spheroids from the ovarian carcinoma SKOV-3 cell line. The spheroid cells were maintained under stem cell conditions, and were found to express the ovarian CSC biomarkers CD44 and CD117. In comparison, SKOV-3 cells grown under differentiating conditions expressed only miniscule levels of these markers, indicating that the spheroids had been enriched or undergone a transformation. The ability of the spheroids to give rise to differentiated cells was investigated over a period of 70 days by growing the aggregates under normal culture conditions. Unfortunately, it was not possible to detect the formation of differentiated cells using light microscopy; although, single cells in suspension were observed after a period of 21 days. The absence of differentiated cells may be due to a change in morphology and growth characteristics that have occurred over time in the SKOV-3 cell line. The spheroids were employed in a phage display selection using the f88-cys5 library to identify peptides with binding affinity for ovarian CSC. The selection revealed that the library contained a large percentage of phage peptide sequences with stop codons, indicating that these clones were morphologically similar to WT phage and as a result may have exhibited growth advantages. In future studies, the selections will be repeated using the fUSE5 library against spheroid cells established from excised human tumors obtained from the University of Missouri Hospital.

Overall the studies in this thesis identified the ovarian cancer SPECT imaging peptide, J18, optical imaging phage clones pM6 and pM9, and demonstrated the possibility of selecting CSC avid peptides using phage display technology. In conclusion, these results show the great potential of phage display derived peptides in radionuclide mediated detection and therapy of ovarian cancer.

CHAPTER 1

INTRODUCTION

When the war on cancer was launched by President Richard Nixon in 1971, the goal was to cure cancer by the bicentennial year 1976. More than 40 years later, the death rate and overall prognosis for patients with adult cancers have improved less than 5% [1]. While the five-year survival rates of a few cancers such as childhood, prostate and testis have improved significantly over the past 60 years, primarily due to patient enrollment in clinical treatment protocols and development of successful detection methods, the prognosis for patients with ovarian cancer has barely improved [2]. Currently, ovarian cancer is the fifth leading cause of cancer deaths in women, and is the most lethal class of gynecological malignancies with an average five-year survival rate of only 44% [3-5]. In the United States, ovarian cancer resulted in over 14,000 deaths in 2013 and approximately 22,000 women are estimated to be diagnosed with the malignancy in 2014 [6]. Ovarian cancer has been termed the silent killer due to a largely symptom-free disease development, which often results in diagnosis at late stage. In fact, 85% of patients are diagnosed with regional or distant metastatic disease, at which point five-year survival rates are merely 72% and 27% for stage III and IV, respectively. In contrast, the prognosis is more optimistic for the minority of patients diagnosed with local ovarian cancer, for which five-year survival rates are above 90% [5, 6]. The difference in prognosis for women diagnosed at local and distant stages of ovarian cancer emphasizes the importance of detection and diagnosis at the earliest possible point in disease progression. Unfortunately, current standard detection methods, which include evaluation of serum levels of the ovarian cancer tumor marker carbohydrate antigen (CA-125) [7], is detectable in only 80% of advanced stage ovarian carcinomas, and is not discernible in early stage disease [7, 8]. Additionally, conditions such as endometriosis and

inflammatory disease may result in elevated levels of CA-125, leading to false positive diagnosis. Pelvic ultrasonography is often combined with evaluation of CA-125 levels to aid in diagnosis; nevertheless, false positive results frequently occur due to benign cysts of the ovaries [7, 9, 10]. Once ovarian cancer is diagnosed, standard treatment of the malignancy includes cytoreductive surgery followed by a chemotherapeutic regimen [11]. While most patients initially respond to this form of treatment, the majority relapses with aggressive and drug resistant tumors within 18 months, with median survival times as low as 24 months post-diagnosis [11, 12]. The development of resistant tumors is believed to be caused by a small subset of cells, known as cancer initiating cells (CIC) or cancer stem cells (CSC). These cells comprise a small subpopulation of the tumor, but are aggressively potent in that they are capable of self-renewal, tumor-initiation and efflux of chemotherapeutic drugs [13-21].

In order to increase the survival rate of ovarian cancer patients, there is an evident need to develop novel and efficacious methods of both detection and therapy. Such new technologies may result from targeting of cell surface antigens specific to ovarian cancer cells and ovarian CSC. Peptide-based molecules as imaging and therapeutic agents are receiving increasing attention due to high-throughput methods such as bacteriophage (phage) display. This well-established technique allows selection of peptide ligands from large phage libraries, and has been used to develop phage particles and peptides for pre-clinical imaging and therapy of various mouse models of cancer [22-44]. While peptide ligands generally display lower binding affinities compared to antibodies, they offer longer shelf life and advantages in regard to tumor targeting by exhibiting low immunogenicity, rapid blood-clearance and renal excretion [45-50]. In contrast, the large

size of phage particles results in long biodistribution times and may elicit mild immunological responses [51, 52]. Nevertheless, individual phage clones can be genetically engineered to display multiple copies of peptide ligands, which provides an avidity effect, and may further be labeled with hundreds of tags for detection and imaging [31, 53-55].

Ovarian Cancer

The majority (90%) of diagnosed ovarian cancers is epithelial of origin, and has for decades been believed to be caused by ovulation-related wound repair and inflammation [56]. Following ovulation, the ovarian surface is repaired by the release of epithelial cells from the follicular rupture; however, these cells can become trapped in the ovarian parenchyma, resulting in formation of inclusion cysts. The microenvironment in these cysts can cause overexposure of the trapped cells to growth factors, thereby increasing the risk of malignant transformation. In correlation to this model, nulliparity, which leads to more ovulations over a lifetime in comparison to women that bear children, has been associated with an increased risk of ovarian cancer, whereas oral contraceptives, pregnancy and lactation have been linked to a reduced risk [56-59].

Recently, a new hypothesis of the origin of ovarian cancer has emerged, which suggests that certain ovarian tumors originate from spilled cancer cells of the fallopian tubes. In fact, early dysplastic tubal regions were identified in the majority of women with ovarian cancer, indicating that these early malignancies may be the site of origin [60, 61]. Additionally, indistinguishable tumor suppressor p53 mutations were found in both ovarian and fallopian tumors of individual patients, which demonstrated that the cancers originated from the same neoplastic event [61]. Taking this together with the fact that early malignant tubal regions were found in several ovarian cancer patients, these studies indicate that the original neoplasm may occur in the fallopian tubes and quickly disseminate to the surface of the ovaries [60, 61]. Further, epidemiological studies have

shown that infrequent ovulation events are not associated with a decreased risk of ovarian cancer in women with poly-cystic ovarian syndrome and that the protective effect of oral contraceptives may in fact be a result of elevated progesterone levels rather than repressed ovulations [62].

While most ovarian carcinomas develop spontaneously, approximately 5% are related to a germ-line mutation in one of the two genes, breast cancer antigen-1 (BRCA1) and breast cancer antigen-2 (BRCA2) [63]. Women that carry either of these mutations have a life-time risk of developing ovarian cancer of 44% and 10%, respectively. The role of normal BRCA proteins expressed in ovaries is to repair DNA breaks incurred during ovulation; however, cells that carry either mutation fail to do so, which leads to an increased risk of malignant transformation [64-66]. In parallel, spontaneous high-grade ovarian cancers are characterized by p53 mutations. This protein responds to DNA damage and, in combination with other proteins, induces cell cycle arrest. These types of tumors progress rapidly, metastasize early and are, therefore, characterized as highly aggressive [67-69]. In contrast, p53 mutations rarely occur in low-grade ovarian cancers. Instead, mutations in proteins involved in cell growth, motility and adhesion, namely the proto-oncogene B-RAF, GTPase KRas, PI3-kinase, β-catenin and phosphate tensin homolog (PTEN) are the most common causes of tumorigenesis [70, 71].

Once malignant cells have been established, further exposure to growth factors, including fibroblast growth factor (FGF), transforming growth factor β (TGFβ) and platelet derived growth factor (PDGF), may trigger epithelial to mesenchymal transition [72-74]. This process leads to loss of differentiation, which is manifested by decreased cell-cell adhesion and apical-basal polarity, as well as enhanced cell motility,

invasiveness and resistance to apoptosis [75, 76]. These characteristics contribute to the aggressive behavior of most ovarian carcinomas, which is demonstrated by rapid invasion of surrounding tissues and metastatic seeding. The seeding of ovarian metastases differs from most other cancers in that spreading occurs via the peritoneal fluid instead of the circulatory system. For these reasons, metastases are often found in the peritoneal cavity and predominantly as fluid containing ascites [77, 78].

The aggressive behavior of ovarian cancer metastases has also been attributed to a group of cells, known as cancer stem cells (CSC). The CSC hypothesis proposes that a heterogeneous tumor contains a small subpopulation of cells that exhibit increased tumorigenicity and that are resistant to traditional radiation and chemotherapy [79]. These cells give rise to differentiated progeny, which comprise the vast majority of the tumor mass and that is sensitive to standard therapeutics [80, 81]. This idea correlates well with what is often observed for advanced ovarian cancer in that most tumors initially respond to treatment, but almost all patients relapse with resistant disease [82]. Initially, CSC were reported in acute myeloid leukemia [83] and have since been found in several solid tumors including melanoma as well as cancers of the breast, prostate, and ovary [14, 84-86]. Ovarian CSC were first isolated by Bapat and co-workers from a patient presented with advanced disease [14]. The cells were shown to display stem cell surface markers including the hyaluronic acid receptor (CD44) and tyrosine-protein kinase Kit (CD117), as well as the intracellular stem cell markers Nanog, Nestin and Oct-4 [14, 20]. Later, ovarian CSC were shown to be capable of tumor initiation, drug efflux, self-renewal and formation of floating ascites-like spheroids in culture [17, 19, 21].

Overall, the CSC hypothesis is exciting due to the potential of elucidating the mechanisms behind drug resistance. Further, the possibility to target and kill these cells may lead to improved therapy and perhaps complete remission. Such efforts would significantly improve the quality of life for ovarian cancer patients as well as overall survival rates.

Ovarian Cancer Diagnosis and Imaging

Currently, the standard clinical detection method of ovarian cancer involves measurement of CA-125 serum levels. CA-125 is a large glycoprotein that is expressed by most forms of ovarian carcinomas [87]. However, detectable levels of the antigen are present in only 80% of advanced ovarian cancers and in as little as 50% of stage I tumors [7, 88, 89]. Moreover, the glycoprotein is linked to other conditions including endometriosis, inflammatory disease and benign ovarian cysts, and is found in several normal tissues [87]. For these reasons, detection of CA-125 suffers from low specificity and sensitivity, and its use as a diagnostic ovarian cancer biomarker is therefore limited [90].

In recent years, the small glycoprotein human epididymis protein 4 (HE4) has emerged as a promising biomarker of ovarian cancer. The antigen is expressed at low levels in normal female genital tissues [91, 92], but is greatly elevated in certain types of ovarian cancer. HE4 has been shown to be a more specific marker of the disease compared to CA-125 [91-95], and its association with endometriosis is negligible [96]. However, overexpression of HE4 in patients with benign masses and in some healthy women has been reported [97], which challenges the otherwise high specificity of this biomarker.

Several novel biomarkers of ovarian cancer are under investigation. Among the most successful is mesothelin, a cell surface protein expressed in mesothelial cells that may be detected in the urine of patients with mesothelioma, pancreatic and ovarian

cancers. Detection of mesothelin has shown high specificity of 95% for early-stage ovarian cancer, which greatly surpasses that of both CA-125 and HE4. Nevertheless, only 42% of localized tumors were found to express detectable levels [98, 99]. Other ovarian cancer biomarkers of interest include vascular cell adhesion protein 1 (VCAM-1) [100], serum amyloid A [101] as well as interleukin (IL) 6 and IL-8 [102]. Although, levels of these antigens in early-stage disease are miniscule, combinations with CA-125 have proven to increase both the sensitivity and specificity compared to CA-125 alone [103-105].

In the clinic, ultrasonography of the pelvic region is often employed in combination with detection of CA-125 to obtain a more accurate diagnosis. The large majority of ovarian tumors are detectable in this manner. Nevertheless, as many as 9% of post-menopausal women present with benign adnexal masses, which are difficult to differentiate from malignant tissue [106]. In cases when CA-125 and ultrasound are insufficient in characterizing adnexal lesions, magnetic resonance imaging (MRI) may be used to determine morphological features and in obtaining a final diagnosis [107]. Another widely used imaging technique of ovarian cancer is computed tomography (CT). However, CT offers lower soft tissue contrast compared to MRI. Consequently, it is used in tumor staging rather than in distinguishing between benign and malignant lesions [108].

Within the past decade, ^{18}F-fluoro-deoxyglucose (^{18}F-FDG) positron emission tomography (PET) has played a large role in imaging of gynecological malignancies [109]. PET imaging was developed to image biochemical processes using molecular probes radiolabeled with positron emitters such as ^{18}F, ^{64}Cu and ^{68}Ga [109, 110]. As the

positron is emitted from the radionuclide and travels through the body, the particle looses energy until it collides and combines with an electron, after which the couple annihilates and emits two 511 keV photons [109]. The two photons are subsequently emitted in opposite directions at 180º apart and detected by a PET scanner, which converts the signal into an image [111]. PET imaging using the molecular probe ^{18}F-FDG exploits the typically elevated glucose metabolism of cancer cells, which causes increased accumulation of the ^{18}F-FDG radiotracer [109]. Nonetheless, ^{18}F-FDG is not specific for malignancies, and increased uptake is also observed in inflammatory diseases and in rapidly proliferating tissues. Further, uptake in the uterus and ovaries is elevated during certain periods of the menstrual cycle, which complicates accurate detection of potential tumors [109, 112-114].

Single photon emission computed tomography (SPECT) was one of the first imaging techniques to be employed clinically and is still widely used today. This method detects the emission of 100-250 keV photons from a γ-ray source, which is converted into an image. Indium-111 (^{111}In) is commonly used in SPECT due to its ideal γ-emissions of 173 and 247 keV and a 2.8 day half-life [111, 115]. Additionally, ^{111}In is produced commercially by proton bombardment of ^{111}Cd or ^{112}Cd and is readily available [110, 116]. Currently, SPECT imaging is not among the standard clinical detection methods of ovarian cancer; however, the method is extensively employed in research and pre-clinical studies. Examples include an ^{111}In-labeled human epidermal growth factor 2 (HER2) binding affibody, which successfully, although with high kidney uptake, imaged ovarian tumors in xenografted mice [117]. Additionally, a VCAM-1 targeting tetrameric peptide was effectively employed in SPECT/CT imaging of ovarian metastases [118-121].

Optical imaging using near-infrared fluorophores is of great interest due to the relatively low toxicity compared to radionuclides and the ease of synthesis. While the use of fluorophores with emission wavelengths in the visible spectrum (<700 nm) is complicated by poor tissue depth and absorption by biological chromophores [122], near-infrared fluorophores (700-900 nm) emit light that is capable of penetrating human tissue at a depth of approximately 1-3 cm [123, 124]. Although tissue penetration of this depth hinders imaging of certain tumors, ovarian cancer metastases, which are typically located along the peritoneal lining, may be imaged using this technique [123]. Nevertheless, while the need for novel detection methods is great, near-infrared optical imaging agents of ovarian cancer are still at the pre-clinical phase. Among these are a fluorescent folic acid-coated nanoparticle, which imaged ovarian metastases in tumor-bearing mice [125], and three alpha-3 integrin binding peptides that successfully imaged xenografted ovarian tumors [123].

Alternatively, fluorescently labeled ovarian cancer targeting agents may be applied during surgery as intraoperative image-guiding agents to aid surgeons in discriminating between normal and malignant tissues [125, 126]. Discrimination of tissues is often difficult and can lead to incomplete removal of cancer cells and unnecessary resection of healthy tissue. Clinical trials have been performed using fluorescently labeled folate to localize and identify ovarian tumors during surgery [127]. This study showed that the cancer specific image-guiding agent significantly improved the ability of the surgeons to identify tumor tissue, suggesting that this new technology may lead to a great improvement in the prognosis for ovarian cancer patients [126, 127].

Ovarian Cancer Therapy

Standard treatment of early and late stage ovarian cancer includes cytoreductive surgery followed by platinum- or taxane-based chemotherapeutics such as cisplatin, carboplatin, paclitaxel or docetaxel [128]. Ovarian cancer is initially highly sensitive to a combination of these drugs; however, the majority of patients quickly revert with incurable resistant disease and median survival times as low as 24 months post-diagnosis [4, 82, 129]. The poor prognosis is believed to be caused by CSC that lead to the re-occurrence of more aggressive tumors, which are capable of drug-efflux and senescence as previously described [13, 14, 20]. To overcome development of resistant disease and to increase average survival rates for ovarian cancer patients, the combination of traditional and newer chemotherapeutics, such as liposomal doxorubicin, gemcitabine and topotecan, has been studied in clinical trials [130]. However, the addition of these drugs to the standard chemotherapeutic regimen has failed to improve both the overall survival and the progression-free survival rates [130, 131].

To improve the overall prognosis for ovarian cancer patients, researchers and clinicians are looking to targeted therapy. So far, bevacizumab (Avastin) is the only U.S. Food and Drug Administration (FDA) approved targeted drug that has shown a noticeable response rate in ovarian cancer patients [132]. Bevacizumab is a recombinant humanized monoclonal IgG1 antibody that targets vascular endothelial growth factor (VEGF). In combination with standard chemotherapy, this anti-angiogenic drug showed

response in almost 31% of platinum-resistant patients whereas all other targeted drugs that are currently in clinical use have resulted in response rates of less than 10% [132, 133]. Fortunately, a few promising drugs have made it to clinical trials, including a poly-ADP-ribose polymerase (PARP) inhibitor (Olaparib), which resulted in a better prognosis compared to standard treatments in patients with BRCA1/2 mutations [134]. Another example is the folate-receptor targeting drug vintafolide, which in combination with liposomal doxorubicin almost doubled the progression-free survival time in patients with resistant disease [135]. Although these drugs have improved the treatment response rates and progression-free survival times in certain groups of patients with advanced resistant ovarian cancer, the overall prognosis has not changed. This may be overcome by delivering cytotoxic radionuclides directly to the cells that are responsible for development of resistance.

Radionuclides can be more cytotoxic than chemotherapeutic drugs, and may therefore be used to kill cells in a more efficient manner. For example, α–emitters are extremely cytotoxic due to their high impact energy transfer and efficient termination of cells independently of dose rate [136, 137]. Further, the combination of short path length and high impact render α–particles excellent for elimination of small tumors, such as metastasis, without exposing surrounding healthy cells to radioactivity [138]. Additionally, the high energy of α-emitters minimizes the risk of resistance by killing cells more efficiently and independently of cellular pathways [139].

Beta-emitters also offer favorable characteristics in regard to radionuclide-based cancer therapies, such as availability and long range emission [140]. These particles deliver long distance cross-fire in the range of a few millimeters, rendering these particles

appropriate for targeting of larger tumors and negate the necessity for the molecular probe to bind every cell. However, the concentration of the radiotherapeutic agent must be sufficient to produce a cross-fire that can reach surrounding cells [140]. While the energy of β-particles is considerable lower compared to α-particles, they are still cytotoxic due to both the direct impact of the particles as well as generation of reactive oxygen species [141]. For this reason, and in order to exploit the cytotoxic effects of radionuclides to eliminate cancer cells, it is important to avoid damage to healthy tissues [140, 141].

Auger electron emitters may also be used for therapeutic purposes; however, these particles are low in energy (<500 eV) and exhibit extremely low emission ranges of a few nanometers [142]. For these reasons Auger electron emitters must be delivered to the nucleus to be cytotoxic, which greatly limits the use of these particles with most cancer targeting agents. Nevertheless, Auger electrons open up the possibility of combining highly effective and localized cytotoxicity, while maintaining very minimal exposure to healthy tissues [143].

A few pre-clinical and clinical studies of radionuclide therapy of ovarian cancer have been performed. For example, Heyerdahl *et al*. investigated the therapeutic efficacy in tumor-bearing mice of an ErbB2/HER2/neu targeting antibody labeled with the α-emitter ^{227}Th and showed that the treatment increased the average survival time compared to the non-radiolabeled antibody [144]. Another example is a clinical trial of a tumor-associated glycoprotein 72 antibody labeled with the β-emitter ^{177}Lu, which resulted in tumor free progression for up to one year in 45% of patients with ovarian cancer [145]. Finally, Mamede *et al*. successfully increased the survival times in tumor-bearing mice

after injection of an Auger electron emitter ^{111}In-labeled dendrimer [146]. These studies demonstrate the great potential of using radionuclides in the treatment of ovarian cancer, which may lead to a significant increase in the overall survival rates.

Phage Display

Phage display is a high-throughput technology that is used to discover novel peptide based ligands by genetically incorporating random peptide sequences onto the coat proteins of phage. The technology was developed by Dr. George P. Smith, who showed that foreign peptides displayed by filamentous phage were capable of binding peptide specific antibodies with high affinity [53]. The best characterized of the filamentous phage is the Ff class that includes the M13, fd and f1 viruses, all of which are structurally similar and 98% identical at the DNA level. Structurally, these phage resemble a flexible rod that measures ~0.9 μm in length and ~65 Å in diameter. The Ff genome is approximately 6.4 kb (ssDNA) and encodes 11 proteins, of which five serve structural functions. Two of these are coat protein III (cpIII) and coat protein VIII (cpVIII). Coat protein VIII is predominant on the phage surface and is usually found in more than 2300 copies along the virion, whereas only five copies of cpIII are present at the tip of the phage particle [55]. Both are well exposed and are for this reason often used in phage display to present foreign peptides, which is done by creating a fusion gene of a coat protein and a foreign insert [53, 54]. Typically, random phage display libraries contain linear or cysteine constrained peptide inserts of up to 45 amino acids long. Among the most common phage display vector systems are the fUSE5 vector, which displays up to five peptide copies on cpIII, and the f88-5 vector system that typically presents several hundred peptide copies on cpVIII [53, 147]. Most phage display libraries contain up to 10^9 different phage clones, each displaying a random peptide. Experimentally, the phage display library is screened against an antigen of interest using

several rounds of affinity selection, elution and amplification in bacteria. The Ff class of phage infects gram-negative bacteria, including *E. coli*, by binding cpIII to the pilus of the bacterium. To produce new virions the phage employs the bacterial machinery, after which progeny is released through the plasma membrane without lysis of the bacterium [55, 148-150]. Since propagation leaves the bacteria intact, amplification is quick and can result in high concentrations of virions that can easily be retrieved and purified for use in analysis or in additional phage display selection rounds [53, 54, 147].

Phage display technology has been employed to discover new peptides that bind varying types of cancer cells. Our laboratory has developed a number of peptides that target cancer cells and their antigens including KCCYSL, IAGLATPGWSHWLAL and NTPCGPYTHDCPVKP, which respectively bind the ErbB-2 receptor, PC-3 prostate carcinoma cells and galectin-3 [29-32, 151]. Other groups have successfully developed peptides that target the tumor vasculature. For example, RGD-containing peptides that bind $\alpha_v\beta_3$-integrin [152, 153] and the SGRSA peptide that targets urokinase plasminogen activator (uPA) [154]. Most tumor targeting peptides that were identified by phage display technology were developed as imaging and/or therapeutic agents of human cancers. Radiolabeling of tumor binding peptides provide effective ways of both *in vivo* imaging, using technologies such as SPECT and PET, and of targeting for therapeutic purposes. While some peptide based therapeutic agents function by binding and inhibiting receptors or other molecules involved in the progression of cancer, radiolabeling of peptides provides a method to target and kill cancer cells independent of intracellular signaling pathways [139].

Peptide Based Cancer Targeting

Antibodies and their fragments are by far the most used targeted cancer imaging and therapeutic agents [50]. Among the most well known examples is the humanized monoclonal antibody trastuzumab (Herceptin) [155], which was developed by phage display technology and binds the cell surface receptor ErbB2/HER2/neu. The antibody is used in the treatment of certain types of both metastatic breast and ovarian cancers and has been proven effective compared to standard chemotherapy alone [155, 156]. Trastuzumab has also been labeled with different radionuclides, including ^{227}Th and ^{111}In, and used in pre-clinical α-therapy and SPECT imaging studies of ovarian and metastatic breast cancer [144, 157].

In comparison to peptide ligands, antibodies exhibit superior affinity; however, they often cause immunogenic related drug resistance, have long biodistribution times and clear through the hepatobiliary system. These characteristics complicate the use of radiolabeled antibodies as imaging and therapeutic agents due to prolonged radioactive exposure to healthy tissues [47, 158]. In contrast, radiolabeled peptides offer low immunogenicity, rapid blood-clearance and are excreted through the kidneys. As a result, peptides provide advantages in regard to SPECT and PET imaging as well as radiotherapy [46, 48]. Additionally, peptides can be developed to be highly target-specific and are, for these reasons, of great interest as *in vivo* tumor imaging and therapeutic agents [50].

An eight amino acid cyclized peptide, octreotide, is currently successfully used in clinical imaging of somatostatin receptor positive tumors in humans [159]. Other peptides

show great promise, such as the peptide analog, CCMSH, of melanoma targeting α-melanocyte stimulating hormone (α-MSH). The CCMSH peptide was labeled with ^{111}In, ^{99m}Tc and ^{188}Re, for SPECT imaging and therapy studies [28, 160]. In additional experiments, the analog was conjugated with the chelator 1,4,7,10-tetraazacyclodecane-1,4,7,10-tetraacetic acid (DOTA) and labeled with ^{64}Cu, ^{86}Y and ^{68}Ga for PET imaging [161, 162] or with ^{212}Pb for melanoma therapy studies in mice. The treatment showed significantly increased survival rates in which 45% of the mice receiving the highest dose of radiation survived the study disease-free [27]. Another example of a tumor targeting peptide is the phage display selected peptide KCCYSL. KCCYSL binds the receptor ErbB2/HER2/neu, which is overexpressed on certain types of malignancies including breast, prostate and ovarian cancers [50, 151]. KCCYSL was labeled with ^{111}In for SPECT imaging of ErbB2/HER2/neu positive tumors in xenografted mice. The study showed rapid tumor uptake and low background in most normal organs except the kidneys, which was indicative of renal clearance [32]. Phage display technology was also employed to select a galectin-3-targeting peptide, which was shown to inhibit the interaction between galectin-3 and the correlating natural carbohydrate ligand, the Thomsen-Friedenreich antigen (TF antigen) [29]. The galectin-3-targeting peptide was further labeled with ^{111}In and shown to successfully image breast cancer xenografted mice while exhibiting low background and rapid renal clearance [36, 163].

To date, very few *in vivo* ovarian cancer targeting imaging agents have been reported; however, many of these targeting moieties involve peptides [121, 123, 164-166]. For example, Aina *et al*. screened libraries of random cyclic peptides and identified an α_3 integrin subunit binding peptide that was found to target ovarian cancer cell lines.

The ligand was labeled with a near-infrared fluorophore and injected intraperitonealy into mice carrying xenografted ovarian tumors and was shown to effectively image and localize tumors [123]. Another research group investigated the tumor targeting capability of an $\alpha_v\beta_3$ integrin binding cyclic RGD peptide, which was labeled with ^{111}In and ^{177}Lu for biodistribution and β-emission therapy studies. The radiolabeled peptide successfully localized to the tumor and resulted in significantly decreased growth of peritoneal masses, demonstrating that peptides may be used as dual purpose theranostic agents [166].

These results demonstrate that radiolabeled peptides offer great promise as both imaging and therapeutic agents of cancer tumors. Further, phage display derived peptides may provide improved detection of early-stage ovarian cancer as well as radionuclide mediated therapy of ovarian CSC.

CHAPTER 2

IN VIVO PHAGE DISPLAY FOR SELECTION OF AN OVARIAN CANCER TARGETING PEPTIDE FOR SPECT/CT IMAGING

Introduction

Ovarian cancer is the fifth leading cause of cancer deaths in women and is the most lethal of gynecological malignancies [5]. In the U.S., ovarian cancer was responsible for 14,000 deaths in 2013, and approximately 22,000 women are estimated to be diagnosed with the malignancy in 2014 [167]. Ovarian cancer has been termed the silent killer due to a predominantly asymptomatic disease development and a quick dissemination of aggressive metastatic cells into the peritoneal cavity. Here, metastases form as fluid filled ascites causing bloating and discomfort, which are often the first symptoms to arise. The late manifestations of ovarian cancer cause ~80% of patients to be diagnosed at late stage disease, at which point five-year survival rates are merely 44% [3, 4, 8]. To the contrary, the minority of women diagnosed at the early stages of ovarian cancer exhibit good five-year survival rates of >90%, which emphasizes the importance of detection and diagnosis at early onset [8]. Currently, standard detection methods involve evaluation of CA-125 serum levels and ultrasonography, which are both mostly successful for late-stage ovarian cancer and often lead to false positive results and may require surgery to obtain final diagnosis [7, 9, 10, 88]. In fact, only 50% of patients with stage I disease test positive for elevated CA-125 serum levels [168], which highlight the need for identification and development of novel detection and diagnostic methods of ovarian cancer.

Various cancers have been successfully imaged for diagnoses and evaluation of disease progression using radionuclide-coupled peptides [25, 159, 163], and while these

ligands generally display lower binding affinities compared to antibodies, they offer advantages in regard to tumor targeting by exhibiting low immunogenicity, rapid blood-clearance and excretion through the urine [46, 48]. High-throughput strategies such as phage display are utilized in the discovery of new peptide ligands that recognize cancer antigens and cancer cell surfaces [22, 50, 151, 169-172]. Phage display is a well-established technique that allows selection of ligands from large phage libraries, in which random peptide sequences are displayed on coat proteins [53]. Cancer targeting peptide ligands are often identified using *in vitro* phage display selections against purified cancer antigens or cultured tumor cells. Although such selections frequently yield peptides that exhibit good binding to cancer cells *in vitro*, these ligands often fail to target tumors *in vivo* due to inadequate pharmacokinetics [50, 173, 174]. In contrast, *in vivo* phage display selections against tumor targets in live animals have resulted in identification of peptides with superior stability and biodistribution. However, most of these peptides have been found to bind the tumor vasculature rather than the actual cancer cells [175-177].

To select peptides with high stability, optimal pharmacokinetic properties and specific binding for ovarian cancer cells, our laboratory has developed a phage display technique that involves initial *in vivo* selection rounds in tumor-bearing mice followed by screening against cultured tumor cells *in vitro*. In the current study, we hypothesized that this rigid selection process against xenografted human ovarian carcinoma (SKOV-3) tumors in mice and enriched cultured SKOV-3 cells would identify peptide ligands that could be utilized in SPECT imaging. This study resulted in identification of an ovarian carcinoma targeting peptide RSLWSDFYASASRGP (J18), which was synthesized with a Gly-Ser-Gly (GSG) spacer and conjugated to a DOTA chelator. The conjugated peptide

(DOTA-GSG-J18) was radiolabeled with ^{111}In and evaluated in regard to its stability under physiological conditions and binding affinity for SKOV-3 cells. The pharmacokinetic properties and SPECT imaging capabilities of ^{111}In -DOTA-GSG-J18 were determined in xenografted mice bearing SKOV-3 tumors, and the results showed that the peptide exhibited good tumor targeting and retention and was able to successfully localize ovarian tumors using SPECT imaging.

Materials and Methods

Chemicals and Reagents

$^{111}InCl_3$ was purchased from Mallinckrodt Chemicals (St. Louis, MO). Unless otherwise stated, chemicals were obtained from Thermo Fisher Scientific (Waltham, MA).

Cell Lines and Cell Culture

The human ovarian adenocarcinoma (SKOV-3), human ovarian adenocarcinoma (OVCAR-3), human melanoma (MDA-MB-435), human embryonic kidney (HEK293) and human normal ovarian (HS-832) cell lines were purchased from American Type Tissue Culture. All cell lines were cultivated in RPMI 1640 (custom) with 10% fetal bovine serum (FBS), 2 mM L-glutamine, 1.7 μM insulin and 48 mg/ml, and maintained at 37°C in 5% CO_2.

Animals and Handling

Solid tumors (1 cm) were established in 4–6-week-old female nude (nu/nu) mice (Harlan, Indianapolis, IN) over a period of 8 weeks. The animals were inoculated subcutaneously in the shoulder under gas anesthesia (3.5% isoflurane, Baxter Healthcare Corp. Deerfield, IL) with $1x10^7$ SKOV-3 cells. All animal studies were conducted according to NIH Guidelines for the Care and Use of Laboratory Animals and the Policy

and Procedures for Animal Research of the Harry S. Truman Veterans Memorial Hospital.

In vivo and *In Vitro* Phage Display Selections of Tumor Binding Phage Clones

For *in vivo* selection of tumor targeting phage clones, a linear 15-mer fUSE5 phage display library (a kind gift from Dr. George P. Smith, [53]) was used. The phage library was pre-cleared against binding to the vasculature and non-tumor targets in nude mice without tumors. For this, the phage library (10^{12} virions) was intravenously injected into the tail-vein of a non-tumor-bearing mouse, after which the blood was collected 15 min post-injection, and phage was purified and amplified as previously described [178]. Next, the pre-cleared phage library (10^{12} virions) was injected into the tail-vein of xenografted SKOV-3 tumor-bearing nude mice and allowed to circulate for 1 h. The animals were sacrificed and tumors were collected and minced, and bound phage were eluted from the tumor tissue using 2.5% 3-[3-(cholamidopropyl) dimethylammonio]-1-proanesulfonate (CHAPS) in TBS. Eluted phage were amplified and employed in two additional rounds of *in vivo* selection as already described. In order to select phage clones with binding to ovarian cancer cells only, the collected phage from the third and final round of *in vivo* selection were used to screen against tumor derived SKOV-3 cells in an *in vitro* assay. For this, tumors were excised from sacrificed nude mice and minced, and the SKOV-3 cells were separated from the remaining tumor tissue cells by incubation with biotinylated antibodies specific for well-known ovarian cancer markers [179-181]. Cells were captured on streptavidin coated magnetic MACS® MicroBeads (Milteniy Biotech, Auburn, CA) and loaded on a magnetic column. Phage (10^{12} virions) from the *in*

vivo selection were incubated with cells for 30 min at 4°C, eluted with 2.5% CHAPS in tris-buffered saline (TBS) and amplified. Between selection rounds, the DNA sequence of the foreign phage display insert was sequenced for detection of potential contamination and identification of selected peptide sequences. Single-stranded DNA isolation from phage was performed using QIAprep Spin Miniprep Kit (Qiagen, Hilden, Germany) and DNA was sequenced at the University of Missouri DNA Core and analyzed with DNA sequence chromatogram viewer software (Chromas 2.23, Technelysium, South Brisbane, Austalia).

Micropanning Assay

Individual phage clones that were identified in the *in vitro* selection were used for micropanning experiments to identify clones with specific affinity for human ovarian adenocarcinoma SKOV-3 cells and low binding to normal ovarian HS-832 cells. Individual phage clones (10^9 virions) were incubated with 10^5 cells (SKOV-3 or HS-832) in serum free Dulbeccos' modified Eagle's medium (DMEM) for 1 h at 37°C. Cells were centrifuged (1,000 g, 1 min) and unbound phage were removed by aspiration. Cells were then washed three times with TBS, and bound phage were eluted with 2.5% CHAPS and collected from the supernatant after centrifugation (1,000 g, 1 min) as described [178]. The collected phage were titered in *Escherichia coli* (*E. coli*) K91 BluKan and titers were calculated.

Peptides

Solid-phase Fmoc chemistry was used to synthesize peptides in a 396 multiple peptide synthesizer (Advanced Chem Tech, Louisville, KY). Peptides were synthesized with a DOTA-chelator or a biotin group linked to a GSG-amino acid spacer at the NH_2-terminus (biotin-GSG-peptide or DOTA-GSG-peptide). Purification of peptides was performed using reverse-phase high-pressure liquid chromatography (RP-HPLC; Beckmann Coulter System Gold HPLC, Beckmann Coulter, Fullerton, CA) on a C18 column (Novapack Reverse Phase, Waters, Milford, MA), lyophilized and stored at -20°C. The peptides were identified by electrospray ionization mass spectrometry (Mass Consortium Corp, San Diego, CA).

Peptide Radiolabeling and Stability

The peptide was radiolabeled with ^{111}In (^{111}In-DOTA-GSG-J18) by incubating 100 μg peptide with 18.5 MBq ^{111}In-Cl_3 (Mallinckrodt, St. Louis, MO) in 0.5 M ammonium acetate buffer, pH 5.0, at 85°C for 1 h. For blocking experiments, 1 mg peptide was incubated with 10^{-4} M non-radioactive indium under similar conditions. The non-radioactive and radiolabeled peptides were purified using RP-HPLC (LC-20A Prominence, Shimadzu, Columbia, MD) on a C18 column (Higgins Analytical Inc., Mountain View, CA; 25-35% acetonitrile/0.1% trifuoroacetic acid) over 20 min. Acetonitrile was removed by further purifying the labeled peptides on an Empore® Extraction Disk C18 cartridge (Phenomenex, Torrance, CA). After removal of acetonitrile, the peptide was eluted with 70% ethanol and the pH adjusted to neutral by adding 0.5 M 2-[4-(2-hydroxyethyl)piperazin-1- ethanesulfonic acid (HEPES; final

concentration) buffer. For animal experiments, the ethanol was evaporated under N_2 and the peptide resuspended in 0.1 M HEPES buffer, pH 7. The peptide stability was analyzed in 0.5 M HEPES buffer, pH 7, and in mouse serum over time (0 h, 1 h, 2 h, 4h, 6 h and 24 h) at 37°C. The peptide degradation was monitored by RP-HPLC on a C18 column.

Fluorescent Microscopy

Peptide binding to cells (SKOV-3, OVCAR-3, MDA-MB-435 and HEK293) was investigated by fluorescent microscopy. Cells were grown to 80% confluency on chamber slides (Lab-Tek, Rochester, NY). Growth medium was aspirated from the slides, and 10 μM J18, J24 or J30 in phosphate buffered saline (PBS) was added for 1 h at 37°C. Next, the slides were washed thrice (PBS), fixed with 10% formalin and then washed (PBS) repeatedly. The cells were blocked (10% FBS, 0.3M glycine, 0.01% Tween-20, PBS) for 1 h at room temperature, and bound peptides were probed with a mouse monoclonal anti-biotin antibody labeled with the fluorophore Cy3 (Sigma Aldrich, St. Louis, MO) for 1 h at room temperature. The slides were then washed three times (PBS, 0.05% Tween-20), and bound peptides was detected using an epifluorescent Nikon T1-SM inverted microscope (Nikon, Melville, NY).

Cell Binding Studies

The binding ability of biotinylated peptides bio-GSG-J18, bio-GSG-J24, bio-GSG-J30 and a non-relevant peptide bio-GSG-N35 (negative control) to SKOV-3 cells were analyzed in an *in vitro* assay. Cells were grown in 96-well tissue culture plates

(TPP, Trasadingen, Switzerland) to 80% confluency. Varying concentrations (10 nM to 300 μM) of peptide in PBS was incubated with the cells for 1 h at 37°C, after which the plates were washed repeatedly (PBS, 1% bovine serum albumin) and fixed with 10% formalin. After extensive washing, the cells were blocked (10% FBS, 0.3 M glycine, 0.05% Tween-20 in PBS), and the bound peptides were then probed by incubation with horseradish peroxidase (HRP) conjugated streptavidin with for 1 h at room temperature. Next, the plate was washed thrice (PBS, 0.05% Tween-20) and HRP substrate 2,2-azino-bis(3-ethylbenzothiazoline)-6-sulfonic acid (ABTS) was added and allowed to develop for 20 min at room temperature. Bound peptides were detected by measuring the absorbance at 405 nm using a μ Quant Universal Microplate Spectrophotometer (Bio-Tek Instruments, Winooski, VT), and the half maximal effective concentration (EC_{50}) was calculated using GraphPad Prism software.

Ovarian carcinoma specificity of radiolabeled peptide (^{111}In-DOTA-GSG-J18) was evaluated in an *in vitro* cell binding assay. Cells, SKOV-3 or HS-832, were released with Gibco Cell Dissociation Buffer, centrifuged (200 g, 5 min) and resuspended in cell binding medium (DMEM, 1% bovine serum albumin). Cells ($1x10^6$) were then incubated with $2x10^5$ cpm of ^{111}In-DOTA-GSG-J18 at 37°C for different periods of time (0 min, 0.5, 1, 2 and 4 h). Next, the cells were pelleted by centrifugation (1,000 g, 1 min), the supernatant was aspirated and the cells were washed thrice with ice-cold 0.1 M HEPES buffer, pH 7. The buffer was removed and the radioactivity bound to the remaining cells was measured using a Genesys™ Genii™ Multi-Well Gamma Counter (Laboratory Technologies, Inc, Maple Park, IL).

In order to determine the half maximal inhibitory concentration (IC_{50}) of the peptide ligand to the ovarian carcinoma cells (SKOV-3), competition experiments were performed with the radiolabeled (^{111}In-DOTA-GSG-J18) and the non-radioactive counterpart (In-DOTA-GSG-J18). Cells ($1x10^6$) were incubated in cell binding medium with $2x10^5$ cpm of ^{111}In-DOTA-GSG-J18 and varying concentrations of In-DOTA-GSG-J18 (10^{-13} to 10^{-4} M) for 1 h at 37°C. Cells were then centrifuged (1000 g, 1 min), the supernatant was removed and the cells were washed extensively with ice-cold 0.1 M HEPES buffer, pH 7. The cell-bound radioactivity was measured by a gamma-counter as previously described, and the IC_{50} value was calculated.

Alanine Scanning Experiments

To further confirm the specific binding of peptide J18 to SKOV-3 cells and to identify the amino acid residues responsible for the interaction, biotinylated alanine scanning versions of the peptide (biotin-GSG-J18-1 to biotin-GSG-J18-15) were synthesized and employed in a modified enzyme-linked immunosorbent assay (ELISA). Cells were grown to 80% confluency on 96-well plates and incubated with various concentrations (10 nM to 100 μM) of biotin-GSG-J18 or alanine scanning versions of the peptide for 1 h at 37°C. Cells were then washed three times with PBS and fixed with 10% formalin. Next, the cells were washed (PBS) extensively and the plate was blocked using 10% FBS, 0.3 M glycine, 0.05% Tween-20 in PBS. Bound biotinylated peptides were then probed by HRP-conjugated streptavidin (Sigma Aldrich, St. Louis, MO) for 1 h at room temperature, after which the plate was washed thrice (PBS, 0.05% Tween-20). Horseradish peroxidase substrate, ABTS, was then added and allowed to develop for 20

min at room temperature followed by detection of peptide binding by measurement of the absorbance at 405 nm using an endpoint assay on a μ Quant Universal Microplate Spectrophotometer (Bio-Tek Instruments, Winooski, VT).

Biodistribution and Near-Infrared Optical Imaging of Phage

The near-infrared fluorophore AF680 (carboxylic acid, succinimidyl ester 5-isomer; Invitrogen, Carlsbad, CA) was dissolved in 2% dimethyl sulfoxide (DMSO) and incubated with phage (0.29 mM coat protein VIII) in 0.5M Na_3citrate, 0.1 M $NaHCO_3$, pH 8.5 for 4 h at room temperature in the dark. The reaction was terminated over night at 4°C by addition of 270 mM ethanolamine, pH 9. Excess hydrolyzed AF680 was removed by dialyzing labeled phage against TBS, pH 7.5 (Slide-A-Lyzer cassette, 10 kDa molecular weight cutoff, Thermo Scientific, Rockford, IL).

AF680-labeled WT, pM6 or pM9 phage (10^{12} virions) were injected into the tail-vein of SKOV-3 xenografted mice and allowed to circulate. For biodistribution experiments, the mice were sacrificed after 4 h, perfused with PBS, and tumors, organs and tissues were excised. For optical imaging experiments, the mice were under gas anesthesia (3.5% isoflurane, Baxter Healthcare Corp. Deerfield, IL), and fluorescence reflectance images were obtained before injection (0 h) and 2 h and 4 h after injection. Images were attained and the fluorescent intensity was measured using a Xenogen IVIS 200 System and analyzed by ImageJ software [182].

Biodistribution of ^{111}In-DOTA-GSG-J18 in SKOV-3 Tumor-Bearing Nude Mice

Female nude mice were injected subcutaneously with $1x10^7$ SKOV-3 human ovarian carcinoma cells in the shoulder and tumors were allowed to form over a period of 6-8 weeks. Mice (n=4) received tail vein injections of approximately 0.17 Mbq of ^{111}In-DOTA-GSG-J18 peptide and were housed separately after administration of radioactivity. The mice were sacrificed by cervical dislocation after 30 min, 1 h, 2 h and 4 h post-injection, and tissues and organs were removed, weighed and counts were determined. Radioactive uptake in the tumor as well as in normal tissues and organs was calculated and expressed as a percentage of injected dose per gram of tissue (%ID/g). For blocking experiments, tumor-bearing mice (n=4) were pre-injected with 100 μg nonradioactive In-labeled DOTA-GSG-J18 peptide. After 5 min, the mice were injected with 0.17 MBq of the corresponding radiolabeled peptide (^{111}In-DOTA-GSG-J18), and the animals were sacrificed after 1 h and the blocking efficiency was evaluated as described previously.

Small Animal SPECT/CT Studies

Nude female mice bearing xenografted SKOV-3 tumors (shoulder) were injected through the tail vein with 13.0 MBq of ^{111}In-DOTA-GSG-J18 and imaged 1 h post injection using a small-animal MicroCAT II SPECT/CT scanner (Siemens Medical Solutions, Malvern, PA) with a high-resolution 2 mm pinhole collimator at the Harry S. Truman Veterans Memorial Hospital Biomolecular Imaging Center. For blocking experiments, mice were pre-injected with 170 μg of nonradioactive In-labeled DOTA-

GSG-J18 peptide. After 5 min, mice were injected with 13.0 MBq of ^{111}In-DOTA-GSG-J18 and imaged after a total of 1 h using a SPECT/CT scanner as described above.

Statistical Analysis

For statistical analysis a Student's t-test was performed to determine significance using Prism Graphpad Software. A P-value of 0.05 or less was considered significant.

Results

Phage Display Selection

In order to select peptides with good *in vivo* pharmacokinetic and tumor targeting properties, phage display selections were initially performed against xenografted SKOV-3 tumors in live nude mice. In the first round of selection, the naive phage display library (15mer, fUSE5) was pre-cleared of vasculature and non-tumor binding phage in nude mice without tumors. The pre-cleared and amplified phage library was then subjected to three rounds of selection in xenografted SKOV-3 tumor-bearing mice. In short, the phage were injected into the tail-vein and allowed to circulate for 1 h, after which the animals were sacrificed and the tumors collected. After each round of selection, the phage were eluted from the tumors, amplified and used in subsequent rounds of selection. Following the third and last round of *in vivo* selection, the phage library was subjected to a final round of selection against tumor derived SKOV-3 cells *in vitro*. Between each round of selection, randomly picked phage clones were collected and the foreign phage display insert was determined for detection of potential contamination and identification of selected peptide sequences by DNA sequencing.

Thirty-one individual phage clones, that were identified in the last round of selection against tumor derived SKOV-3 cells, were used for micropanning experiments to identify clones with specific affinity for human ovarian carcinoma cells. These phage clones were incubated with SKOV-3 (cancer) or HS-832 (normal) cells, after which bound phage were collected and titered in *E. coli* (K91 BluKan). Results showed that

Table 2.1. Micropanning assay to determine binding of selected phage clones to SKOV-3 and HS-832 cells.

Phage No.	*Peptide sequence*	*SKOV-3 to HS-832 ratio*
pJ1	RTEVPVLSFTSPLTG	1.76
pJ2	GDVWLFKTSTSHFAR	1.91
pJ3	AREYGTRFSLIGGYR	0.21
pJ4	HAAFEPRGDVRHTLL	2.00
pJ5	LGRAGQSYPSFARGL	0.52
pJ6	PIFPVVSSSGSSSSP	1.58
pJ7	PLSHGSVVYPRSSLG	1.36
pJ8	RRDTVPRSLSAPLSW	0.59
pJ9	PAVASTSSLIIDGPF	2.29
pJ10	HPPLASVWHVSVPL	0.83
pJ11	LHDFRSPIYASLLGF	1.53
pJ12	AGDGGLGRVAAGARV	1.15
pJ13	RVFHLWPHPTSTLSA	0.25
pJ14	APLSYNFASMPFMSG	0.73
pJ15	HPGWFDSAWFRAVSR	1.24
pJ16	ARDSRCGGFLGCGVT	1.36
pJ17	AMVRGFSFGMSRGSD	1.94
pJ18	RSLWSDFYASASRGP	6.57
pJ19	SYSVVNSPWCDGTCD	1.25
pJ20	SRDGLHSFCYVGCPP	0.40
pJ21	GVGDADGFIPVISAV	0.59
pJ22	PVFFRLSPVTEGGGV	1.40
pJ23	FPSYPFIAYSLQTPV	1.23
pJ24	RRLPHLMPFEGSVFL	3.55
pJ25	GPHFDYRTGLGWRFG	1.35
pJ26	LGKGLTGSALSLSAL	2.29
pJ27	YGVTPSPRSPWATAH	3.43
pJ28	VFVDGARYSTASDSL	2.83
pJ29	GAGIFGPWGVFAAVP	1.21
pJ30	GYRSAFVPFVARGGH	3.65
pJ31	RYRVGFTPGTIAAVL	1.13

Collected phage from the *in vitro* phage display selection against cultured and purified SKOV-3 tumor cells were evaluated for their binding to ovarian carcinoma SKOV-3 and normal ovarian HS-832 cells. SKOV-3 or HS-832 cells were incubated with individual phage clones and eluted using 2.5% CHAPS. Phage binding was determined by titer and the SKOV-3 to HS-832 ratio was calculated.

three phage clones (pJ18, pJ24 and pJ30) showed the highest SKOV-3 to HS832 binding ratios, indicating preferable binding to the human ovarian carcinoma cell line (Table 2.1). Based on this data, the correlating peptides RSLWSDFYASASRGP (J18), RRLPHLMPFEGSVFL (J24) and GYRSAFVPFVARGGH (J30) were chosen to be synthesized and biotinylated to compare cell binding characteristics using fluorescent microscopy, as well as EC_{50} values, and to determine if the binding was mediated by the displayed peptides or by inherent phage proteins.

Cell Binding of Biotinylated J18, J24 and J30

Biotinylated peptides, bio-GSG-J18, bio-GSG-J24, bio-GSG-J30 and non-relevant peptide bio-GSG-N35 (negative control), were synthesized using solid-phase Fmoc chemistry. In order to further evaluate if the observed binding in the micropanning study was mediated by the displayed peptides or by non-specific phage interactions, the peptides were incubated with SKOV-3 cells. Binding was measured by a colorimetric assay; in which varying concentrations of peptides (10 nM to 300 μM) was incubated with SKOV-3 cells (Figure 2.1). The selected peptides were found to show increased binding compared to bio-GSG-N35 and exhibited EC_{50} values of 22.2 ± 10.6 μM, 29.0 ± 6.9 μM and 33.7 ± 11.5 μM (mean ± SE), demonstrating that the binding was facilitated by the peptide sequences and not by inherent phage proteins.

Fluorescent Microscopy

The binding characteristics of the biotinylated peptides were further evaluated using fluorescent microscopy (Figure 2.2). These studies revealed that peptide

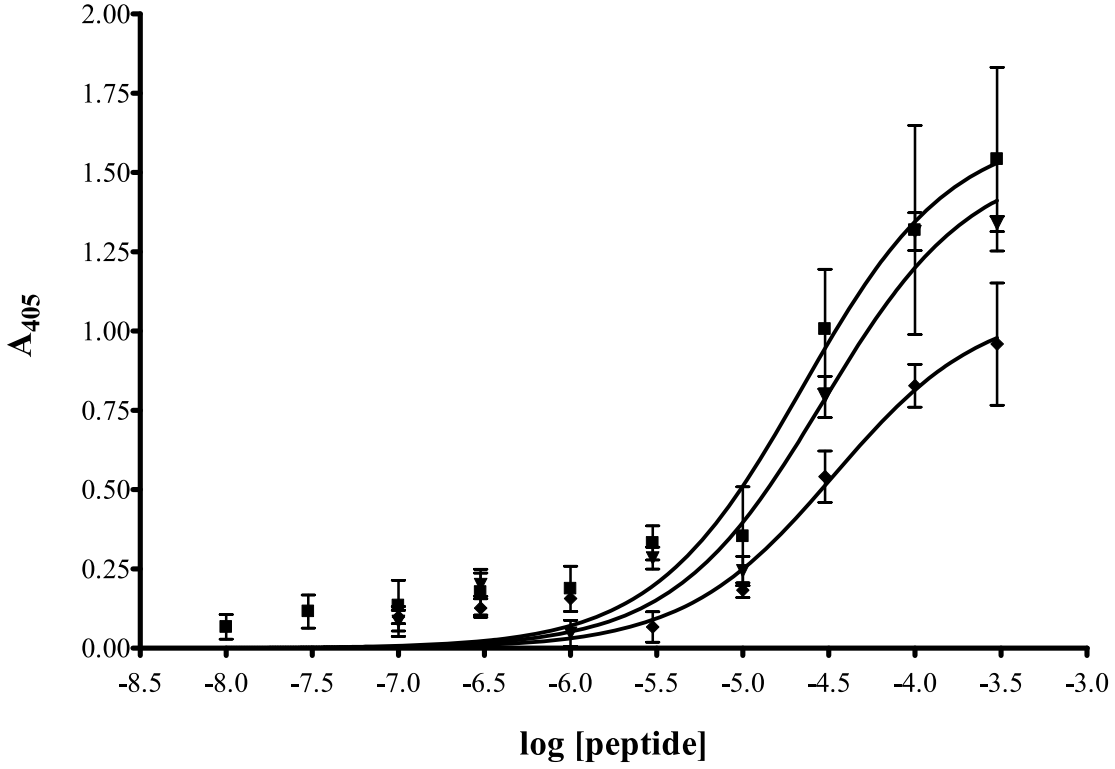

Figure 2.1. Binding properties of biotinylated peptides J18, J24 and J30 to ovarian carcinoma (SKOV-3) cells. Cells were grown to 80% confluency on 96-well plates, and then incubated with varying concentrations (10 nM to 300 μM) of biotin-GSG-J18 (■), biotin-GSG-J24 (▼) or biotin-GSG-J30 (♦) for 1 h at 37°C. Plates were washed with PBS and fixed with 10% formalin. Biotinylated peptides were detected by HRP-conjugated streptavidin, and measurement of absorbance at 405 nM after addition of HRP-substrate ABTS. EC_{50} values for biotin-GSG-J18, biotin-GSG-J24 and biotin-GSG-J30 were calculated to be 22.2 ± 10.6 μM, 29.0 ± 6.9 μM and 33.7 ± 11.5 μM (mean ± SE), respectively. Measurements were performed on a μ Quant Universal Microplate Spectrophotometer (Bio-Tek Instruments,Winooski, VT).

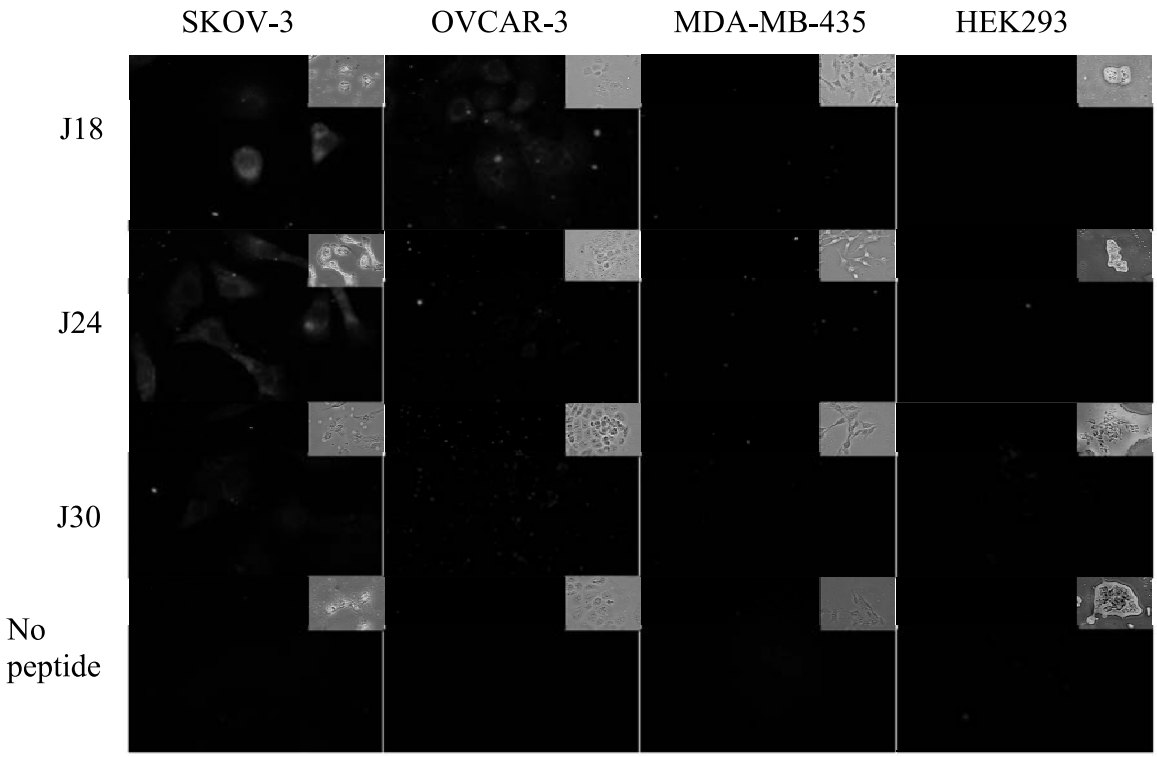

Figure 2.2. Fluorescent microscopy of peptide binding to SKOV-3, OVCAR-3, MDA-MB-435 and HEK293 cells. Cells were incubated with 10 μM bio-GSG-J18, bio-GSG-J24 or bio-GSG-J30 peptides for 1 h at 37°C. Bound peptides were probed by a mouse monoclonal anti-biotin antibody and detected using an epifluorescent Nikon T1-SM inverted microscope (Nikon, Melville, NY).

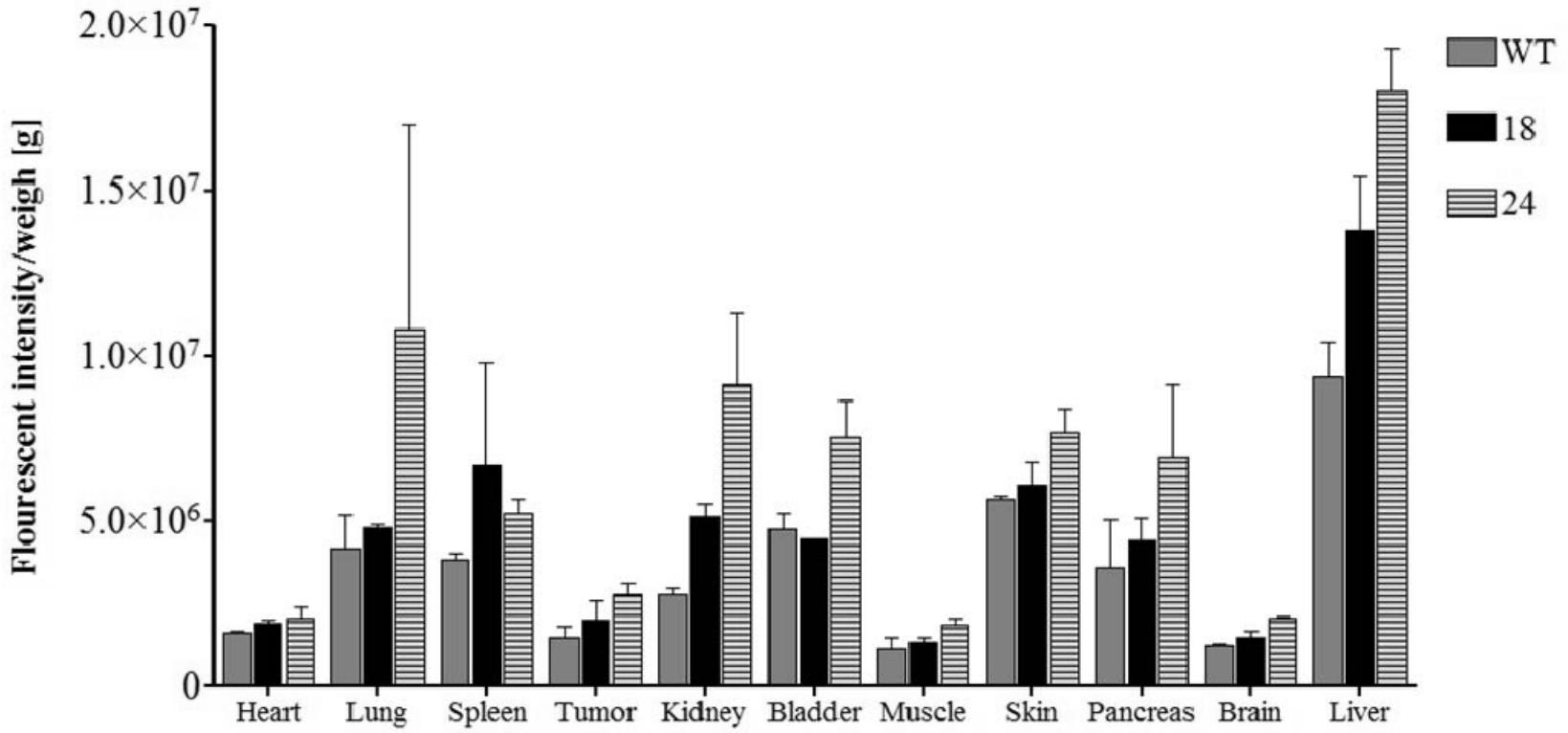
Flourescent intensity/weigh [g]
2.0×10^7
1.5×10^7
1.0×10^7
5.0×10^6
0
WT
18
24
Heart
Lung
Spleen
Tumor
Kidney
Bladder
Muscle
Skin
Pancreas
Brain
Liver

Figure 2.3. Biodistribution of AF680-labeled pJ18, pJ24 and WT phage in SKOV-3 xenografted nude female mice. Mice were injected with 10^{12} virions of phage. After 4 h the animals were sacrificed and the organs, tissues, and the tumor were excised, weighed, and the fluorescent intensity was measured using a Xenogen IVIS 200 System. Fluorescent uptake was normalized to the weight of each organ, and reported as fluorescent intensity per gram.

bio-GSG-J18 displayed increased binding for the SKOV-3 and human ovarian carcinoma OVCAR-3 cell lines, while exhibiting minimal affinity for MDA-MB-435 and HEK293 cells. Peptide bio-GSG-J24 showed the highest binding to SKOV-3 cells and little to no binding to other cell lines. Similarly, bio-GSG-J30 exhibited the highest affinity for SKOV-3 cells; however, this binding was minimal. For this reason, in addition to displaying the highest EC_{50} value of the three peptides, bio-GSG-J30 was eliminated from further studies.

Biodistribution and Near-Infrared Optical Imaging of AF680-Labeled Phage

In order to evaluate the tumor targeting capabilities of the selected peptides J18 and J24, the corresponding phage clones, pJ18, pJ24 as well as WT, were labeled with the near-infrared fluorophore AF680, and employed in biodistribution and optical imaging studies. The biodistribution of the AF680-labeled phage clones was investigated in female nude mice bearing xenografted human SKOV-3 tumors. Phage were injected into the tail-vein of the animals; after 4 h the mice were sacrificed by cervical dislocation and the fluorescent intensity in the tumors and in normal tissues was measured (Figure 2.3). Phage clone pJ18 exhibited fluorescent tumor uptake after 4 h; however, the levels were not significantly higher compared to WT. To the contrary, tumor uptake of pJ24 was significantly higher compared to WT phage, but also showed increased levels in most other organs (lung, spleen, kidney, bladder, skin and liver). For all phage, the liver exhibited increased fluorescent uptake compared to other organs, indicating that the phage were excreted through the reticuloendothelial system. This observation was further confirmed by elevated uptake by the spleen and lungs; however, the kidneys also

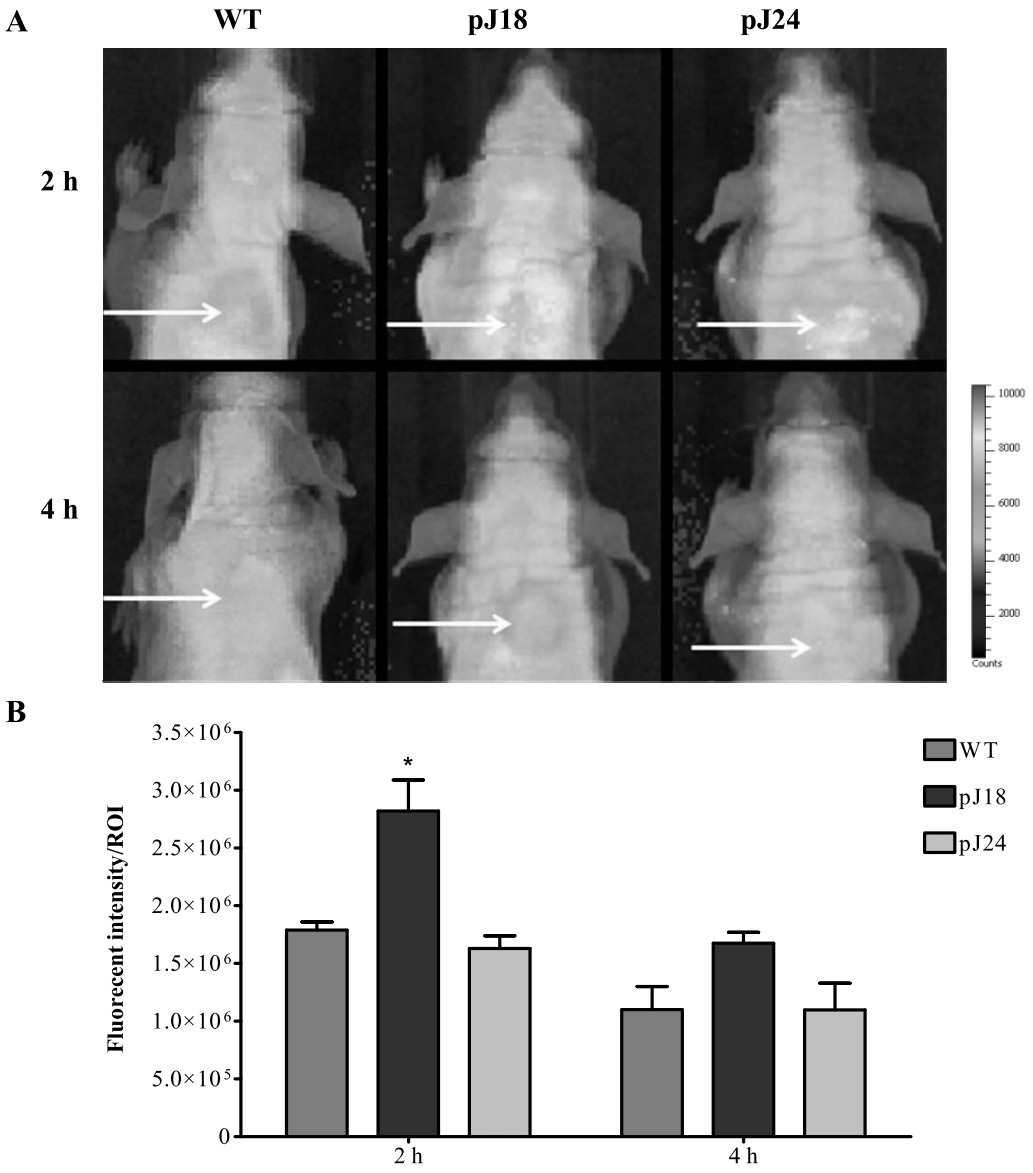

Figure 2.4. *In vivo* optical imaging of SKOV-3 xenografted tumors in female nude mice using AF680-labeled pJ18, pJ24 and WT phage. The mice were injected with 10^{12} virions of phage and imaged under anesthesia at 2 h and 4 h post-injection. **A)** Fluorescence reflectance images of SKOV-3 xenografted mice. Tumor location is indicated by a white arrow. **B)** Quantification of fluorescent signal intensity of region of interest (ROI). Fluorescence reflectance images were obtained using a Xenogen IVIS 200 System, and the fluorescent signal intensity was quantified using ImageJ software. * p=0.03.

displayed increased fluorescent intensity, especially for J24. These results suggest that the kidneys may be a minor excretion route for both J18 and J24, but not for WT phage, which showed only minimal uptake in these organs. Phage uptake in other organs (heart, muscle and brain) was comparatively lower and did not differ between the clones.

Near-infrared optical imaging of nude mice carrying xenografted SKOV-3 tumors was performed to investigate the imaging properties of phage clones pJ18 and pJ24 (Figure 2.4a). AF680-labeled phage (pJ18, pJ24 or WT) were tail-vein injected into the animals and circulated for up to 4 h. The mice were imaged before the injection (0 h) to determine autofluorescence, as well as 2 h and 4 h post-injection. The obtained images revealed that the SKOV-3 tumors were easily localized and exhibited sufficient tumor-to-background contrast. Additionally, the tumor signal intensity of phage clone pJ18 and was significantly higher in comparison to WT at 2 h post-injection (Figure 2.4b). The tumor uptake was lower after 4 h for all three phage clones.

The higher tumor uptake and more rapid biodistribution of pJ18 compared to pJ24 are great advantages in regard to radionuclide imaging [183], and for these reasons, peptide J18 was chosen for further analysis.

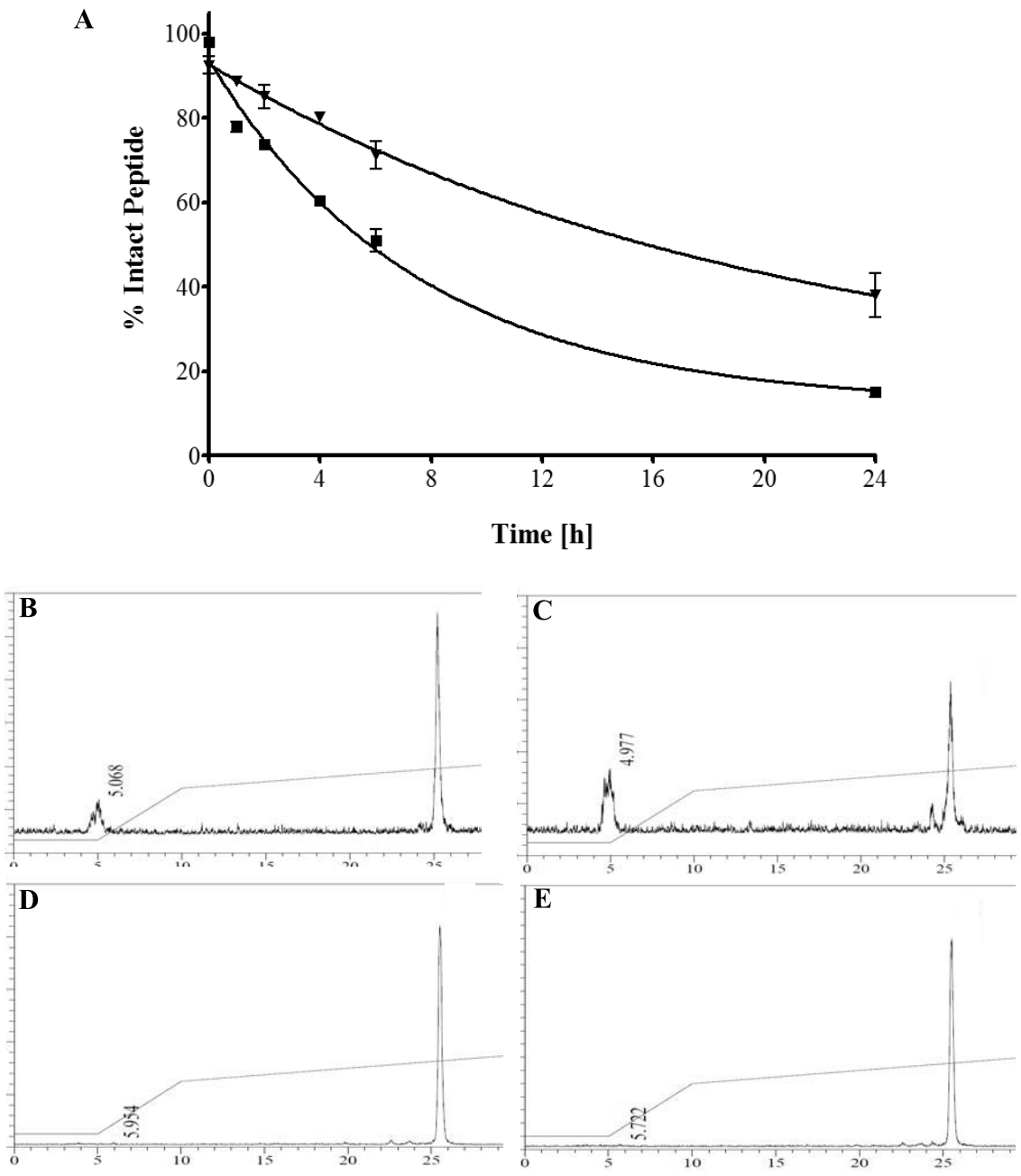

Figure 2.5: Stability of ^{111}In-DOTA-GSG-J18 under physiological conditions. **A)** Time course of intact radiolabeled peptide in mouse serum (■) and HEPES buffer (▼) at 37ºC. **B-E)** HPLC chromatograms of collected radiolabeled peptide in mouse serum after 1 h **(B)** and 4 h **(C)** and in HEPES buffer after 1 h **(D)** and 4 h **(E)**. Half-lives of ^{111}In-DOTA-GSG-J18 in mouse serum and HEPES buffer were calculated to be 5.2 h and 14.0 h, respectively.

Peptide Synthesis, Radiolabeling and Stability

Solid-phase Fmoc chemistry was used to synthesize the DOTA-labeled peptide DOTA-GSG-J18. The GSG spacer was introduced between the DOTA group and the NH_2-terminus of the peptide to avoid potential steric hindrance. The peptide DOTA-GSG-J18 was successfully labeled with ^{111}In or non-radioactive indium in 0.5 M ammonium acetate buffer, pH 5.0, at 85°C for 1 h and purified by RP-HPLC. The radiolabeled peptide and its non-radioactive counterpart eluted with retention times of 24.6 min and 24.5 min, respectively. High labeling efficiency of 98% and radiochemical purity of 98.6 ± 1.6 % (mean ± SD), for ^{111}In-DOTA-GSG-J18 were observed. The yield of radiolabeled peptide was 20% after HPLC and C-18 cartridge purification.

The stability of radiolabeled peptide ^{111}In-DOTA-GSG-J18 was evaluated in 0.5M HEPES buffer, pH 7, and in mouse serum at 37ºC for different time intervals and analyzed by RP-HPLC. The radiolabeled peptide exhibited a half-life of 14.0 h and 5.2 h in HEPES buffer and mouse serum, respectively (Figure 2.5).

Cell Binding of ^{111}In-DOTA-GSG-J18

The specificity of the radiolabeled peptide for ovarian cancer was determined in an *in vitro* cell-binding assay using SKOV-3 and HS-832 cells. For this, ^{111}In-DOTA-GSG-J18 was incubated with $1x10^6$ cells for different periods of time, and the bound radioactivity was measured and calculated as percentage of the total counts per minute (% total cpm). Binding of the radiolabeled peptide to both cell lines increased from 0 min

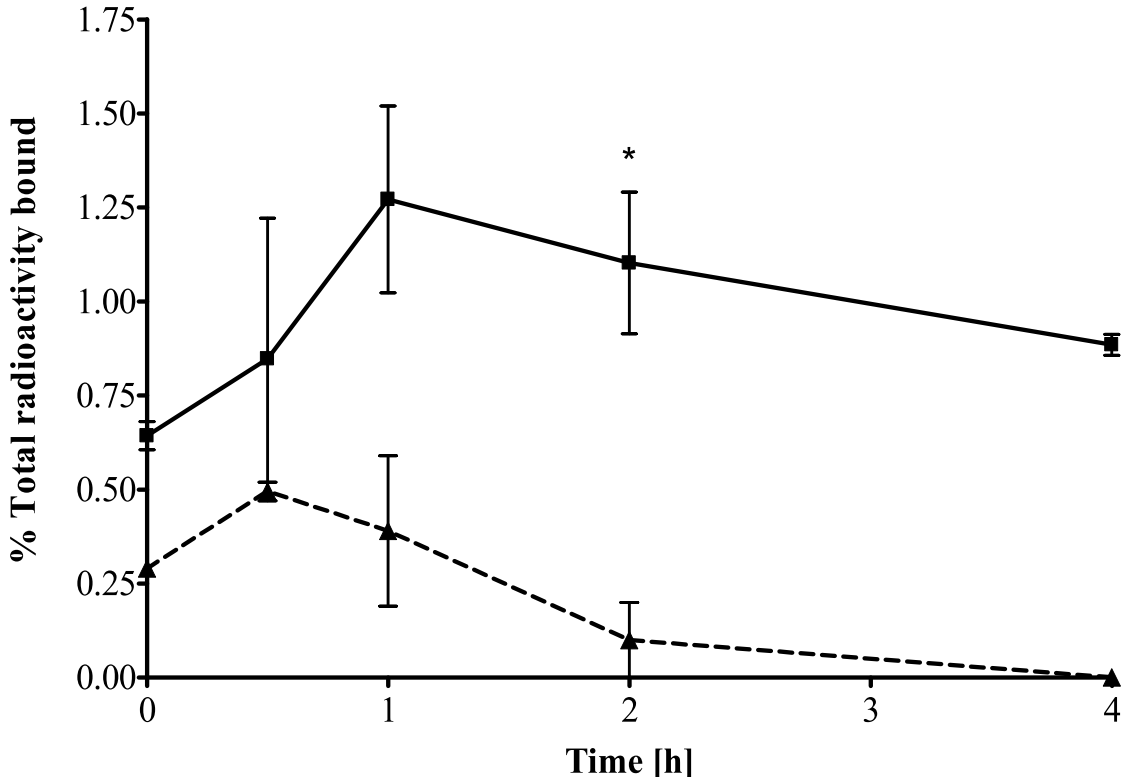

Figure 2.6. Binding properties of ^{111}In-DOTA-GSG-J18 to ovarian carcinoma (SKOV-3) (■) and normal ovarian (HS-832) (▲) cells. Cells ($1x10^6$) were incubated with $2x10^5$ cpm of radiolabeled peptide for 30 min, 1 h, 2h or 4 h. Although, binding of ^{111}In-DOTA-GSG-J18 to SKOV-3 cells was significantly higher at 2 h, binding to HS-832 cells was also observed. * $p < 0.05$.

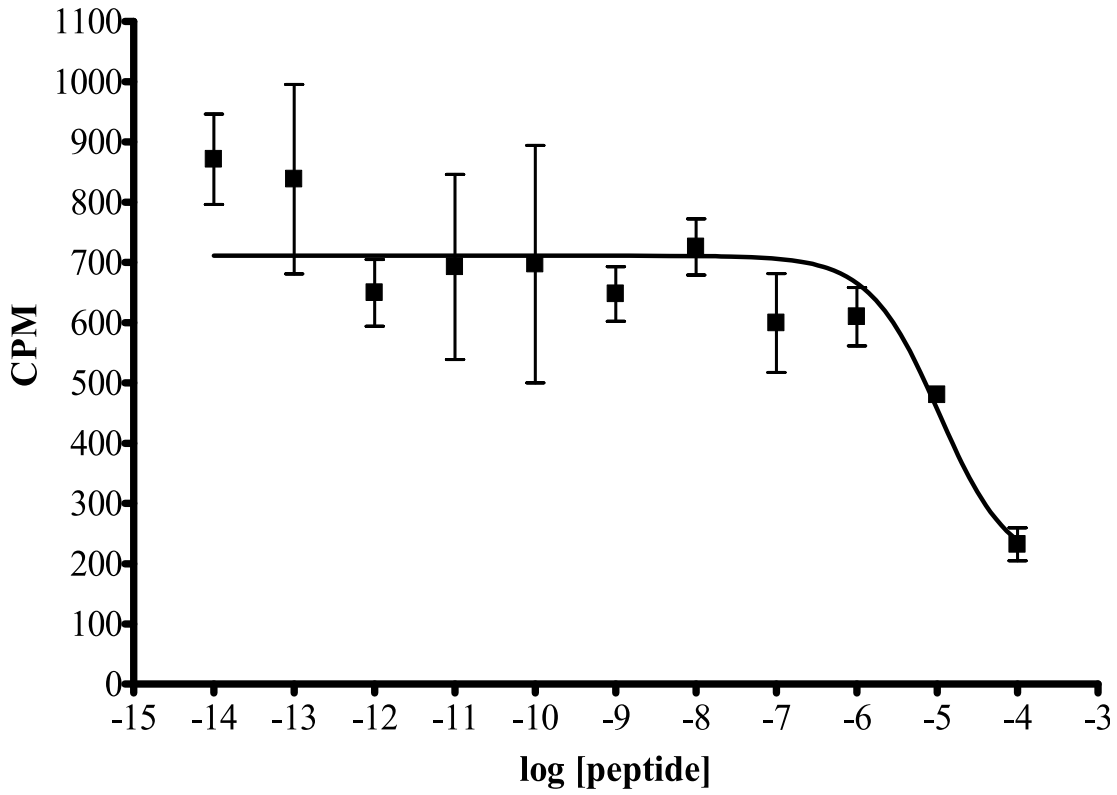

Figure 2.7. Cell binding competition study of ^{111}In-DOTA-GSG-J18 and its non-radioactive counterpart. SKOV-3 cells ($1x10^6$) were incubated with $2x10^5$ cpm of ^{111}In-DOTA-GSG-J18 and various concentrations (10^{-14} to 10^{-4} M) of the correlating non-radiolabeled peptide In-DOTA-GSG-J18 for 1 h at 37ºC. Bound radioactive peptide was measured in cpm by a Genesys™ Genii™ Multi-Well Gamma Counter (Laboratory Technologies, Inc, Maple Park, IL). The IC_{50} value was 10.5 ± 1.1 μM (mean ± SE).

to 1 h, after which the binding gradually decreased. Nevertheless, in comparison to normal ovarian (HS-832) cells, ^{111}In-DOTA-GSG-J18 exhibited significantly higher binding to ovarian carcinoma (SKOV-3) cells after 2 h, demonstrating specificity for this cell line (Figure 2.6).

Further validation of the specific binding of radiolabeled peptide (^{111}In-DOTA-GSG-J18) to SKOV-3 cells was determined by an *in vitro* competition assay in the presence of different concentrations of the correlating non-radioactive peptide (In-DOTA-GSG-J18). The results showed that the amount of bound radioactivity decreased in a dose-dependent manner with increasing concentrations of non-radiolabeled peptide, indicating that binding of ^{111}In-DOTA-GSG-J18 was out-competed by In-DOTA-GSG-J18 (Figure 2.7). Based on these data, an IC_{50} value of ^{111}In-DOTA-GSG-J18 for human ovarian carcinoma SKOV-3 cells was calculated to be 10.5 ± 1.1 μM (mean ± SE).

Alanine Scanning Experiments

A sequential alanine scanning experiment of peptide J18 was performed to identify the amino acid residues responsible for the binding to ovarian carcinoma cells. For this purpose, biotinylated peptides, each with a single alanine substitution (inherent alanine residues were substituted with serine), were synthesized and employed in a modified ELISA (Table 2.2). Various concentrations (10 nM to 100 μM) of peptides were incubated with SKOV-3 cells for 1 h at 37ºC, after which the binding was measured colorimetrically at 405 nm, and the half maximal effective concentration (EC_{50}) for each peptide was calculated (Figure 2.8). These results showed that alanine substitutions of

Table 2.2. Alanine scanning peptides.

Peptide No.	*Peptide Sequence*
J18	RSLWSDFYASASRGP
J18-1	**A**SLWSDFYASASRGP
J18-2	R**A**LWSDFYASASRGP
J18-3	RS**A**WSDFYASASRGP
J18-4	RSL**A**SDFYASASRGP
J18-5	RSLW**A**DFYASASRGP
J18-6	RSLWS**A**FYASASRGP
J18-7	RSLWSD**A**YASASRGP
J18-8	RSLWSDF**A**ASASRGP
J18-9	RSLWSDFY**S**SASRGP
J18-10	RSLWSDFYA**A**ASRGP
J18-11	RSLWSDFYAS**S**SRGP
J18-12	RSLWSDFYASA**A**RGP
J18-13	RSLWSDFYASAS**A**GP
J18-14	RSLWSDFYASASR**A**P
J18-15	RSLWSDFYASASRG**A**

A sequential alanine scanning experiment of peptide J18 was done to elucidate the mechanism of peptide binding to SKOV-3 cells. Each biotinylated peptide was synthesized with a single alanine substitution. Inherent alanine residues were substituted with serine.

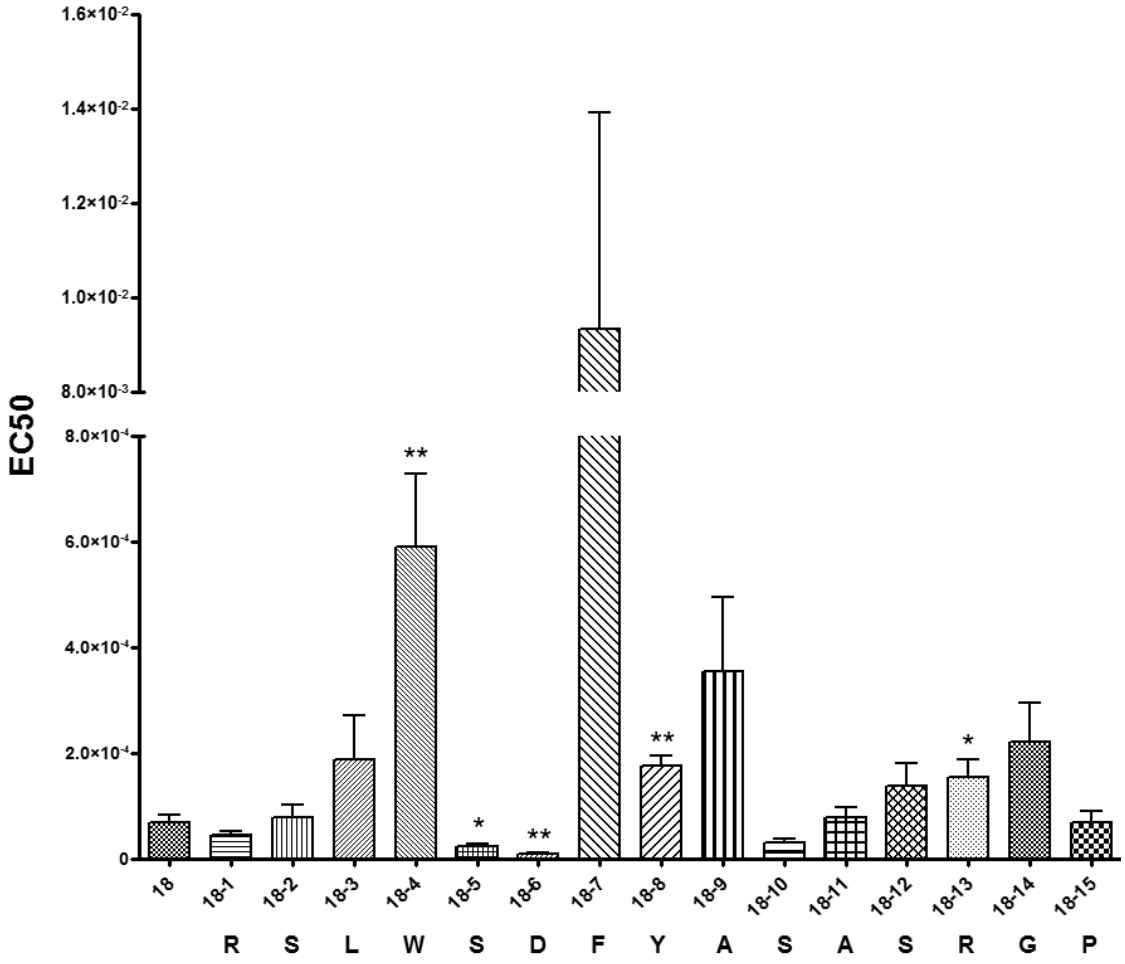

Figure 2.8. Sequential alanine scanning experiment of peptide biotin-GSG-J18. The SKOV-3 binding of various concentrations (10 nM to 100 μM) of biotinylated peptides (J18-1 to J18-15) with single sequential alanine substitutions (inherent alanine residues were substituted with serine) was analyzed by a modified ELISA. EC_{50} values were calculated for each peptide.

* $p < 0.05$, ** $p < 0.01$.

tryptophan (J18-4), tyrosine (J18-8) and arginine (J18-13) significantly increased the EC_{50} values compared to J18, indicating that these residues are important in the binding to SKOV-3 cells. Although not significant, the alanine substitution of phenylalanine (J18-7) showed similar results, suggesting that this amino acid is likewise involved in the binding interaction. In contrast, substitutions of serine (J18-5) and aspartic acid (J18-6) resulted in significantly lower EC_{50} values of approximately 10-fold, demonstrating that the affinity of the peptide may be improved upon.

Pharmacokinetics of ^{111}In-DOTA-GSG-J18 in SKOV-3 Tumor-Bearing Mice

Indium-111 labeled DOTA-GSG-J18 peptide was evaluated in regard to its pharmacokinetic properties in female nude mice bearing xenografted SKOV-3 tumors. The mice were tail-vein injected with 0.17 Mbq of the radioligand and sacrificed after 30 min, 1 h, 2 h and 4 h, and the tumor and organ uptakes were determined (Table 2.3). Radioactive uptake in the tumor was calculated to be 1.63 ± 0.68, 0.60 ± 0.32, 0.31 ± 0.12 and 0.10 ± 0.02 % ID/g at 30 min, 1 h, 2 h and 4h, respectively. Blood clearance of the radioligand was apparent exhibiting levels of 2.37 ± 0.94, 0.40 ± 0.24, 0.03 ± 0.03 and 0.19 ± 0.02 % ID/g at 30 min, 1 h, 2 h and 4h, respectively. The tumor-to-blood ratio increased from 0.69 at 30 min to 1.50 and 6.00 at 1 h and 2 h, respectively, indicating rapid blood clearance and kinetically favorable tumor uptake and retention. Equally high tumor-to-muscle ratios were shown as early as 1 h post-injection. Radioactive uptake in the normal organs was, as expected, the highest in the kidneys due to renal clearance

Table 2.3: Biodistribution of ^{111}In-DOTA-GSG-J18 in SKOV-3 tumor-bearing nude mice.

Pharmacokinetics of ^{111}In-DOTA-GSG-J18					
%ID/g					
Tissues	30 min	1 h[†]	1 h- block	2 h[††]	4 h
Tumor	1.63 ± 0.68	0.60 ± 0.32	0.31 ± 0.12[*]	0.18 ± 0.03	0.10 ± 0.02
Blood	2.37 ± 0.94	0.40 ± 0.24	0.23 ± 0.11	0.03 ± 0.03	0.19 ± 0.02
Heart	0.67 ± 0.27	0.13 ± 0.08	0.07 ± 0.03	0.02 ± 0.01	0.05 ± 0.01
Lung	2.42 ± 0.48	1.06 ± 0.82	0.83 ± 0.19	0.49 ± 0.36	0.62 ± 0.32
Liver	1.42 ± 0.37	0.51 ± 0.48	0.37 ± 0.02	0.23 ± 0.11	0.84 ± 0.13
Spleen	1.77 ± 0.46	0.68 ± 1.01	0.16 ± 0.03	0.19 ± 0.24	1.58 ± 0.36
Stomach	0.36 ± 0.14	0.11 ± 0.04	0.08 ± 0.03	0.04 ± 0.02	0.04 ± 0.00
Large intestine	0.34 ± 0.17	0.15 ± 0.05	0.07 ± 0.02	0.27 ± 0.06	0.28 ± 0.19
Small intestine	0.63 ± 0.29	0.32 ± 0.11	0.15 ± 0.04	0.15 ± 0.08	0.06 ± 0.01
Intestines	0.49 ± 0.22	0.25 ± 0.08	0.12 ± 0.03	0.20 ± 0.07	0.15 ± 0.08
Kidneys	6.71 ± 3.08	2.70 ± 0.95	1.98 ± 0.29	1.67 ± 0.43	1.75 ± 0.17
Brain	0.09 ± 0.03	0.03 ± 0.01	0.02 ± 0.00	0.01 ± 0.00	0.01 ± 0.00
Muscle	0.32 ± 0.17	0.06 ± 0.03	0.04 ± 0.01	0.01 ± 0.00	0.01 ± 0.00
Pancreas	0.65 ± 0.18	0.11 ± 0.05	0.08 ± 0.01	0.02 ± 0.01	0.04 ± 0.01
Bone	0.31 ± 0.13	0.06 ± 0.05	0.05 ± 0.03	0.02 ± 0.01	0.08 ± 0.02
Skin	1.28 ± 0.68	0.22 ± 0.11	0.22 ± 0.08	0.09 ± 0.03	0.10 ± 0.01
Uptake ratio					
Tumor to blood	0.69	1.50	1.35	6.00	0.53
Tumor to muscle	5.10	10.00	7.75	18.00	10.00

Data are represented as %ID/g (mean ± SD), or as uptake ratio of tumor to normal tissue (blood and muscle) for female nude mice (n=4) bearing human ovarian SKOV-3 xenografted tumors. Mice were sacrificed at different times post-injection of ^{111}In-DOTA-GSG-J18.

[†] n=7

[††] n=5

[*] p=0.03, significant difference between tumor uptake of radiolabeled peptide 1 h post-injection with and without the presence of its non-radioactive counterpart.

being the major route of excretion for most peptide ligands [183]. The kidney uptake was highest after 30 min at 6.71 ± 3.08 and decreased to 2.70 ± 0.95, 1.67 ± 0.43 and 1.75 ± 0.17 % ID/g at 1 h, 2h and 4 h, respectively. Of all other organs, only the lungs, liver and spleen demonstrated noticeable radioligand uptake, which decreased rapidly after 1 h. Very little radioactivity was detected in the remaining organs and bone. In order to determine the specificity of tumor uptake, the radiolabeled peptide was subjected to *in vivo* competition studies with its non-radioactive counterpart. SKOV-3 tumor-bearing mice (n=4) were injected with 100 μg of peptide labeled with non-radioactive In, followed by an injection of 0.17 Mbq of ^{111}In-labeled peptide, and the tumor and organ uptakes were evaluated after 1 h. The results indicate that the non-radioactive peptide ligand successfully blocked uptake of the radioactive counterpart by approximately 48% (P=0.03). The non-radioactive ligand did not significantly (P>0.05) affect the uptake of the ^{111}In-labeled peptide in normal organs including the kidneys, lung, liver and spleen.

SPECT/CT Tumor Imaging

In order to evaluate the tumor imaging ability of ^{111}In-DOTA-GSG-J18, female nude mice carrying xenografted SKOV-3 tumors (shoulder) were injected into the tail-vein with 13.0 MBq of the radiolabeled peptide, and a whole-body SPECT/CT scan was performed of the live animals after 1 h (Figure 2.9a). The xenografted human ovarian tumor was clearly visualized with high tumor-to background contrast, and the kidney uptake was concurrent with the pharmacokinetic data. Excretion of the radioligand was visible in the bladder, while little to no radioligand uptake was detected in other normal organs and bone. For determination of peptide tumor specificity, mice were tail-vein

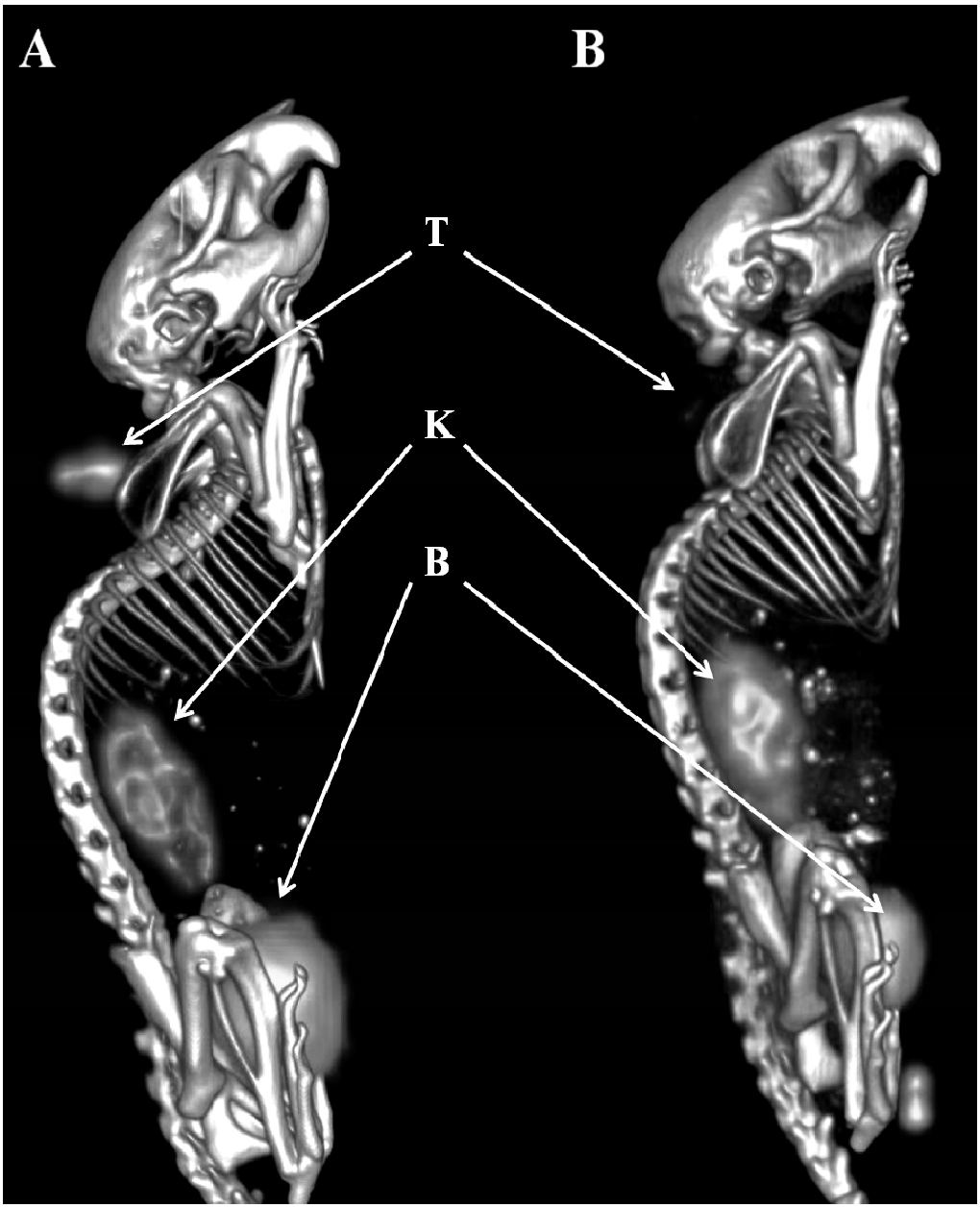

Figure 2.9. SPECT/CT study with nude mice carrying xenografted SKOV-3 tumors. **A)** ^{111}In-DOTA-GSG-J18 (13.0 MBq) or **B)** In-DOTA-GSG-J18 followed by ^{111}In-DOTA-GSG-J18 (13.0 MBq) were injected into the tail vein of SKOV-3 tumor-bearing nude mice. The live image was acquired 1 h post-injection under isoflurane anesthesia in a Siemens small-animal SPECT/CT scanner. The pictures show left lateral fused SPECT/CT images. T=tumor, K=kidneys and B=bladder.

injected with 170 μg of peptide labeled with non-radioactive indium, followed by an injection of 13.0 MBq of ^{111}In-DOTA-GSG-J18 and a whole-body SPECT/CT scan of the live animal 1 h post-injection. The image showed that the tumor uptake of ^{111}In-DOTA-GSG-J18 was successfully blocked by its non-radioactive counterpart (Figure 2.9b), while radioactive uptake in the kidneys as well as other organs and the bone was unchanged, indicating that the radioligand exhibits specificity for the SKOV-3 tumor.

Discussion

Ovarian cancer is among the leading causes of cancer deaths in women. The poor prognosis is a direct result of asymptomatic disease development and a lack of adequate diagnostic methods, causing the majority of patients to be diagnosed at regional or distant stages [1, 3, 4, 6, 8]. Currently, CA-125 is the only biomarker significantly associated with ovarian cancer, and measurement of its serum levels is a standard diagnostic method in the clinic. However only 50% of stage I patients show elevated levels of this tumor marker [168]. In addition, elevated CA-125 levels may be caused by other conditions such as endometriosis and inflammatory diseases, and may therefore lead to false-positive results that require surgery to obtain final diagnosis [9, 184, 185]. As a consequence, the low levels and/or absence of CA-125 during early stages of ovarian cancer and its elevated presence in non-malignancies render its detection more useful as a follow-up tool to monitor progressed disease rather than as a diagnostic method [168]. In recent years another ovarian cancer biomarker, HE-4, has been intensely studied. HE4 is overexpressed in some forms of ovarian cancer and has been shown to be a more specific marker of the disease than CA-125 [91-95]. Many other biomarkers of ovarian cancer are under investigation, including epidermal growth factor (EGF) [186], IL-6 [186], IL-8 [186, 187] and monocyte chemoattractant protein-1 (MCP-1) [186]; however, the majority shows high specificity while exhibiting low sensitivity or vice versa [188]. Taking the lack of adequate diagnostic tools together with the low survival rate of ovarian cancer, it emphasizes the great need for discovery and development of novel detection

methods. Better diagnostics will not only allow for detection of less progressed disease, but will also greatly improve mortality rates.

While peptides often exhibit lower binding affinities to their target compared to antibodies, the former offer advantages in regard to low immunogenicity, rapid blood-clearance as well as renal excretion [46, 48]. Peptide-based radionuclide imaging agents are rapidly evolving due to the implementation of combinatorial strategies such as phage display technology, which allows high-throughput selection and identification of cancer targeting peptide ligands [32, 151, 152, 169, 171, 189-194]. Several peptides have been identified by phage display selections against known cancer antigens and have demonstrated excellent binding properties in *in vitro* assays. Examples of such targeting agents include peptides that bind to the cysteine rich protein 1 (CRIP-1) [171], prostate specific antigen (PSA) [170, 172], and ephrin type-A receptor 2 (ephA2) [195]. Unfortunately, while the majority of peptides selected by such methods are excellent "binders" *in vitro*, they lack stability, suffer from low solubility and exhibit poor pharmacokinetic properties *in vivo*. To overcome these problems, researchers have argued that *in vivo* phage display selections offer advantages over *in vitro* screenings, in that the harsh environment of a live animal allows only stable peptides with optimal pharmacokinetic properties to reach and bind the target [196-198]. A limited group of peptides have been identified in this manner, of which one of the most well-known examples is the identification of a RGD-containing peptide that binds vasculature expressed $\alpha_v\beta_3$-integrin, and has been employed in both positron emission tomography (PET) and SPECT imaging of the human tumor vasculature in xenografted mice [152, 199, 200]. Other examples of peptides selected via *in vivo* phage display include the

rhabdomyosarcoma targeting sequence CQQSNRGDRKRC [194], as well as several peptides that bind tumor vasculature receptors such as interleukin 11 receptor [175], aminopeptidase P [176] and the ePHa4 receptor [177].

While many of these peptides show great promise, the majority of peptides that have been identified using *in vivo* phage display target the tumor vasculature rather than tumor cells. Instead, our laboratory has developed an *in vivo/in vitro* phage display screening method designed to select tumor cell targeting peptides with high *in vivo* stability and good pharmacokinetic properties. Initially, non-target binding phage was depleted from the library in a negative selection round in non-tumor bearing mice, which was followed by selection of tumor targeting phage against human ovarian carcinoma SKOV-3 xenografted animals. In order to select specifically for peptides binding to ovarian cancer cells, an additional *in vitro* selection was carried out against cultured enriched tumor SKOV-3 cells. This rigid screening process was followed by micropanning experiments, which resulted in the identification of three phage clones (pJ18, pJ24 and pJ30) that exhibited high ovarian cancer (SKOV-3) to normal ovarian (HS-832) binding ratios of 6.57, 3.55 and 3.65, respectively.

In order to further evaluate and compare the ovarian cancer binding properties, the phage displayed peptides (J18, J24 and J30) were synthesized with a biotin group and employed in cell binding and fluorescent microscopy studies. The cell binding studies revealed that all three peptides bound to SKOV-3 cells in a sigmoidal dose-response manner, indicating that the interaction was caused by specific binding. Further, these results confirmed that the phage binding observed in the micropanning experiments was facilitated by the displayed peptides and not by inherent phage proteins. The EC_{50} values

were calculated for bio-GSG-J18, bio-GSG-J24 and bio-GSG-J30 to be 22.2 ± 10.6 μM, 29.0 ± 6.9 μM and 33.7 ± 11.5 μM (mean ± SE), respectively, demonstrating that peptide J18 exhibited higher binding affinity. Additionally, these EC_{50} values are consistent with what has previously been found for peptides identified by *in vivo* phage display selections [201].

Fluorescent microscopy studies were done to further evaluate the peptide binding characteristics. These results showed that peptide bio-GSG-J18 exhibited increased binding to the SKOV-3 and OVCAR-3 cell lines, while bio-GSG-J24 showed affinity for SKOV-3 cells and minimal binding to other cells. Peptide bio-GSG-J30 displayed the highest affinity for SKOV-3 of all cell lines; nevertheless, this binding was negligible. Taken together these results suggested that the biotinylated peptides bio-GSG-J18 and bio-GSG-J24 bound ovarian cancer specific antigens, and may as a result be utilized as ovarian carcinoma imaging agents. Further, the different binding characteristics of J18 and J24 for SKOV-3 and OVCAR-3 cells indicate that the peptides may target different antigens. SKOV-3 cells are known to exhibit more invasive potential compared to OVCAR-3, and to express higher levels of epidermal growth factor receptor (EGFR) [202]. The higher affinity of J18 for SKOV-3 may therefore suggest that the peptide binds an antigen with similar expression profiles in the two cell lines, such as EGFR. The high SKOV-3-to-OVCAR-3 binding ratio of J24 may indicate that the peptide targets an antigen that is involved in invasiveness and is comparatively overexpressed in the more aggressive cell line. For these reasons, peptide J18 may be binding to an antigen present in a wider array of ovarian cancer types and could, therefore, be useful in more broad applications, while J24 may be utilized to provide a more specialized targeting strategy.

Unfortunately, J30 displayed both low binding to both ovarian carcinoma cells lines and exhibited the highest EC_{50} value of the three peptides, and was for these reasons eliminated from further studies.

In order to evaluate the potential tumor targeting abilities of the selected peptides, the corresponding phage were employed in biodistribution and optical imaging studies. This type of testing the phage prior to the peptides alone was previously performed with the notion that phage virions exhibit high stability under physiological conditions [203], and may therefore aid the peptides in tumor targeting. Hence, if phage clones fail to adequately target and image the tumors, the correlating single peptides would do so as well. Such form of pre-testing enables selection of the fittest peptides and avoids unnecessary and costly studies.

The biodistribution and optical imaging of fluorescently labeled phage, pJ18, pJ24 and WT, was explored in SKOV-3 xenografted nude mice. Although fluorescent tumor uptake was observed for pJ18 after 4 h, the levels were not significantly different from WT. This observation suggested that the phage clone may have exhibited optimal uptake at earlier time points; in fact the optical imaging study revealed that significant tumor retention was obtained after 2 h. These results may be caused by increased uptake and excretion rates of pJ18, which are further validated by the likewise low levels in other normal tissues. In correlation, the surface charge and displayed functional groups of nanoparticles are known to influence both cellular uptake and excretion; consequently, the net positive charge at physiological pH of peptide J18 (displayed on phage) may be the reason behind the observed rapid pharmacokinetics. In fact, nanoparticles with an overall positive charge are associated with fast cellular uptake and excretion, which

moreover may cause an increase in the rate of tumor targeting [204, 205]. In contrast to these observations, pJ24 showed significantly increased tumor uptake after 2 h and 4 h, as evident from both the biodistribution and imaging studies. However, this phage also exhibited increased levels in most other organs, which indicated that the clone displays elevated background binding compared to pJ18 and WT. For all phage clones, the liver exhibited the highest fluorescent uptake compared to other tissues, suggesting that the phage were cleared through the reticuloendothelial system. These results were further confirmed by increased retention in the spleen and lungs; nevertheless, the kidneys also displayed increased fluorescent intensity, especially for pJ24. This observation suggests that the kidneys may be a minor excretion route for both pJ18 and pJ24. Previous biodistribution studies of phage have shown similar results in regard to reticuloendothelial excretion [31, 206-208]. While the large size and biochemical properties of nanoparticles, including phage, are known to greatly affect biodistribution and excretion [205], the display of peptides have shown to partly re-direct the clearance [31]. Taking these observations into account, the pharmacokinetic results in this study may indicate that peptides J18 and J24 are steering the excretion system towards the kidneys. Phage uptake in other organs (heart, muscle and brain) was comparatively lower and did not differ between the clones. The low uptakes were possibly caused by the tight junctions that connect heart and muscles cells, and challenge extravasation of large particles into these tissues. Additionally, the blood-brain barrier excludes the vast majority of particles above 400 kDa, which greatly limits the ability of phage to enter the brain [209]. Taken together, the biodistribution and optical imaging studies show that the peptides, J18 and J24, influence the binding characteristics of the phage particles, and

enable specific targeting and imaging of SKOV-3 tumors. Due to the rapid pharmacokinetics of pJ18, which are a great advantage in regard to subsequent radionuclide peptide studies owing to decreased toxicity [183], peptide J18 was chosen for further studies.

Peptide J18 was synthesized with an N-terminal DOTA chelator and GSG spacer and labeled with ^{111}In. The radiolabeled peptide demonstrated excellent stability under physiological conditions with *in vitro* half-lives of 14 h and 5.2 h in HEPES buffer and mouse serum, respectively. These results indicated good potential *in vivo* stability as well as low susceptibility to serum peptidases and proteolysis, which is often of great concern for natural amino acid peptides [210]. A comparison of the binding patterns of the radiolabeled peptide for ovarian carcinoma and normal ovarian cells were investigated at varying time points in an *in vitro* assay. Although ^{111}In-DOTA-GSG-J18 showed binding to HS-832 cells, the peptide exhibited significantly higher binding to SKOV-3 cells after 2 h. These results may indicate that the radiolabeled peptide binds to an antigen that is overexpressed by SKOV-3 cells but is present at low levels on normal ovarian cells. Several cell receptors are known to exhibit such expression patterns, including the folate receptor α, which is found on most normal cells, but is greatly overexpressed by ovarian tumors, among others [211]. Other examples include the epithelial cellular adhesion molecule (EpCAM) and the ErbB2/HER2/neu receptor, which are stably expressed in most normal tissues, but is found at greatly elevated levels in varying types ovarian carcinomas [180, 212]. Based on this data, an IC_{50} value of 10.5 ± 1.1 μM (mean ± SE) for the radiolabeled peptide was calculated, which is in correlation with what has previously been reported for phage display peptides selected against live cells [201].

To validate the specific sequence-mediated interaction and to identify the amino acid residues responsible for binding to SKOV-3 cells, an alanine scanning experiment of peptide J18 was performed. Alanine substitutions of three amino acids, tryptophan (J18-4), tyrosine (J18-8) and arginine (J18-13), resulted in significantly higher EC_{50} values compared to peptide J18, suggesting that these residues are involved in, and important for, the interaction with SKOV-3 cells. Additionally, a strong tendency towards decreased binding affinity was observed for the alanine substitution of phenylalanine (J18-7), indicating that this residue may be important for the binding interaction. On the other hand, substitutions of serine (J18-5) and aspartic acid (J18-6) resulted in an approximately 10-fold decrease in EC_{50} values that were significantly different compared to J18. Many receptor-ligand interactions, including those of drugs and their corresponding cellular targets, involve aromatic amino acids present in both the ligand and the hydrophobic binding pocket of the protein [213]. Therefore, the finding that the tryptophan, tyrosine and phenylalanine residues are important for the interaction between peptide J18 and SKOV-3 cells is not surprising and correlate well with the literature. Although counterintuitive, arginine has also been shown to greatly contribute to the binding of ligands to aromatic amino acids and to greatly improve the stability of the interaction. In fact, peptides containing this amino acid have been found to associate with aromatic residues in proteins by cation-π bonding between the guanidinium group of arginine and the electron cloud of the ring [213-216]. In contrast, the presence of the serine (J18-5) and aspartic acid (J18-6) residues negate the binding affinity of the peptide, perhaps by disturbing hydrophobic interactions between the aromatic amino acids and the antigen. By substituting the polar amino acids serine and aspartic acid with alanine the

peptide becomes more hydrophobic, which may stabilize both intramolecular and potential peptide-protein interactions [217, 218].

In vivo characterization of peptide J18 included pharmacokinetic studies and SPECT imaging. A competition biodistribution study demonstrated specific binding of ^{111}In-DOTA-GSG-J18 to the tumor while radioactive uptake in other organs was nonspecific. The biodistribution study further showed good tumor uptake and retention as well as high target-to-background ratios. Tumor-to-blood and tumor-to-muscle ratios both peaked after 2 h, indicating rapid blood clearance and low background uptake, while maintaining kinetically favorable tumor retention. Additionally, low levels of radioactivity in the blood as well as rapid clearance indicate good stability of the radionuclide-chelator complex as free ^{111}In would bind to metal conjugating serum proteins and result in prolonged circulation. The kidneys exhibited the highest radioactive uptake of all organs, suggesting renal clearance of the peptide. Both the small molecular size and the positive charge of the peptide at physiological pH indicates that the vast majority of the peptide should be cleared through the kidneys [219], which is indeed evident from the biodistribution results, and correlates with the fact that renal clearance is the preferred route of excretion for most radiolabeled peptides [183]. Renal retention of radiolabeled compounds may cause prolonged exposure to high radiation doses and consequently nephrotoxicity [220]. Nevertheless, the biodistribution results showed that kidney uptake of ^{111}In-DOTA-GSG-J18 rapidly decreased after only 1 h, which suggests favorable retention kinetics and indicates limited kidney exposure. Studies have shown that coinjection of positively charged amino acids decreases nonspecific renal retention of radiolabeled peptides, and such a procedure may be pursued in the future in an effort

to lower unnecessary kidney uptake [45, 221]. Nonspecific retention of radioactivity was low in most other organs, although the liver and spleen showed some uptake, indicating a minor excretion route through the hepatobiliary system, which is possibly due to relatively hydrophobic parts of the peptide sequence and the fact that increased lipophilicity tends to direct a compound towards hepatic excretion rather than through the renal route [222-224]. Finally, the lungs showed some retention of radioactivity, which may be due to high perfusion and increased exposure to the blood circulation, however, the binding was non-peptide specific.

In vivo SPECT/CT imaging using ^{111}In-DOTA-GSG-J18 in SKOV-3 xenografted mice revealed high tumor-to-background ratios, and successfully enabled localization of the tumor. In correlation with the pharmacokinetic studies, the majority of the radioactivity was found in the kidneys and renal excretion of the peptide was clearly evident from the high levels visualized in the bladder. Very low radioactivity was detected in any other organs including the liver, lungs and spleen emphasizing the potential use of this peptide for detection of ovarian cancer. Furthermore, tumor uptake of the radioactive peptide was successfully blocked by injection of the non-radioactive counterpart showing specificity of the peptide for the SKOV-3 tumor.

To date, very few *in vivo* ovarian cancer targeting imaging agents have been reported. The majority of these targeting moieties generally involve peptides [121, 123, 164, 165], ligand coated nanoparticles [125, 225], as well as antibodies and antibody fragments [117, 226-230], while the imaging modalities mostly include near-infrared fluorescent probes for optical imaging [123, 125, 231-233] and radionuclide labels for radioscintigraphy, PET or SPECT [117, 121, 164, 165, 226-229, 234]. Recently, ovarian

metastases were imaged and localized after injection of folic acid coated fluorescent high-density lipoprotein nanoparticles targeting folate receptor α in tumor-bearing mice [125]. While, these nanoparticles were able to image tumors in a mouse model, the biodistribution of these large complexes showed high uptake in the liver and spleen when administered intravenously. To the contrary, intraperitoneal injections of the imaging agent significantly reduced non-tumor uptake. However, such a strategy requires initial knowledge of the approximate tumor location. Aina *et al*. reported three cyclic peptides with high affinity for alpha-3 integrin on ovarian cancer cells that successfully imaged xenografted ovarian tumors in mice using near-infrared fluorophores. The excretion route of these peptides was mainly through the kidneys and gastrointestinal tract and showed no accumulation in the liver or spleen [123]. Even though fluorescent imaging agents of ovarian cancer in mice models have been reported, *in vivo* optical imaging is currently applicable only to surface tissues due to limited depth penetration of near-infrared light [124]. More promising are radiolabeled imaging probes that offer deep tissue penetration and, when combined with PET or SPECT, deliver high resolution images. PET and SPECT imaging were both applied to evaluate the imaging capabilities of ErbB2/HER2/neu binding affibody. The affibody was labeled with ^{18}F, ^{68}Ga, and ^{111}In and injected into mice carrying SKOV-3 xenografted tumors. Both PET and SPECT images revealed excellent tumor uptake of the radiolabeled affibody, but also showed very high kidney retention (>100 %ID/g) and slow whole body clearance [117]. Such prolonged radioactive organ exposure carries a risk of toxicity [220] and is unwanted in humans. Weissleder and co-workers developed a tetrameric peptide targeting VCAM-1, a protein associated with peritoneal metastasis of ovarian cancer, using phage display [118-

120] and employed it in SPECT/CT imaging of SKOV-3 metastases in a mouse model. Peritoneal metastases were successfully imaged and localized after intraperitoneal injection of the ^{111}In-labeled peptide. Further, tumor retention was maintained for up to two weeks, while radioactive uptake in other organs was minimal [121]. This study showed that radiolabeled peptide imaging of xenografted ovarian tumors may be achieved while maintaining good pharmacokinetic properties. Although the VCAM-1 targeting peptide exhibited excellent homing and imaging capabilities of peritoneal metastases, its use is limited to advanced stages of ovarian cancer. In the same study by Scalici *et al.*, VCAM-1 was found to be expressed on ~25% and 75 % of tumors from stage II and III patients, respectively, while protein was not detectable on stage I tumors [121]. These studies, although successful, emphasize the ongoing need for novel imaging agents of ovarian cancer that will aid in the detection and diagnosis of both early and late stage disease.

Here, we demonstrated that ^{111}In-DOTA-GSG-J18 images xenografted SKOV-3 tumors in live nude mice using SPECT/CT. In addition, the peptide showed rapid clearance through the kidneys thereby lowering the risk of toxicity caused by prolonged exposure to radioactivity. This peptide may be useful in advancing the diagnosis of ovarian cancer and allow detection of early stages of the malignancy and provide an opportunity to increase survival rates.

Conclusion

The SKOV-3 specific peptide J18 was selected by an *in vivo/in vitro* phage display screening process and evaluated for its binding and pharmacokinetic properties as well as SPECT/CT imaging capabilities. The peptide demonstrated good tumor uptake and retention in biodistribution studies and successfully imaged SKOV-3 tumors in xenografted nude mice. In conclusion, the J18 peptide may be an effective imaging agent of ovarian cancer for diagnostic purposes.

Acknowledgements

We acknowledge the contributions of Lisa Watkinson, Terry Carmack and Marie Dickerson. This work was supported by a VA Merit Review Award BX000964 and the NIH 1R21CA134960.

CHAPTER 3

IN VITRO HIGH-THROUGHPUT PHAGE DISPLAY SELECTION OF OVARIAN CANCER AVID PHAGE CLONES FOR *IN VIVO* NEAR-INFRARED OPTICAL IMAGING

Introduction

Ovarian cancer has been termed the “silent killer” due to quick and asymptomatic development of aggressive disease that is characterized by rapid invasion of surrounding tissues and metastatic seeding in the peritoneal cavity [77, 78]. In 2014, 22,000 women are estimated to be diagnosed with ovarian cancer and 14,000 women will succumb to the disease in the US [167]; establishing ovarian cancer as the most prevalent and lethal class of gynecological malignancies, and as the overall fifth leading cause of cancer deaths in women [3, 4]. Standard treatment of early-stage ovarian cancer involves surgical removal of the primary tumor followed by a chemotherapeutic regimen that leads to good overall five-year survival rates of >90%. Nevertheless, due to symptom free disease development and limited detection methods, the vast majority of ovarian cancer patients are diagnosed at the regional or distant stages, at which point five-year survival rates drops to 44% [3, 4]. Current screening for ovarian cancer includes detection of the serum tumor marker CA-125 and pelvic ultrasonography [7, 9, 88]. However, these methods often lead to false positive diagnosis, require surgery to obtain final diagnosis, and are generally limited to detection of advanced stage disease [7, 9, 10, 88, 184]. These limitations and the poor prognosis of late-stage ovarian cancer emphasize the need for discovery of disease associated biomarkers and the development of novel detection methods.

Phage display technology was pioneered by Dr. George P. Smith in 1985 [53], and is a powerful method to select and identify peptide based cancer targeting agents. The technology is based on genetic incorporation of random peptide sequences onto the

coat proteins of filamentous phage, creating large peptide libraries capable of containing up to 10^9 individual peptide-displaying phage clones [53, 54]. The large number of individually displayed ligands allows high-throughput screening of these against various protein and carbohydrate targets [26, 29, 31, 36, 38, 39, 50, 169, 235]. To date, phage display has been utilized to develop high affinity peptide-based targeting molecules against a number of malignancies such as breast, melanoma, prostate, lung, lymphoma and liver cancer [32, 34, 36, 39, 236-238]. Most commonly, such phage-display derived peptides have been synthesized and utilized outside of the phage moiety as cancer targeting agents for imaging and radiotherapy studies. Even though such peptides can be developed to exhibit good target binding affinities and excellent biodistribution, the process of selecting peptide ligands and validating binding properties is often time-consuming, and is especially challenging and costly when translating such targeting agents into use *in vivo*. To the contrary, cancer targeting phage can be developed relatively quickly and at low cost by eliminating the challenges that are involved in translating targeting agents from *in vitro* to *in vivo* use. The high stability and good biodistribution, as well as the ability of genetically modified phage to undergo cell internalization [239], make phage excellent nanoparticles for molecularly targeted imaging and drug delivery. Phage have successfully been employed as cancer targeting agents for tumor imaging as well as drug and gene delivery. For example, molecularly targeted phage have been used to image Lewis lung carcinoma and prostate cancer in mice models using near-infrared fluorophores [31, 193], cancer associated biomarkers (secreted protein, acidic and rich in cysteine; SPARC and phosphatidylserine) using iron oxide nanoparticle-labeled phage for MRI [43, 240], and tumor vasculature associated

integrin $\alpha_v\beta_3$ using ^{64}Cu-labeled phage for positron emission tomography (PET) [241]. Further, phage have been employed to deliver targeted antibiotics to sites of infection [242], doxorubicin to SPARC expressing cancer cells [243], and to deliver and subsequently express genes in target cells [191, 244, 245].

Here, our laboratory reports a rapid and cost effective method of developing novel ovarian carcinoma targeting phage using phage display technology. Specifically, phage clones were selected from a fUSE5 15-mer peptide library by screening against human ovarian carcinoma (SKOV-3) cells. Identified phage were further subjected to micropanning experiments and *in vitro* cell binding studies to discriminate between clones with high specific affinity and inherent nonspecific binding to SKOV-3 cells. Based on these results, two phage clones (pM6 and pM9) were labeled with the near-infrared fluorophore (AF680) and analyzed for their ovarian tumor targeting and optical imaging abilities *in vivo*. Both fluorescently labeled phage successfully bound and imaged xenografted SKOV-3 tumors in female nude mice.

Materials and Methods

Materials

Cell culture reagents were purchased from Invitrogen (Carlsbad, CA). Unless otherwise stated, chemicals were purchased from Sigma Chemical Co. (St. Louis, MO).

Cell Lines

Human ovarian adenocarcinoma (SKOV-3), human ovarian (HS-832) and human embryonic kidney (HEK293) cells were obtained from American Type Tissue Culture. SKOV-3 and HEK293 cells were grown in general maintenance medium containing RPMI 1640 (custom) with 10% FBS, 2 mM L-glutamine, 1.7 μM insulin, 48 mg/ml gentamicin at 37°C in 5% CO_2. Human ovarian cells (HS-832) were maintained in DMEM high glucose with 20% FBS and 48 mg/ml gentamicin at 37°C in 5% CO_2.

Animals

All animal studies were conducted according to NIH Guidelines for the Care and Use of Laboratory Animals and the Policy and Procedures for Animal Research of the Harry S. Truman Veterans Memorial Hospital. Solid tumors were established in female 4–6-week-old nude nu/nu mice (Harlan, Indianapolis, IN) over a period of 8 weeks, resulting in approximately 1 cm-sized tumors. SKOV-3 cells ($1x10^7$) were inoculated subcutaneously under gas anesthesia (3.5% isoflurane, Baxter Healthcare Corp.

Deerfield, IL) in the shoulder of each mouse. Following *in vivo* biodistribution, the mice were sacrificed and tumors and organs were excised and analyzed as described later.

Selection of Tumor-Targeting Phage

A coat protein III displaying 15-mer peptide library (fUSE5) was a kind gift from Dr. George P. Smith [53]. Phage particle concentration in virions per mL (V/mL) was determined spectrophotometrically by measuring absorbance at 260 nm and 280 nm. The number of transducing units (TU) was determined by tittering in *E. coli* K91 Blue Kan. In order to exclude phage that bind to non-cancerous cells, the phage display library was initially negatively selected (pre-cleared) against normal human ovarian HS-832 cells. Approximately $4x10^{13}$ V/mL were incubated with $1x10^{6}$ HS-832 cells and allowed to bind for 30 min at 4°C. Unbound phage were collected from the supernatant after centrifugation (1,000 x g, 1 min) and amplified in *E. coli* K91 Blue Kan as previously described [178]. For selection of ovarian carcinoma binding phage, the purified preparation (10^{13} V/mL) was incubated with approximately $2x10^{6}$ SKOV-3 cells for 30 min at 4°C. Cells were washed extensively with TBS and bound phage were eluted with 2.5% CHAPS. Collected phage were amplified as previously described and used in subsequent selection rounds. In whole, four rounds of selection against SKOV-3 cells were performed. All phage were stored at 4°C for further use. Between selection rounds, random phage clones were chosen for DNA sequencing of the foreign phage display insert for detection of potential contamination and continuous evaluation of the selection process.

Micropanning Assay

Selected phage were subjected to a micropanning assay to identify clones with specific binding to SKOV-3 compared to HS-832 cells. Individual phage clones (10^9 virions) were incubated with $1x10^5$ cells in DMEM for 1 h at 37°C. Cells were centrifuged (1,000 x g, 1 min) and unbound phage were removed by aspiration. Next, cells were washed three times with TBS and bound phage were eluted with 2.5% CHAPS. Collected phage were used to infect *E. coli* K91 Blue Kan, and the ratio of phage titer in SKOV-3 cells to HS-832 cells was calculated.

Fluorescent Microscopy

Binding of phage to SKOV-3, HS-832 and HEK293 cells was evaluated using fluorescent microscopy. Cells were grown on microscope chamber slides (Lab-Tek, Rochester, NY) and incubated with WT, pM6 or pM9 phage (10^{10} V/mL in TBS, 1% BSA) for 1 h at 37°C. The cells were then washed three times with TBS and fixed with 10% formalin. Next, fixed cells were washed (TBS, 1% BSA) extensively and blocked with 6% BSA in TBS, and then incubated with a rabbit polyclonal anti-phage antibody (courtesy of Dr. George P. Smith) for 1 h at room temperature. A fluorescein isothiocyanate (FITC)-labeled α-rabbit antibody was then added, incubated for 1 h at room temperature in the dark and washed three times (TBS, 0.05% Tween-20). The binding of phage was detected with an epifluorescent Nikon T1-SM inverted microscope (Nikon, Melville, NY).

Phage and Peptide Binding to SKOV-3 Cells by Modified Enzyme-Linked Immunosorbent Assay (ELISA)

Human ovarian carcinoma cells (SKOV-3) were grown to 80% confluency in a 96-well tissue culture plate (TPP, Trasadingen, Switzerland). The growth medium was aspirated and replaced with different concentrations of WT, pM6 or pM9 phage (10^9-10^{11} V/mL in TBS, 1% BSA). Cells were incubated for 1 h at 37°C, washed three times with TBS and fixed with 10% formalin. The cells were washed (TBS, 1% BSA) extensively and then blocked with 6% BSA in TBS. Next, a rabbit polyclonal anti-phage antibody (courtesy of Dr. George P. Smith) was added and the plate was incubated for 1 h at room temperature. After extensive washing (TBS, 1% BSA), a secondary HRP-conjugated anti-rabbit antibody (Santa Cruz Biotechnology, Santa Cruz, CA) was added and the plate was incubated for 1 h at room temperature in the dark. The plate was washed (TBS, 0.05% Tween-20) three times and HRP substrate ABTS was added and allowed to develop for 20 min at room temperature. The binding of phage was detected by measuring the absorbance at 405 nm using an endpoint assay on a μ Quant Universal Microplate Spectrophotometer (Bio-Tek Instruments, Winooski, VT).

To compare the binding of phage and their correlating free peptides, biotinylated peptides M6 and M9 were synthesized with a GSG-spacer between the biotin group and the NH_2-terminus using solid-phase Fmoc chemistry in a 396 multiple peptide synthesizer (Advanced Chem Tech, Louisville, KY). To determine cell binding and the EC_{50} values, varying concentrations (100 nM to 300 μM) of peptides M6, M9 or a non-relevant N35 peptide (negative control) were incubated with SKOV-3 cells grown to 80% confluency on 96-well plates for 1 h at 37°C. Next, cells were washed (PBS, 1% BSA)

extensively and fixed with 10% formalin. After repeated washing, cells were blocked with 10% FBS, 0.3 M glycine, 0.05% Tween-20 in PBS. Bound biotinylated peptide was then probed by incubation with HRP-conjugated streptavidin for 1 h at room temperature. The plate was washed (PBS, 0.05% Tween-20) three times and ABTS was added and developed for 20 min at room temperature. The peptide binding was detected by measuring the absorbance at 405 nm as previously described.

Fluorescent Labeling of Phage

Alexa Fluor-680 (AF680) carboxylic acid, succinimidyl ester 5-isomer (Invitrogen, Carlsbad, CA) was dissolved in dimethyl sulfoxide (DMSO; 2% final concentration) and added to phage (0.29 mM final concentration of coat protein VIII) in 0.5M Na_3citrate, 0.1 M $NaHCO_3$ pH 8.5. The solution was incubated for 4 h at room temperature in the dark, after which the labeling reaction was stopped by addition of 270 mM ethanolamine, pH 9 over night at 4°C. To remove excess hydrolyzed AF680, labeled phage were dialyzed against TBS, pH 7.5, over two days changing the buffer four times (Slide-A-Lyzer cassette, 10 kDa molecular weight cutoff, Thermo Scientific, Rockford, IL).

Biodistribution of AF680-Labeled Phage

Nude (nu/nu) mice carrying xenografted SKOV-3 tumors (~1 cm) were intravenously injected with AF680-labeled WT, pM6 or pM9 phage (10^{12} virions). The animals were sacrificed after 4 h and perfused with PBS. For comparison of tumor

uptake, tumors and organs were excised and the fluorescent intensity was measured using a Xenogen IVIS 200 System and analyzed by ImageJ software [182].

In Vivo Near-Infrared Optical Imaging of SKOV-3 Tumors

Wild type, pM6 or pM9 phage labeled with AF680 (10^{12} virions) were injected intravenously into the tail vein of female SKOV-3 tumor-bearing nude (nu/nu) mice. Fluorescence reflectance images of the mice were obtained while the animals were under gas anesthesia (3.5% isoflurane, Baxter Healthcare Corp. Deerfield, IL) before injection (0 h) as well as 2 h and 4 h post-injection. The mice were sacrificed after the last imaging time point (4 h) and the tumors and organs were excised. The imaging was performed using a using a Xenogen IVIS 200 System system and analyzed by ImageJ software.

Statistical Analysis

Statistical analysis was performed to determine significance using an unpaired Student's t-test and Prism Graphpad Software. A P-value of 0.05 or less was considered significant.

Results

Phage Display Selections

A 15-mer phage display library (fUSE5) was pre-cleared in a selection round against human ovarian cells (HS-832), and the resulting phage were amplified in *E. coli* K91 Blue Kan. The selected phage were used in four subsequent screening rounds against human ovarian carcinoma cells (SKOV-3). After the last round of selection, the DNA of 96 random phage clones were sequenced to identify the foreign peptide inserts and to determine if these phage had been previously reported (PepBank, PSI-BLAST) [246, 247]. Based on these results, nine unique phage clones (pM1 to pM9) were identified and analyzed for their binding specificity to SKOV-3 and HS-832 cells in a micropanning assay. Two phage clones (pM6 and pM9) showed elevated SKOV-3 to HS-832 and peptide-displaying phage to WT-phage binding ratios and were chosen for evaluation in further studies (Table 3.1).

Fluorescent Microscopy

Fluorescent microscopy was used to further evaluate the binding characteristics of selected phage and to compare to the binding of WT phage (Figure 3.1). Both phage clones pM6 and pM9 showed increased affinity for human ovarian carcinoma SKOV-3 cells while exhibiting very limited binding to human ovarian HS-832 cells, thereby demonstrating specificity for SKOV-3 cells. To the contrary, WT phage exhibited limited binding to both cell lines, suggesting that binding is facilitated by the displayed peptides

Table 3.1. Micropanning assay to determine specificity of selected phage clones.

Clone No.	*Sequence*	*SKOV-3 to HS-832 ratio*	*Peptide-phage to WT ratio*
pM1	YHGGLSLGWISDWHA	1.6	5.4
pM2	YKSLGTFVMDHFWDS	1.0	2.4
pM3	GEVFFSFVPDWKVQS	1.5	5.1
pM4	GWFFPPLATDAWRLT	1.6	210.2
pM5	LWSPIFSMTAQRGSR	1.3	6.1
pM6	MQSVSGWFPWESVAY	11.1	19.0
pM7	THVELGRSNAVFWAL	0.5	48.3
pM8	VRMAPILIHDAARDR	2.3	20.6
pM9	CAFCEFLPRAYGVSW	3.5	31.9

Phage collected from the fourth round of selection were evaluated for specificity to SKOV-3 and HS-832 cells. The phage clones were incubated with either SKOV-3 or HS-832 cells and eluted using 2.5% CHAPS. Binding of phage was determined by titer and the SKOV-3 to HS-832 ratio and peptide-displaying phage to WT ratio were calculated.

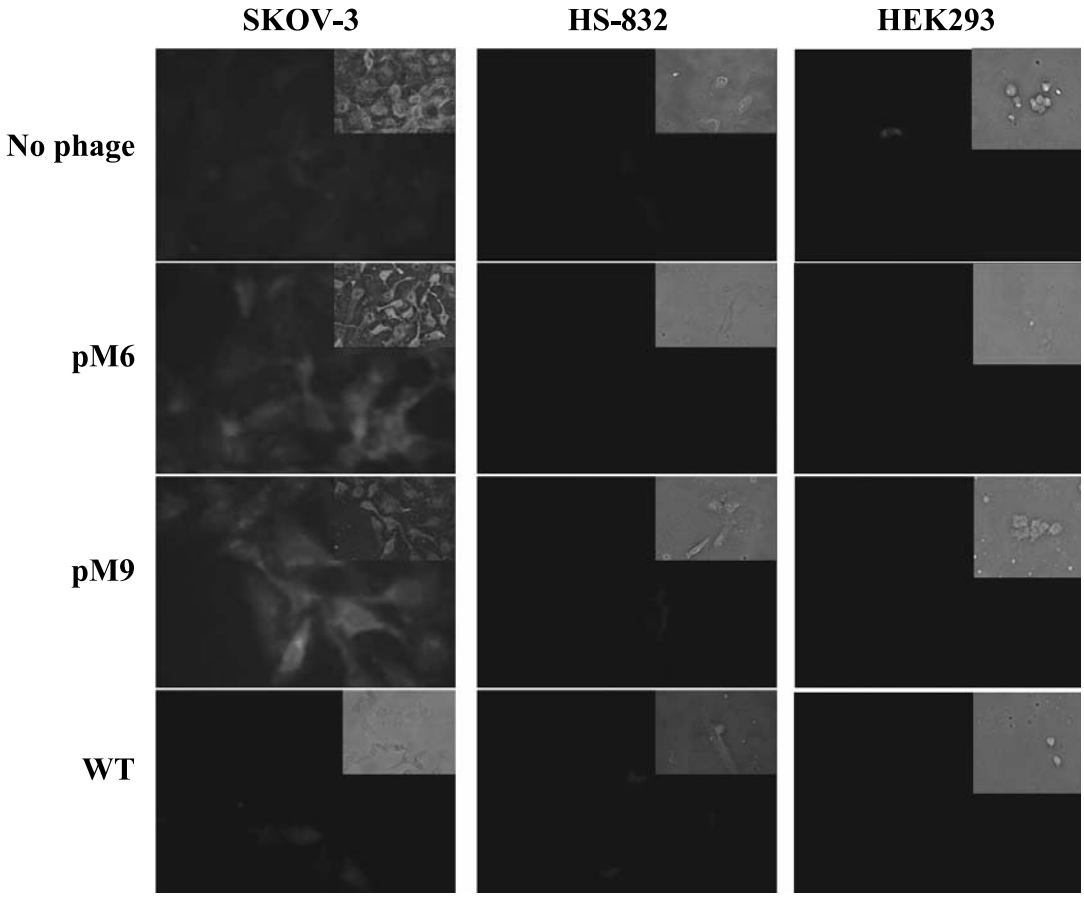

Figure 3.1. Fluorescent microscopy of phage binding to human ovarian carcinoma SKOV-3, ovarian HS-832 and embryonic kidney HEK293 cells. Cells were grown on microscope chamber slides to 80% confluency and incubated with 10^{10} V/mL of pM6, pM9 or WT phage for 1 h at 37°C. Next, the slides were washed with (TBS, 1% BSA) and fixed with 10% formalin. The binding of phage was detected by a rabbit polyclonal anti-phage antibody and a secondary FITC-labeled anti-rabbit antibody. Fluorescence was detected by an epifluorescent Nikon T1-SM inverted microscope (Nikon, Melville, NY).

A

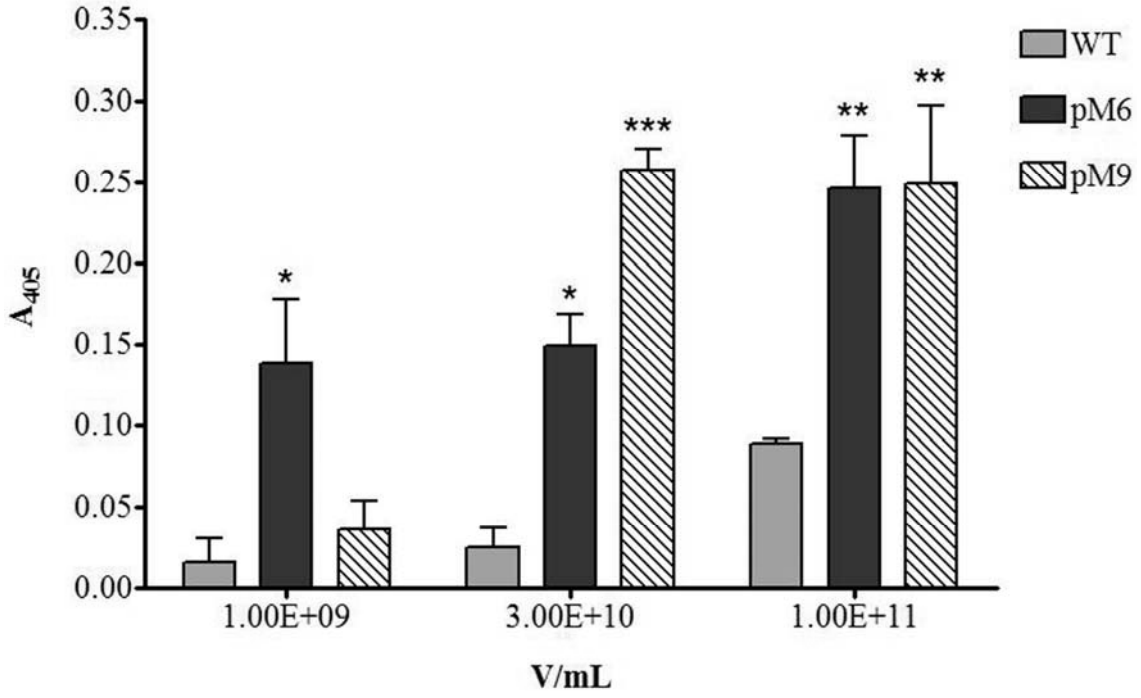
0.35
0.30
0.25
0.20
0.15
0.10
0.05
0.00
A405
WT
pM6
pM9
*
*
***
**
**
1.00E+09
3.00E+10
1.00E+11
V/mL

B

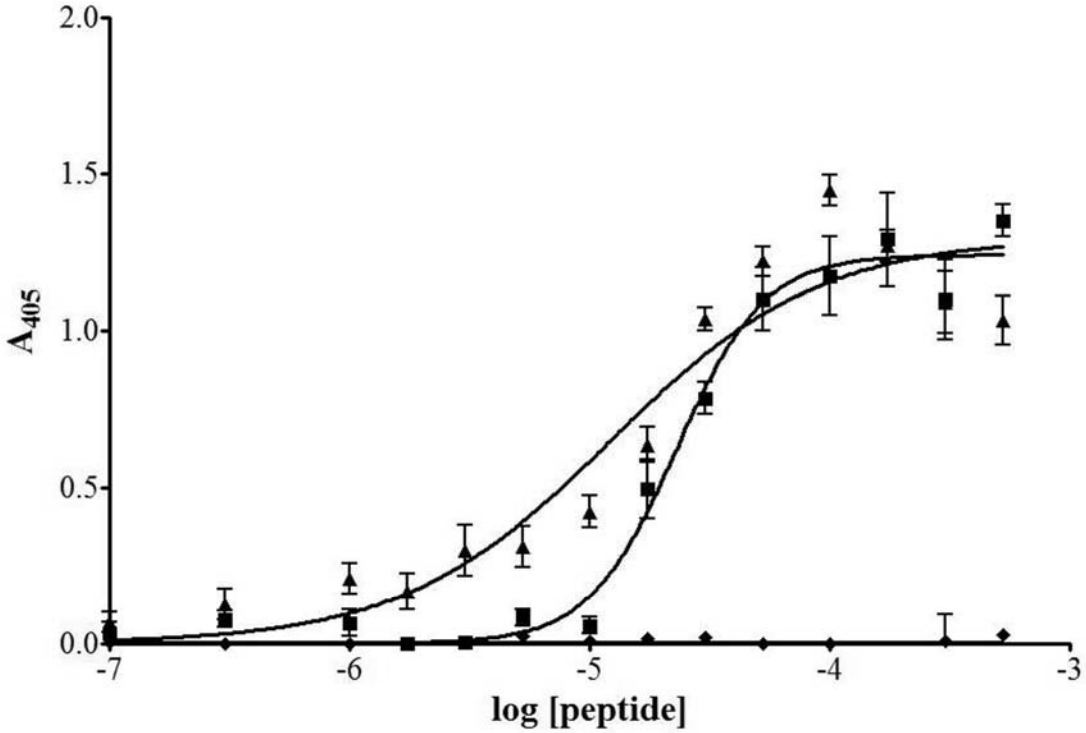
2.0
1.5
1.0
0.5
0.0
A405
-7
-6
-5
-4
-3
log [peptide]

Figure 3.2. Binding properties of selected phage to human ovarian carcinoma SKOV-3 cells. **A)** Cells were grown to 80% confluency in 96-well plates and incubated with different concentrations (10^9, $3x10^{10}$ and 10^{11} V/mL) of WT, pM6 or pM9 phage for 1 h at 37°C. Next, phage and cells were washed with TBS and fixed with 10% formalin. Bound phage were detected by a rabbit polyclonal anti-phage antibody followed by a secondary HRP-conjugated anti-rabbit antibody. Horseradish peroxidase substrate, ABTS, was added and the absorbance at 405 nm was measured after 20 min. **B)** Cells were incubated with varying concentrations (100 nM to 300 μM) of biotinylated peptide M6 (■), M9 (▲) or negative control N35 (♦) for 1 h at 37°C. Plates were washed with PBS and fixed with 10% formalin. Biotinylated peptides were probed with HRP-conjugated streptavidin, and binding was detected by measurement of absorbance at 405 nM after addition of ABTS. EC_{50} values for M6 and M9 were determined to be 22.9 ± 2.0 μM and 12.2 ± 2.1 μM (mean ± STD). Measurements were performed on a μ Quant Universal Microplate Spectrophotometer. * $p < 0.05$, ** $p < 0.01$, *** $p < 0.001$.

and not by intrinsic phage proteins. Additionally, the specificity of the selected phage for a non-relevant normal human embryonic kidney HEK293 cells was investigated. These results showed that both phage clones pM6 and pM9 exhibited very little affinity for this cell line, indicating specificity for ovarian carcinoma cells. Taken together, these data demonstrate that pM6 and pM9 phage exhibit specific binding to SKOV-3 cells, and that this binding is facilitated by the displayed peptides.

Modified Enzyme-Linked Immunosorbent Assay (ELISA)

In order to further explore the binding of phage clones pM6 and pM9 to ovarian cancer cells, a modified enzyme-linked immunosorbent assay (ELISA) was developed. The binding properties of the selected phage and WT phage were compared to ensure that the binding was facilitated by the displayed foreign peptide, rather than by natural phage coat proteins. Results showed that, at concentrations of 10^9, $3x10^{10}$ and 10^{11} V/mL, phage clone pM6 exhibited significantly higher binding to SKOV-3 cells compared to WT phage, whereas pM9 showed significantly higher binding at $3x10^{10}$ and 10^{11} V/mL (Figure 3.2a). These results confirm the microscopy data and additionally demonstrate that the binding of pM6 and pM9 to SKOV-3 cells is mediated by the displayed peptides, and is not caused by inherent non-specific binding of the phage particle. To further validate this observation, the binding characteristics of phage pM6 and pM9 were compared to that of the correlating free peptides M6 and M9 (Figure 3.2b). Peptide binding to SKOV-3 cells was found to correlate well with that of phage, and showed that both M6 and M9 exhibited increased binding to this cell line compared to a non-relevant

control peptide (N35). EC_{50} values for M6 and M9 were determined to be 22.9 ± 2.0 μM and 12.2 ± 2.1 μM (mean ± STD).

Biodistribution Studies

The pharmacokinetic properties and *in vivo* optical imaging capabilities were investigated by labeling phage clones pM6, pM9 and WT with the near-infrared fluorophore AF680. Each phage particle was labeled with approximately 270 molecules of AF680. For the biodistribution study, AF680-labeled phage was injected into the tail-vein of SKOV-3 xenografted nude female mice and allowed to circulate for 4 h, after which the animals were sacrificed and the fluorescent uptake in normal organs and tissues, and in the tumor was measured (Figure 3.3). The reticuloendothelial system was found to be the major route of excretion for all three phage, which was evident from elevated uptake in the liver, lungs and spleen. However, the kidneys also showed increased fluorescent uptake, indicating that renal clearance may provide a minor excretion route. Phage clone pM6 showed increased uptake in the kidneys, liver and spleen, and exhibited significantly higher fluorescent levels in the tumor compared to pM9 and WT. In contrast, tumor uptake of pM9 after 4 h showed no difference compared to WT phage, and additionally showed the lowest fluorescent levels in the lungs and pancreas of all three phage. Phage accumulation in other organs including the heart, muscle and brain was very low and was similar for all phage clones. In all, these data demonstrate that phage clone pM6 exhibit good tumor uptake 4 h post-injection and may, therefore, be used as an *in vivo* imaging agent. To the contrary, pM9 failed to show elevated tumor binding after 4 h, suggesting that excretion of this phage clone occur more

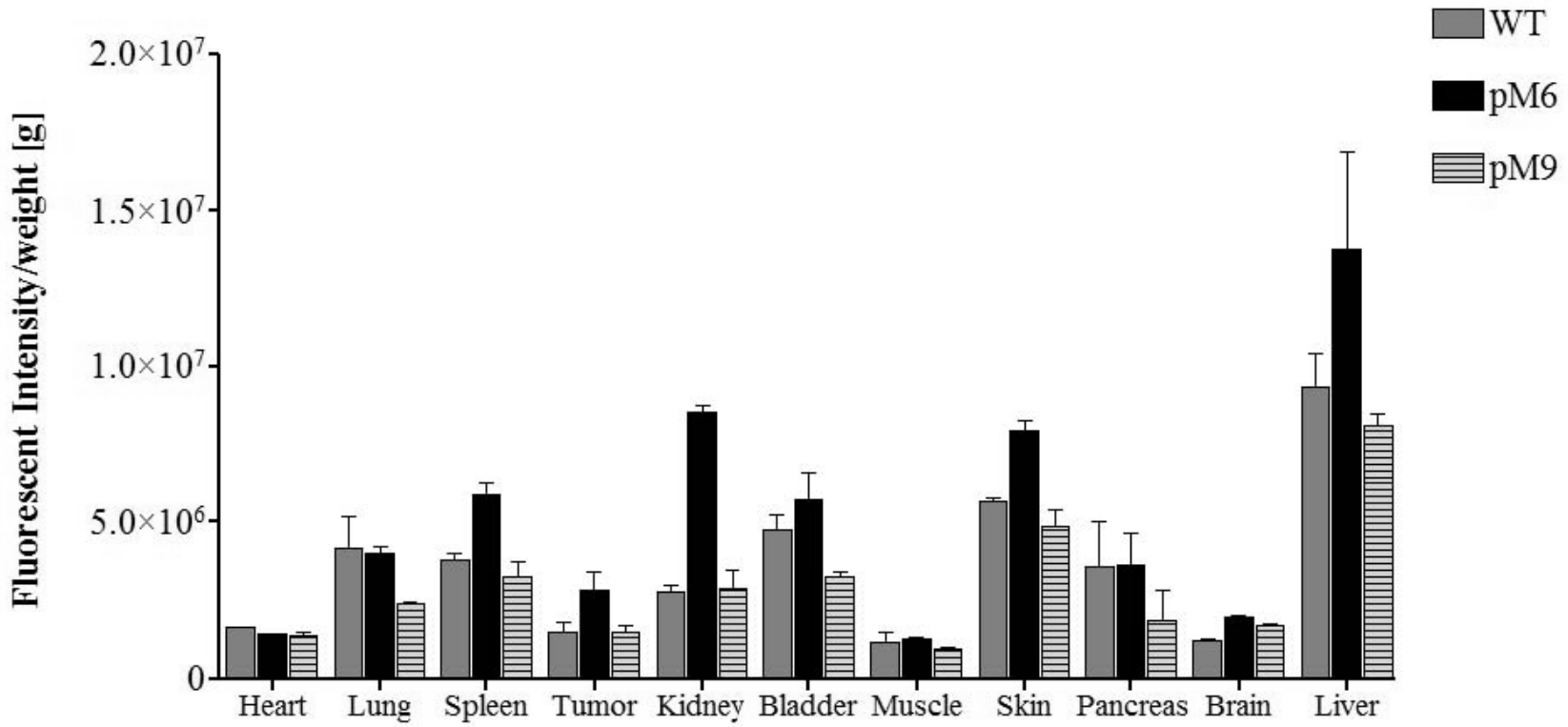
WT
pM6
pM9
Fluorescent Intensity/weight [g]
2.0×10^7
1.5×10^7
1.0×10^7
5.0×10^6
0
Heart
Lung
Spleen
Tumor
Kidney
Bladder
Muscle
Skin
Pancreas
Brain
Liver

Figure 3.3. Biodistribution of AF680-labeled pM6, pM9 and WT phage in SKOV-3 xenografted nude female mice. Mice were injected with 10^{12} virions of AF880-labeled phage and were allowed to circulate for 4 h, after which the animals were sacrificed. Normal organs, tissues, and the tumor were excised and weighed, and the fluorescent intensity was measured using a Xenogen IVIS 200 System. Fluorescent uptake was normalized to the weight of each organ, and reported as fluorescent intensity per gram.

rapidly and that uptake may be more optimal at earlier time points. For these reasons, subsequent *in vivo* optical imaging was performed at 2 h and 4 h post-injection.

In Vivo Near-Infrared Optical Imaging

To explore the *in vivo* imaging capabilities of phage clones pM6 and pM9, near-infrared optical imaging of female nude mice carrying xenografted SKOV-3 tumors was performed (Figure 3.4a). Prior to injection of AF680-labeled phage, the animals were imaged to determine levels of autofluorescence (0 h). In short, AF680-labeled phage (pM6, pM9 or WT) were injected into the mice and allowed to circulate, after which fluorescence reflectance images of the live animals were obtained after 2 h and 4 h. The acquired images showed that the ovarian carcinoma tumors were easily visualized with adequate tumor-to-background contrast at both 2 h and 4 h post-injection. Further, results showed that the tumor signal intensity of phage clone pM6 peaked at 2 h and was significantly higher compared to that of WT phage at both time points (Figure 3.4b). In correlation, phage clone pM9 exhibited peak tumor signal intensity after 2 h, which was significantly higher compared to WT phage. Concurrently with the biodistribution data, tumor uptake of pM9 was lower compared to pM6 after 4h and was no longer significantly different from the WT. Taken together, these results indicate that the peptides displayed on phage clones pM6 and pM9 are capable of influencing the binding properties of the phage particles to specifically target and image ovarian tumors.

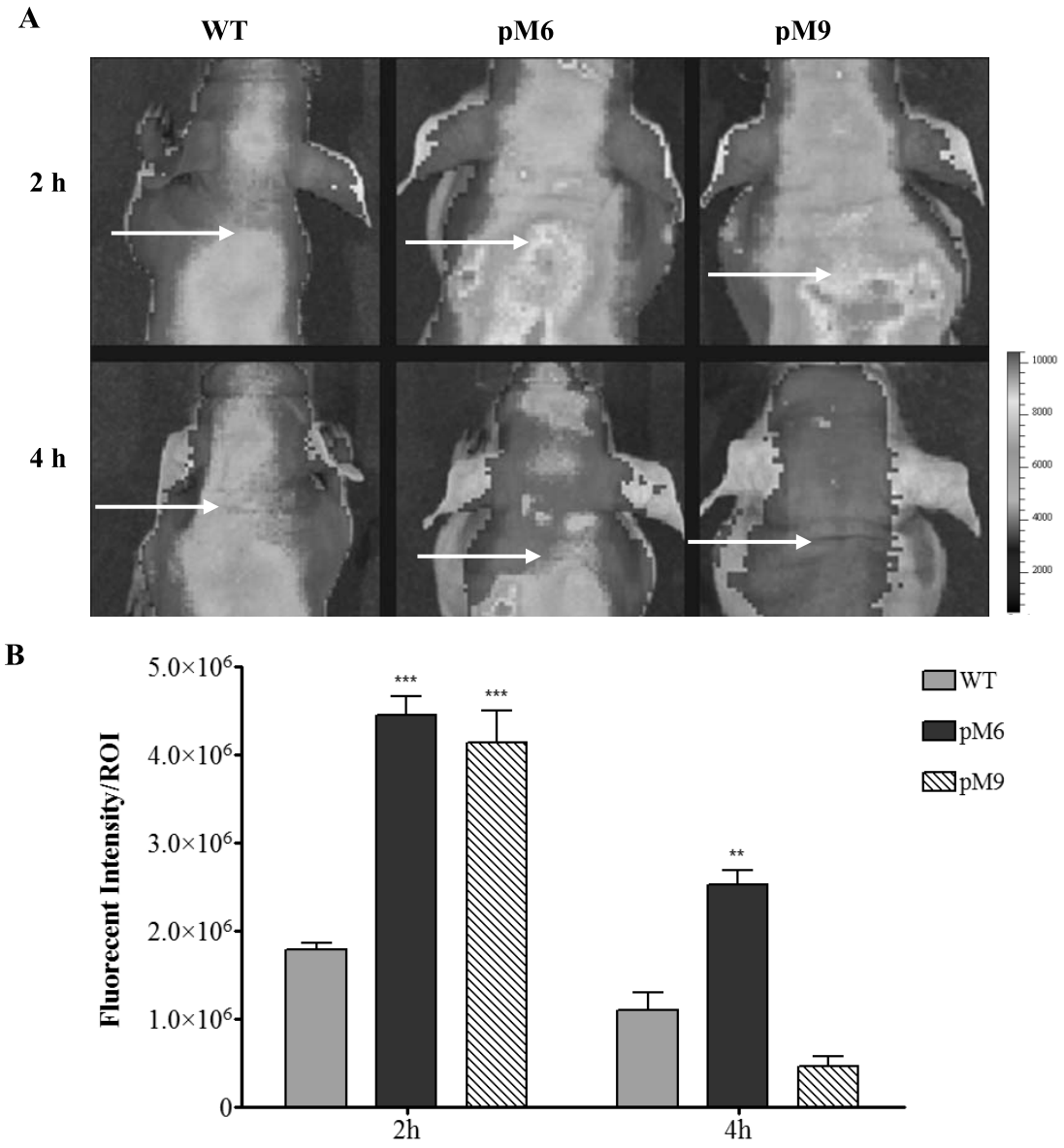

Figure 3.4. *In vivo* optical imaging of SKOV-3 xenografted tumors in female nude mice using AF680-labeled pM6, pM9 and WT phage. The mice were injected with 10^{12} virions of AF680-labeled phage and imaged under anesthesia after 2 h and 4 h. **A)** Fluorescence reflectance images of SKOV-3 tumor bearing mice. Tumor location is indicated by the white arrow. **B)** Quantification of fluorescent signal intensity of ROI. Fluorescence reflectance images were obtained using a Xenogen IVIS 200 System, and the fluorescent signal intensity of ROI was quantified using ImageJ software. ** $p < 0.01$, *** $p < 0.001$.

Discussion

Peptide phage display technology has mostly been employed as a method of identifying and developing free peptides that target tumors and may be used as imaging agents. However, phage particles as tumor targeting agents offer several advantages compared to free peptides including increased stability and prolonged biodistribution [239]. Further, due to the large size of phage, labeling with fluorophores or radiotracers has minimal influence on the overall binding and pharmacokinetics, whereas the function of peptides may easily be disrupted by additional tags [31, 48]. The large size of phage also allows attachment of numerous labels, which results in signal amplification and provides increased sensitivity during imaging. Finally, development of phage imaging agents is cost effective and more time efficient in comparison to peptides, in that synthesis, labeling and validation of the latter is often lengthy and challenging. In contrast, filamentous phage do not require synthesis, as they are biological non-pathogenic particles that replicate in *E. coli* [55, 248].

Phage display technology often results in selection of a number of clones that appear to exhibit excellent binding affinities. However, biological amplification in *E. coli* can establish a selective pressure for phage that exhibit advantageous growth properties, such as high infectivity and proliferation rates, and these phage may be incorrectly identified as clones with high target binding affinity [249]. For this reason, the nine phage clones that were identified in this study the last round of phage display selection were subjected to a micropanning assay, in which they were evaluated for their specificity for

human ovarian carcinoma SKOV-3 and human ovarian HS-832 cells. This "weeding out" of potentially unwanted phage, revealed that two clones, with the displayed peptide sequences MQSVSGWFPWESVAY (M6) and CAFCEFLPRAYGVSW (M9), exhibited specificity for ovarian carcinoma SKOV3 cells and showed increased binding compared to WT phage.

Further characterization of the *in vitro* binding properties of these phage clones involved fluorescent microscopy and a modified ELISA. The fluorescent microscopy studies provided evidence of pM6 and pM9 phage binding and specificity for cultured SKOV-3 cells, and further showed that these clones exhibited minimal binding to normal ovarian cells (HS-832) and human embryonic kidney (HEK293) cells. These results indicate that the selected phage clones may target (an) ovarian cancer specific antigen(s), and may therefore be potential ovarian carcinoma imaging candidates. Additionally, the affinity of pM6 and pM9 for SKOV-3 cells was elevated compared to WT phage, suggesting that the interaction was facilitated by the displayed peptides and not by non-specific binding of the phage particle.

To further validate this claim, a modified ELISA was developed, which showed that pM6 and pM9 phage displayed significantly increased binding at concentrations of 10^9 to 10^{11} V/mL and $3x10^{10}$ to 10^{11} V/mL, respectively, compared to WT. Although low, the WT phage also showed binding, which is not unexpected since these particles are known to bind to various materials including plastic [250]. In parallel to these results, varying concentrations (100 nM to 300 μM) of correlating free peptides M6 and M9 showed increased binding to SKOV-3 cells compared to a negative control peptide (N35), confirming that binding is in fact mediated by the peptide ligands and is not

facilitated by inherent phage proteins. Additionally, both peptides were shown to bind to ovarian carcinoma cells in a sigmoidal dose-response manner. Based on this data, EC_{50} values of 22.9 ± 2.0 μM and 12.2 ± 2.1μM (mean ± STD) for M6 and M9, respectively, were calculated, demonstrating that the latter peptide displays higher affinity for SKOV-3 cells compared to M6. These values are in correlation with what has been previously reported for peptides selected by phage display technology [201]. Taken together, these *in vitro* investigations demonstrated that selected phage pM6 and pM9 displayed preferential binding for ovarian carcinoma cells and exhibited minimal affinity for normal ovarian and human embryonic kidney cells. Further, it was shown that binding to SKOV-3 cells was facilitated by the displayed peptides, M6 and M9 and was not a result of non-specific binding of the phage particle.

In vivo characterization of phage clones pM6 and pM9 included pharmacokinetic evaluation (biodistribution) and optical imaging. The near-infrared fluorophore AF680 was used to label pM6, pM9 and WT phage for these studies, which were carried out in human ovarian carcinoma SKOV-3 xenografted nude mice. At 4 h post-injection, the biodistribution study revealed that the reticuloendothelial system was the major route of excretion for pM6, pM9 and WT phage. This observation was evident from increased fluorescent uptake in liver, lungs and spleen, and is in correlation with what has been previously found in our laboratory [31, 52] and by others [206, 208]. Additionally, the kidneys and bladder showed elevated uptake of pM6, indicating that renal clearance may be a minor route of excretion for this phage clone. In fact, Newton *et al*. have previously found that peptide-displaying phage can exhibit increased kidney uptake compared to WT [31], suggesting that the peptide may re-direct part of the excretion system towards

renal clearance. Uptake of pM9 in organs involved in the reticuloendothelial and renal excretion systems was lower overall compared to pM6, suggesting that clearance of pM9 is more rapid in comparison. Uptake of pM9 was similar to that of WT phage in spleen, kidneys and liver, indicating that the excretion patterns of these two phage clones are comparable. However, fluorescent levels in lungs, bladder and pancreas were lower for pM9 than WT, suggesting that the peptide displayed on this phage clone may be responsible for decreased binding in these organs. In accordance, the size and biochemical properties of phage and other nanoparticles have been shown to influence the uptake in different organs and tissues as well as the rate of excretion [205]. Tumor uptake of pM6 was significantly higher in comparison to pM9 and WT phage, which may be indicative of prolonged tumor retention of the former. In contrast, there was no significant difference in tumor uptake between pM9 and WT, again suggesting that the pharmacokinetics and clearance rate of pM9 is more rapid compared to pM6, and that tumor uptake and retention may occur at earlier time points. Finally, muscle, brain and heart showed minimal uptake of all fluorescently labeled phage, which was most likely due to limited ability of large phage particles to enter these organs and tissue. In fact, muscle and heart cells are connected by tight junctions that challenge extravasation of phage into the tissue, whereas the blood-brain barrier excludes the vast majority of particles above 400 kDa [209].

The *in vivo* imaging capabilities of selected phage clones were likewise explored in nude mice carrying xenografted SKOV-3 tumors. Peak tumor signal intensity was observed after 2 h for pM6, pM9 and WT phage, suggesting that this time point is the most optimal for *in vivo* imaging. Although low levels of WT phage were found to locate

to the tumor, the signal intensities of pM6- and pM9-phage were significantly higher, indicating that tumor targeting was mediated by the displayed peptides. Importantly, high tumor-to-background contrast allowed easy visualization and localization of the ovarian carcinoma tumors, which was consistent for pM6 at both 2 h and 4h post-injection. In correlation with the biodistribution data, pM9 showed low tumor signal intensity after 4 h. This may be caused by higher uptake and excretion rates of this phage, which is also evident from the low uptake in normal organs at this time point. Physiochemical properties, such as surface charge and functional groups, are widely accepted factors that influence cellular uptake and excretion of nanoparticles. Thus, the positive charge at physiological pH of peptide M9 may be the cause of the rapid clearance observed in both the biodistribution and *in vivo* imaging studies. In fact, positively charged nanoparticles are known to exhibit rapid cellular uptake and clearance, which additionally may lead to faster tumor targeting [204, 205]. Taken together, these results demonstrate that both phage clones pM6 and pM9 are capable of targeting and imaging human ovarian carcinoma tumors in xenografted mice, and that the binding of the phage to the cancer cells is mediated by the displayed peptides.

Conclusion

In conclusion, this study demonstrated the ability of phage selected for binding to cultured SKOV-3 cells to target and image ovarian tumors *in vivo*. This proves that it is possible to select and develop successful targeting agents in a time efficient and cost effective manner.

Acknowledgements

This work was supported in part by a Merit Review Award from the Veterans Administration BX000964 (SLD) and the NIH 1R21CA134960. The authors would like to acknowledge the contributions of Lisa D. Watkinson, Terry L. Carmack and the VA Biomolecular Imaging Core.

CHAPTER 4

PEPTIDE PHAGE DISPLAY FOR DISCOVERY OF NOVEL BIOMARKERS FOR IMAGING AND THERAPY OF CELL SUBPOPULATIONS OF OVARIAN CANCER

Introduction

Ovarian cancer is an aggressive disease that is characterized by a symptom free onset and early metastasis. Neoplastic cells rapidly invade surrounding tissues through the peritoneal fluid and metastasize predominantly as ascites in the peritoneal cavity [77, 78]. Approximately 80% of patients are diagnosed at late-stage disease, which leads to significantly decreased five-year survival rates of merely 30-45% [3, 4]. Furthermore, ovarian cancer often develops resistance to therapy after initial platinum-based treatment, and even though most patients respond to chemotherapy, the majority relapses within 18 months and succumbs to disease [4, 12, 59, 129]. Ovarian cancer is a very heterogeneous disease that comprises three major types: epithelial, stromal and germ cell, of which the former represents about 95% of diagnosed cases. Epithelial ovarian cancer can be further divided into eight subtypes: endometrioid, mucinous, serous, clear cell, transitional, squamous, undifferentiated and mixed epithelial that each exhibit different molecular and morphological characteristics [56, 57, 59, 251]. In addition to the large diversity among ovarian cancer subtypes, the largely asymptomatic early stages of the disease complicate diagnosis and treatment. At present, standard detection methods include measurement of the serum tumor-marker CA-125 as well as pelvic ultrasonography [7, 9, 88]. However, CA- 125 levels are often negligible in early-stage disease and elevated in only 80% of advanced stage ovarian cancer. In addition, false positive CA-125 levels are common for a range of other conditions such as endometriosis, inflammatory disease and other cancers, and the method is, therefore, often not sufficient to be diagnostic. Several

attempts have been made to find novel serum tumor markers of early-stage ovarian cancer, including measurements of soluble epidermal growth factor receptor (sEGFR) [252, 253], soluble cytokeratin 19 fragments [254], serum human kallikreins [255-258] and VEGF [259, 260]. However, most of these biomarkers are limited to advanced stage or metastatic disease and are, therefore, not sufficiently sensitive for early-stage ovarian cancer screening and diagnosis. For these reasons, it is necessary to develop new detection methods for both early- and advanced stage ovarian cancer.

Treatment of ovarian cancer most often includes cytoreductive surgery followed by a range of chemotherapies dependent on disease stage [12]. Combinations of the drugs paclitaxel, carboplatin and cisplatin are often used to treat both early and late-stage disease following surgery and most patients respond to this treatment. Nonetheless, the majority of patients relapsed within 18 months with therapy resistant disease, which cause median survival times as low as 24 months post diagnosis [12, 59, 129, 261]. Such poor prognosis seems to result from chemotherapy treatment that targets only the bulk of the tumor cells and fails to target the more aggressive cancer stem cells (CSC). This process most likely causes the occurrence of more aggressive tumors that are resistant to therapy (Figure 4.1) [13, 17, 262].

Ovarian Cancer Stem Cells

Cancer stem cells were first observed in acute myeloid leukemia [83] and have since been discovered in several solid tumors including breast, prostate, melanoma and ovarian cancer [14, 84-86]. Ovarian CSC were first isolated by Bapat and co-workers (2005) from ascites in a patient with advanced disease. The cells were shown to display

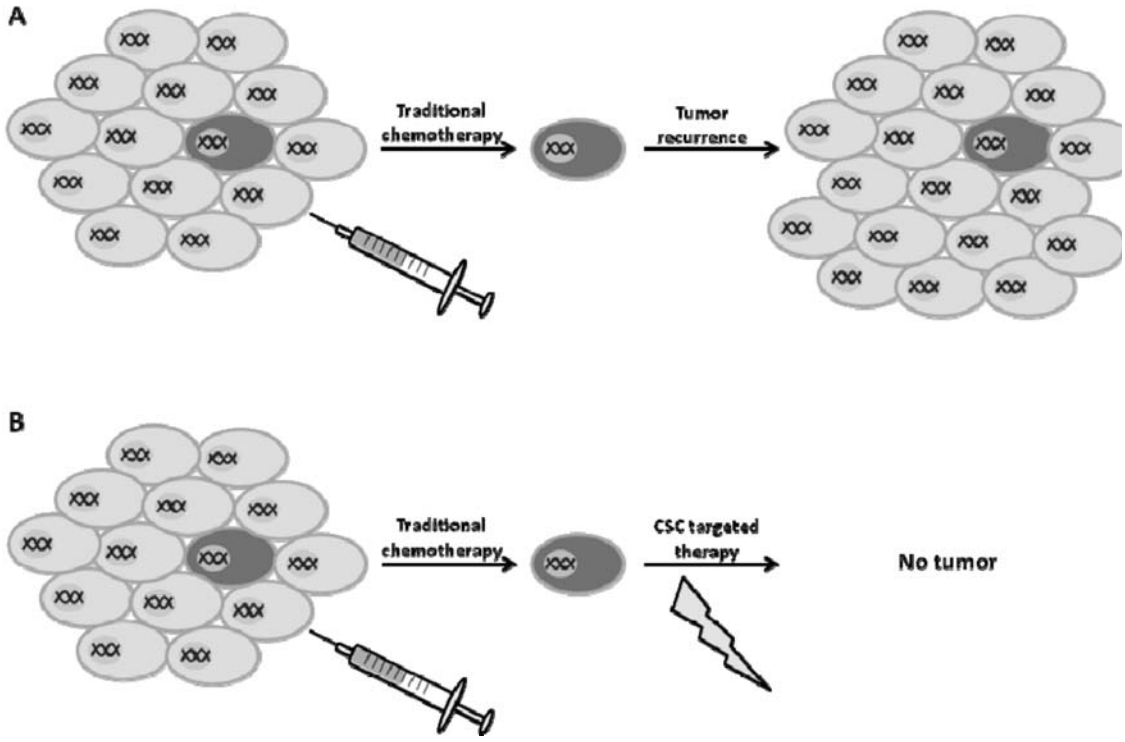

Figure 4.1. Traditional and CSC targeted therapies in ovarian cancer. **A)** Traditional chemotherapy fails to target CSC, which allows successive regrowth of the tumor. **B)** CSC targeted therapy in combination with traditional chemotherapy eradicates both tumor populations and hinder tumor recurrence.

the stem cell surface markers CD44 (hyaluronic acid receptor) and CD117 (ckit) as well as the intracellular stem cell markers Nestin, Oct-4 and Nanog [14, 20, 84-86]. Later, ovarian CSC were found to express aldehyde dehydrogenase (ALDH) and the cell surface marker CD133 (prominin-1), [263, 264]. The expression of these CSC biomarkers has been correlated with increased resistance to chemotherapeutic drugs. In fact, CD44 positive cells have been associated with resistance to the chemotherapeutic drugs carboplatin and paclitaxel [20], and CD133 expression has been correlated with resistance to cisplatin [263]. A subpopulation of cells expressing the biomarkers CD44 and CD117 from primary human ovarian tumors were shown to form floating spheroids in culture when grown under stem cell conditions (serum free, EGF, bFGF and insulin). The spheroids visually resembled spheroids found in ovarian cancer ascites [14, 17] as well as cultured spheroids from breast and neural tissue stem cells [265, 266]. Later CD133 and ALDH positive cells from ovarian epithelial carcinomas were also shown to form spheroids in culture and in addition cause formation of larger and more rapid tumors compared to CD133 and ALDH negative cells [264]. The aggressiveness of CSC is also evident from their ability to initiate tumor formation. In fact, as few as 100 dissociated spheroid cells have been found to establishment full tumors in mice, whereas up to $1x10^5$ of unselected cells were unable to initiate malignant growth [19]. In addition, these cells were capable of serial propagation and establishment of heterogeneous tumors with original phenotype after several rounds of propagation. The chemoresistance of CSC is associated with expression of the membrane efflux transporter ABCG2 [13, 267, 268], which has been found to be upregulated in CSC from primary ovarian tumors and in both murine and human ovarian cancer cell lines [13, 19, 21]. Increased drug-efflux in CSC

has been based on their ability to efflux the lipophillic dye Hoechst 33342 [13, 15, 17]. Side populations of mouse ovarian cancer cells exhibiting reduced Hoechst 33342 staining have been shown to increase tumorigenesis in nude mice [17]. A side population has also been observed in the human ovarian cancer cell line SKOV-3, where approximately 10% of the cells showed reduced Hoechst 33342 staining [13].

Taking these results together it seems likely that the development of molecules that target CSC may hold the key to increase the therapeutic efficiency for ovarian cancer. So far most studies have focused on drug candidates that inhibit cellular signaling pathways [269], however, it may be necessary to target CSC cell surface biomarkers that are independent of the ABCG2 drug-efflux system. Cancer stem cell targeting radiolabeled peptides may provide an efficient method to eradicate the CSC subpopulation.

Bacteriophage Display

Bacteriophage (phage) display technology was first developed by Dr. George P. Smith in 1985 [53]. The high-throughput technology involves the expression of combinatorial peptide libraries on filamentous phage coat proteins, and is often utilized to select high affinity ligands [53-55]. The best characterized of the filamentous phage is the Ff class, which structurally resemble a flexible rod. The Ff genome encodes 11 proteins; two of these are cpIII and cpVIII, which are surface exposed and are, for this reason, used to display the foreign peptides on the phage surface [53-55]. One of the most common phage display vector systems is the fUSE5 vector, which displays up to five copies of the peptides on cpIII. Another commonly used phage display vector is the f88 vector system,

which displays several hundred copies of the peptide on cpVIII. Experimentally, the phage display library is most often screened against an antigen of interest using several rounds of affinity selection, elution and amplification. The amplification step is relatively straight forward in that the Ff class of phage infects gram-negative bacteria, such as *E. coli*, and uses the bacterial machinery to produce progeny phage, which are released without lysis through the bacterial plasma membrane [3, 53-55, 147-150, 270]. Phage display technology has been employed to discover novel peptides that bind cancer cells. For example, RGD-peptides have been developed that target the tumor vasculature by binding to αvβ3-integrin (vitronectin receptor) [152, 153]. The SGRSA peptide has been found to have high binding affinity to uPA [154] and the peptide CGNSNPKSC to bind to gastric cancer endothelium [271]. Our laboratory has developed a number of peptides that target cancer cells. Among these are the peptide KCCYSL that binds to the ErbB2/HER2/neu receptor [32, 151], which is a member of the epidermal growth factor (EGF) receptor family and is upregulated in both ovarian and breast carcinoma. The ErbB2/HER2/neu oncogene is overexpressed in approximately 15-30% of ovarian carcinomas and is associated with an increased risk of progression and death, especially among women diagnosed with stage I and II ovarian carcinoma [272, 273]. In addition, the peptides IAGLATPGWSHWLAL and ANTPCGPYTHDCPVKR were selected for binding to the prostate carcinoma cell line PC-3 [31, 39] and galectin-3, respectively [29, 36, 38, 235]. Furthermore, a number of peptides have been developed that bind to the TF carbohydrate antigen, which is present on approximately 90% of human carcinoma cells and is involved in cell adhesion and migration [26, 169, 274, 275]. Most of these tumor targeting peptides have been developed to function as imaging and/or therapeutic agents

of human cancers. Radiolabeling of tumor targeting peptides provides an effective method of eradicating cancer cells as well as imaging tumors *in vivo* using technologies such as SPECT and PET.

New Ovarian Cancer Cell Targeting Peptides

In order to efficiently select ovarian targeting peptides with high affinity for a tumor and desirable pharmacokinetics, it is important to initially pre-clear the phage display library from peptide motifs that bind to normal vasculature. This may be accomplished by intravenously injecting non-tumor bearing mice with an appropriate volume of $>10^{14}$ virions/mL of phage display library followed by a 15 minute incubation time. Mice will then be sacrificed, the blood harvested and unbound phage amplified and purified for further rounds of selection. For *in vivo* selections against ovarian carcinoma, our laboratory has used SCID mice carrying SKOV-3 human carcinoma cell xenografted tumors. After injection of pre-cleared phage library tumor bound phage may be eluted after excision by using detergents. Amplified and purified phage may then be used for further rounds of *in vivo*/*ex vivo* selections [31, 41, 147]. Selected phage clones may additionally be analyzed for their binding affinity by micropanning experiments, in which phage are incubated with different carcinoma and normal cell lines. Phage binding affinity can then be evaluated by comparing the number of infectious units (TU/mL) between the cancerous and normal cell lines. In order to analyze the binding affinities of peptides outside of the phage environment, biotinylated or radiolabeled peptides may be synthesized and used in *in vitro*/*in vivo* binding studies [31, 40]. *In vivo* selection of ovarian carcinoma specific peptides can be an inefficient procedure. One potential barrier

is the presence of many tissue types within the tumor such as endothelial cells and connective tissue. Determination/selection of the targeted tissue for each selected peptide can be difficult when the *in vivo* milieu is so complex. Thus, an additional round of *ex vivo* selection may be added to try and select peptides that bind directly to ovarian carcinoma tumor cells. For this purpose MACS® technology may be utilized to separate ovarian carcinoma tumor cells from undesired tissue types. In order to avoid non-specific binding of phage, the phage may first be selected negatively against the MACS column and streptavidin labeled magnetic beads. Cells from excised human ovarian carcinoma tumors from xenografted mice may then be labeled with a mixture of biotinylated antibodies against known ovarian cancer biomarkers and then bound to streptavidin magnetic beads. Cells can then be loaded onto a MACS separation column and incubated with phage from previous selection rounds, and bound phage may then be eluted from cells using detergents and subsequently amplified and purified. A good candidate for a known ovarian cancer biomarker includes EpCAM, which is overexpressed in a variety of carcinomas, as well as normal epithelial tissues. Overexpression of EpCAM is present in ~70% of ovarian carcinomas and is significantly related to overall decreased survival [276]. ErbB2/HER2/neu is a member of the EGF receptor family and is also overexpressed in both ovarian and breast carcinoma. The ErbB2/HER2/neu oncogene is overexpressed in approximately 15-30% of ovarian carcinomas and is associated with an increased risk of progression and death, especially among women diagnosed with stage I and II ovarian carcinoma, which makes it an interesting cell surface biomarker for ovarian cancer [272, 273].

New Ovarian Cancer Stem Cell (CSC) Targeting Peptides

Selection of phage display derived peptides with high binding affinity for ovarian CSC is complicated by the fact that CSC only represents a small percentage of the entire tumor mass [17, 83]. Thus, CSC must initially be enriched from the remaining regular cancer cells. This may be done, as described above, utilizing MACS® technology using antibodies against known ovarian CSC biomarkers such as CD44, CD117 and CD133 [14, 20, 263, 264]. Alternatively, CSC can be selected by growing ovarian cancer cells in stem cell appropriate medium [20, 21]. Successful separation of CSC may be visualized by formation of spheroids in culture and staining with antibodies against ovarian CSC biomarkers. It may be advisable to further select CSC using flow cytometry cell sorting using antibodies against the known ovarian CSC biomarkers [17, 21]. Further, normal cancer cells may be separated during this process and used for negative selections. Even though the nature of CSC prevents selection of phage display derived peptides *in vivo*, pre-clearing of the phage display library may still be performed in non-tumor bearing mice as described above. In the early stages of selections, it is also important to consider the tumor microenvironment, in that CSC comprise only a small part of the tumor bulk [14, 17]. Thus in order to ensure specific binding, the library may be further pre-cleared against normal ovarian cancer cells before selecting for binding to CSC. Such a selection should be done *ex vivo* using cultured normal tumor tissue, and may be performed by utilizing MACS® technology as previously described. However, if the normal cancer cells have already been separated from CSC using flow cytometry, it will be sufficient to use non-labeled cells in suspension. Experimentally, it may be difficult to obtain large numbers of ovarian CSC, and it can be essential to cultivate CSC in appropriate stem cell

medium [14, 17, 20, 21] after separation from the tumor bulk. Cultured ovarian CSC form three dimensional spheroids in stem cell medium and it may be necessary to dissociate the cells to a single cell suspension for the phage display selection. For the selection, the MACS® technology may be employed by labeling ovarian CSC with antibodies against the known biomarkers CD44, CD117 and CD133 [14, 20, 263, 264]. Alternatively, CSC in suspension or grown on plates can be used instead. It is important to note that cells grown under such conditions must be tested for the presence of ovarian CSC biomarkers before selection in order to ensure that cells have not differentiated. Furthermore, it is imperative to use a large number ($>10^{13}$ virions) of phage in the first selection rounds in order to guarantee high diversity of phage clones [277]. After initial rounds the number of phage may be lowered to increase selection stringency. As previously described, selected phage clones may be further analyzed for their binding affinity by micropanning experiments, in which phage are incubated with normal ovarian cancer cells and ovarian CSC. The corresponding peptides of identified high binding clones may then be synthesized and biotinylated or radiolabeled, and analyzed for their tumor targeting abilities [31, 40]. Peptides with high binding affinity for CSC will most likely not be applicable as imaging agents due to the low percentage of CSC in a tumor. However, the chemotherapeutic abilities of such radiolabeled peptides can be evaluated in *in vivo* therapy studies using xenografted mice [27, 28, 33, 278]. Most likely, radiolabeled peptides for CSC tumor therapy must be combined with other forms of chemotherapy, such as more traditional platinum based drugs, in order to eradicate all cells in a tumor [279]. Thus, in a mouse therapy study it may be necessary to compare the therapeutic effects of drugs such as carboplatin and paclitaxel, which are standard in

current ovarian cancer treatment, to the effects of the radiolabeled peptide, as well as to a combined approach.

Radiolabeled Peptides for Tumor Imaging and Therapy

While antibodies and their fragments are by far the most used cancer targeting imaging and therapeutic agents [50], peptides exhibit better biodistribution properties [45-49]. High kidney uptake has, however, been observed with peptides, which poses a problem in regard to tumor imaging near the kidney and with toxicity caused by accumulation of radiolabeled peptides [45, 49, 50, 280]. Thus, lowering renal uptake is important and may be done by changing parts of the peptide sequence, trying different radionuclides and chelators or by co-administration of lysine or arginine [45, 49, 281].

Radiolabeling of tumor targeting peptides affords a proficient way of *in vivo* imaging using technologies such as SPECT and PET. SPECT was one of the first imaging modalities used clinically, and is widely employed in cancer imaging today; frequently utilizing both ^{99m}Tc (6 h half-life) and ^{111}In (2.8 day half-life). PET is an emerging imaging technique that offers certain advantages compared to SPECT in regard to sensitivity as well as quantitation [282]. The positron-emitting tracer ^{18}F-FDG is a commonly used PET tracer for imaging of cells with elevated glucose metabolism [283]. However, the uptake of ^{18}F-FDG is not increased in all cells, and has not shown great promise in early stage ovarian cancer diagnosis [284]. Therefore, alternative PET tracers are being developed that instead target antigens on cancer cells [110, 282]. A well-known example is octreotide, an eight amino acid cyclized peptide, that has been successfully utilized in imaging of somatostatin receptor positive tumors in humans when labeled with

^{111}In-diethylenetriaminepentaacetic acid (DTPA) [159]. Other examples include the α-MSH analog, which has been conjugated with the chelator DOTA and labeled with ^{64}Cu, ^{86}Y and ^{68}Ga for PET imaging of melanoma [161, 285], as well as peptides identified by our laboratory that bind ovarian, breast, and prostate tumors [32, 38-40, 163, 286]. The phage display selected peptide KCCYSL that bind ErbB2/HER2/neu has been radiolabeled with ^{111}In and used for SPECT/CT imaging of human MDA-MB-435 breast, and OVCAR-3 and SKOV- 3 ovarian xenografted tumors (Figure 4.2) [32, 40, 151, 163].

Whereas many cancer therapeutic agents function by binding and inhibiting receptors or other molecules involved in the progression of cancer, radiolabeling of peptides provides a method to target and eradicate cancer cells independent of peptide function and intracellular signaling pathways [139]. Labeling peptides with β-particle emitting radioisotopes are being used for targeted tumor radiotherapy and offer advantages in regard to varying degrees of energy emission. High energy β-emitters such as ^{90}Y (2.7 day half-life) are appropriate for the treatment of large tumor burdens, whereas medium and lower-energy β-emitters, such as ^{177}Lu (6.7 day half-life) may be more suitable for treating smaller tumors, residual tumor or metastatic deposits found in ovarian cancer [287, 288]. One example of a radiolabeled peptide being developed for tumor therapy is the α-MSH peptide analog, CCMSH, which targets melanoma cells. The α-MSH analog has been conjugated with DOTA and labeled with ^{212}Pb and used in melanoma therapy studies in mice. The treatment showed significantly increased survival rates, in which 45% of the mice receiving the highest dose of radiation survived the study disease-free [27, 28].

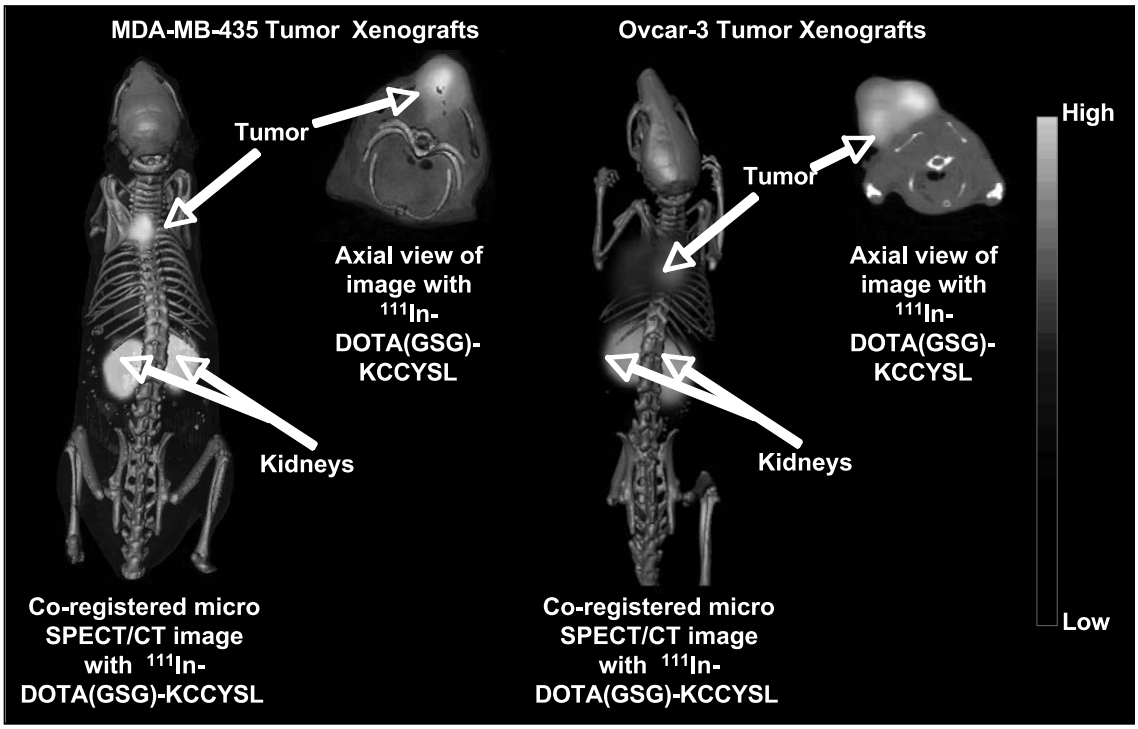

Figure 4.2. SPECT imaging of ^{111}In-DOTA-GSG-KCCYSL ErbB2 targeting peptide in MDA-MB-435 breast and OVCAR-3 ovarian tumor bearing SCID mice. MDA-MB-435 breast and OVCAR-3 ovarian tumor xenografted SCID mice were injected in the tail vein with 11.1 MBq of ^{111}In-DOTA-GSG-KCCYSL peptide or ^{111}In-DOTA-GSG-KYLCSC scrambled peptide and imaged by microSPECT/CT one hour later.

These results demonstrate that radiolabeled peptides offer great promise as both cancer imaging and therapeutic agents. Peptides that target early stage ovarian cancer cells could be developed into diagnostic imaging/therapeutic agents. Furthermore, peptides may be developed that target tumor subpopulations such as ovarian CSC.

Identification of Antigens Targeted by Selected Phage Displayed Peptides

Both phage and peptides can be used in formats that allow identification of targeted antigens. Previous studies have utilized cross-linking of phage or peptides to antigens as a means of identifying peptide targets [289, 290]. Kelly *et al.* have employed photolinker and biotin labeled phage to bind and capture target antigens on the cell surface. After binding and cross-linking, cell lysates were incubated with streptavidin beads. Antigens were eluted by reversing the crosslink and subsequently used in sodium dodecyl sulfate polyacrylamide gel electrophoresis (SDS-PAGE) followed by tryptic digest and mass spectrometry analysis [289]. However, these techniques can suffer from lack of specificity due to the use of multiple cross-linkers and the large size of filamentous phage. In addition, phage are known to aggregate and exhibit high non-specific binding to cells, which may result in identification of numerous irrelevant proteins via mass spectrometry. Alternatively, uniquely designed immobilized fusion proteins may offer a powerful means of isolating specific targets of phage display selected peptide sequences. For example a recombinant fusion protein containing a phage display selected peptide can be developed to aid the antigen capture process. Such a fusion protein may contain an N-terminal protein, such as thioredoxin, which acts as a soluble fusion partner linked to a matrix specific binder and a series of protease cleavage

sites. Our laboratory has adapted a thioredoxin fusion protein that remains soluble in *E. coli* cytosol and can be purified, during immobilization on S-protein sepharose (Figure 4.3). Thioredoxin is removed by cleavage with a protease, leaving the phage display peptide still bound to the S-protein sepharose. The immobilized peptide complex will then be accessible for binding to its target protein. The phage display derived peptide and the corresponding antigen may then be released from the S-protein sepharose by cleavage with a second protease. Once bound target proteins from cell lysates have been obtained they may be analyzed by 2D gel electrophoresis and identified by proteomic methodologies.

Here we hypothesize that spheroids may be established from cultured SKOV-3 cells, and that these aggregates will morphologically resemble ovarian CSC and express relevant biomarkers. Further, these spheroids may be utilized in phage display selections to identify peptides with affinity for ovarian CSC, and that such peptides may be employed as radionuclide therapy agents.

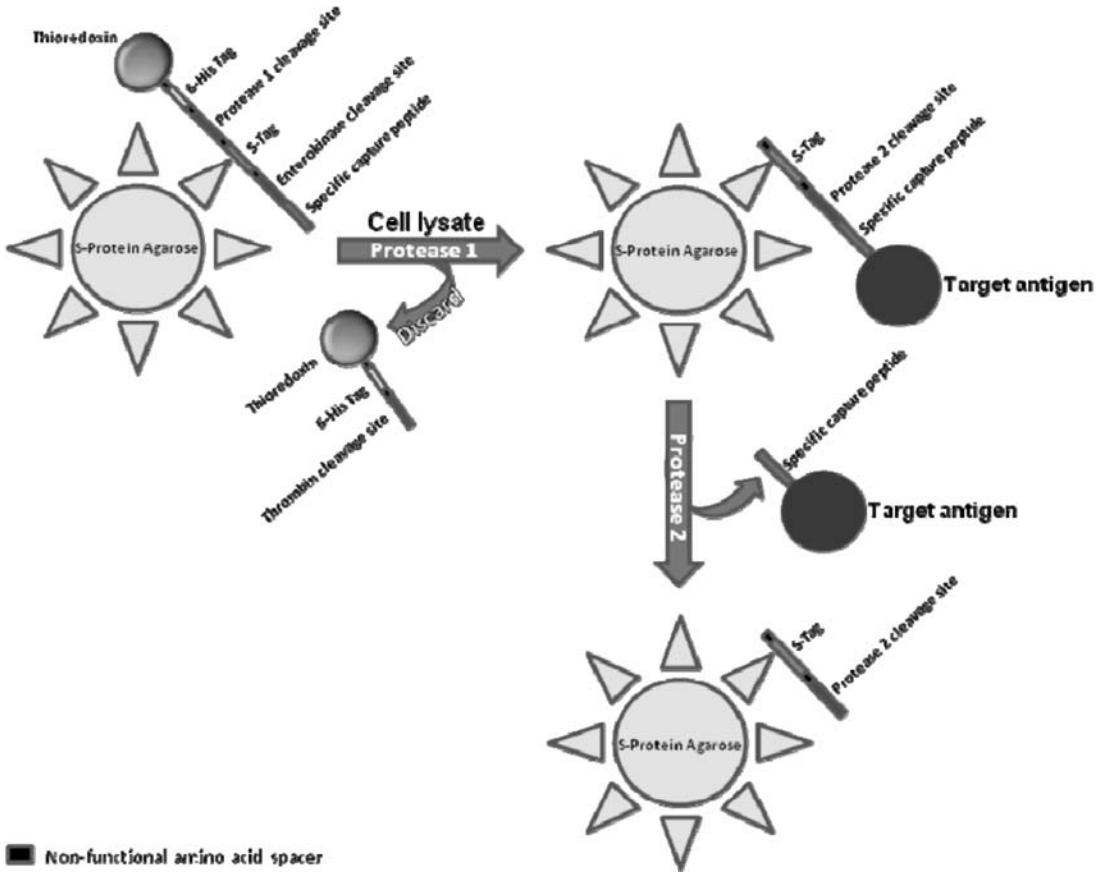

Figure 4.3. Isolation of bacteriophage targets using immobilized heterofunctional thioredoxin fusion proteins. Thioredoxin acts as a solubilizer and allows the complex to bind to the column matrix in aqueous solution. After cleavage of thioredoxin, cell lysate is added to let the phage display derived peptide capture target antigens, which are eluted from the column by protease cleavage.

Materials and Methods

Chemicals and Reagents

Tissue culture reagents were from Invitrogen (Carlsbad, CA). Unless otherwise stated, chemicals were purchased from Sigma Chemical Co. (St. Louis, MO).

Cell Lines and Tissue Culture

The human ovarian adenocarcinoma (SKOV-3) and human cervical cancer (HeLa) cell lines were purchased from American Type Tissue Culture. The cell lines were grown under differentiating conditions in RPMI 1640 (custom) with 10% FBS, 2 mM L-glutamine, 1.7 μM insulin and 48 mg/ml, at 37°C in 5% CO_2. For establishment of SKOV-3 spheroids, cells were lifted by 0.2% Trypsin-EDTA and transferred to ultra-low attachment cell culture plates and grown under stem cell conditions (DMEM/F12 supplemented with 20 ng/mL EGF, 10 ng/mL basic fibroblast growth factor, bFGF; and 10 μg/mL insulin). After 7 days under these conditions, SKOV-3 spheroids were transferred to differentiating conditions and monitored for up to 70 days.

Fluorescent Microscopy

SKOV-3, SKOV-3 spheroids and HeLa cells were fixed in ice cold methanol for 2 min at -20ºC on microscope slides. Cells were then washed with PBS and blocked with 10% FBS, 0.3 M glycine, 0.01% Tween-20 in PBS for 1 h at room temperature. Next, chicken anti-human CD44 and goat anti-human CD117 antibodies were added and

incubated for 30 min at room temperature, and slides were washed with PBS. Secondary anti-chicken antibody labeled with FITC and anti-goat antibody labeled with TEXAS Red fluorophores, were incubated with the cells for 30 min at room temperature in the dark, and then washed extensively (0.01% Tween-20, PBS). Cells were viewed with an epifluorescent Nikon T1-SM inverted microscope (Nikon, Melville, NY).

Phage Display Selections

A coat protein VIII displaying 15-mer peptide library (f88cys5) was a kind gift from Dr. George P. Smith (NCBI accession #AF246454). The concentration of phage particles (V/mL) and transducing units (TU) were determined by measuring absorbance at 260 nm and 280 nm and by tittering in *E. coli* K91 Blue Kan, respectively. The library was initially pre-cleared in a negative selection round against SKOV-3 cells grown under differentiating conditions by incubating $1x10^{13}$ virions with $1x10^{6}$ cells for 1 h at 4°C. Cells were pelleted by centrifugation (1,000 x g, 1 min) and unbound phage were collected from the supernatant and used in a subsequent positive selection round. Bound phage were eluted with 2.5% CHAPS. Both collections of phage were amplified in *E. coli* K91 Blue Kan as described per previous methods [178]. For positive selection against SKOV-3 spheroids, $1x10^{13}$ virions of purified phage were incubated with $1x10^{6}$ cells for 1 h at 4°C. Next, cells were washed thrice with TBS and bound phage were eluted with 0.1 M HCl, pH 2, and then 2.5% CHAPS or. Collected phage were amplified in *E. coli* as previously described. After each selection round, the DNA of random phage clones were sequenced to identify the foreign phage display inserts and to monitor the selection process.

Results

Characterization of SKOV-3 Spheroid Cells

Spheroids of the human ovarian carcinoma cell line SKOV-3 were established under stem cell conditions, which was evident from formation of cell aggregates over a period of 1-3 days (Figure 4.4). To determine if the SKOV-3 spheroids were capable of giving rise to attached differentiated cells, a well-known characteristic of cancer stem cells, the spheroids were transferred to differentiating conditions and monitored for up to 70 days (Figure 4.5). After 21 days and, until the end of the experiment (70 days), single cells in suspension were observed; however the spheroids failed to produce cells that morphologically resembled attached differentiated SKOV-3 cells.

To further determine if the spheroid cells were in fact cancer stem cell-like, expression of the ovarian cancer stem cell markers CD44 and CD117 were evaluated using fluorescent microscopy of SKOV-3, SKOV-3 spheroids and in HeLa cells, a cell line known to express both markers (Figure 4.6). As expected, the HeLa cells expressed both CD44 and CD117, which confirmed the functionality of the assay. Further, results showed that the SKOV-3 spheroids expressed increased levels of both markers compared to SKOV-3 cells grown under differentiating conditions, indicating that the former had been enriched or undergone transformation. Based on these results, the SKOV-3 spheroid cells were used in phage display selection rounds to identify clones with binding affinity for ovarian cancer stem cells.

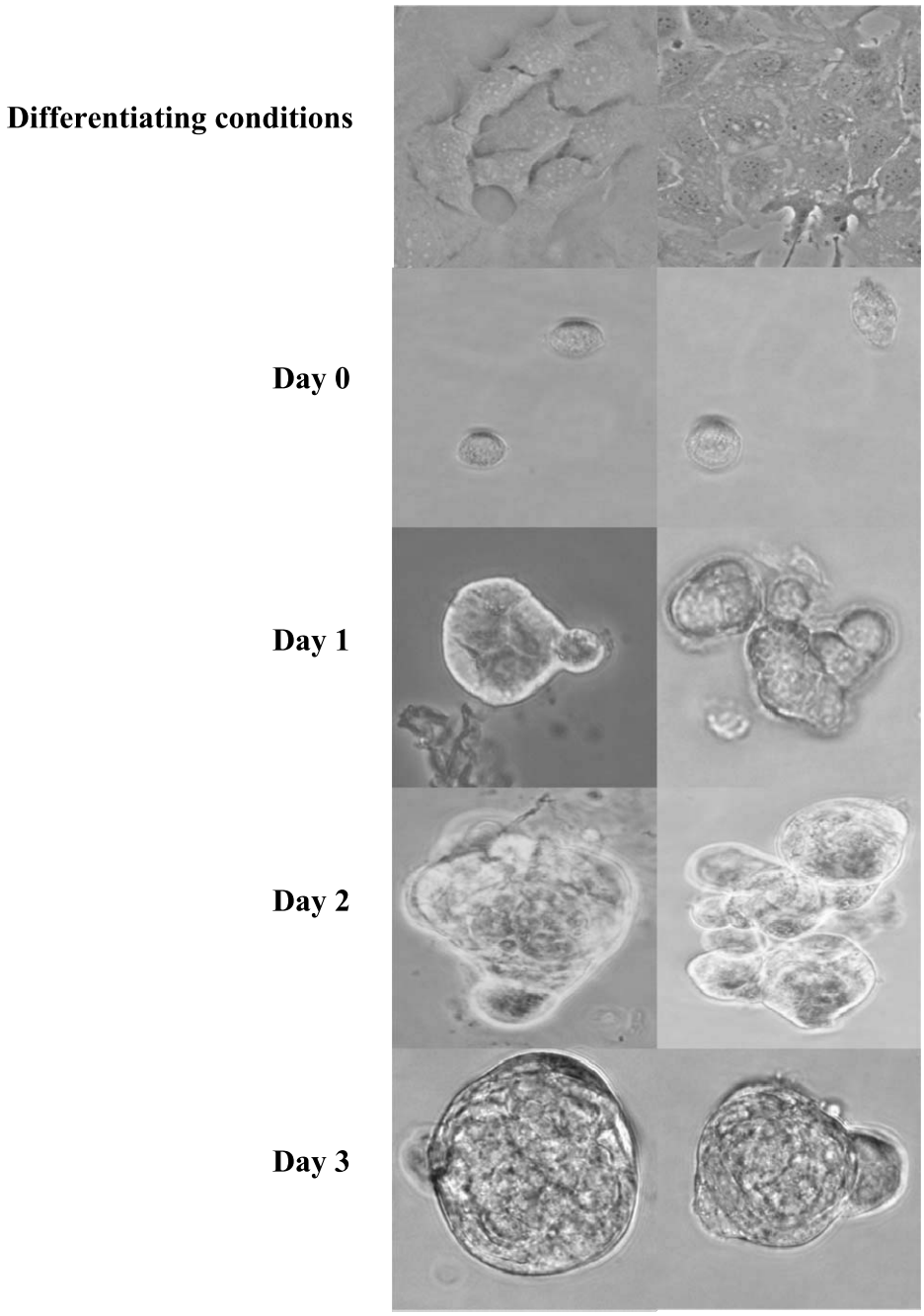

Figure 4.4. Growth of SKOV-3 spheroid cells. SKOV-3 cells were grown in differentiating medium, and then transferred to stem cell conditions (Day 0). Spheroids formed over a period of three days (Day 1 to Day 3). Cells were detected by light microscopy (Nikon T1-SM inverted microscope; Nikon, Melville, NY).

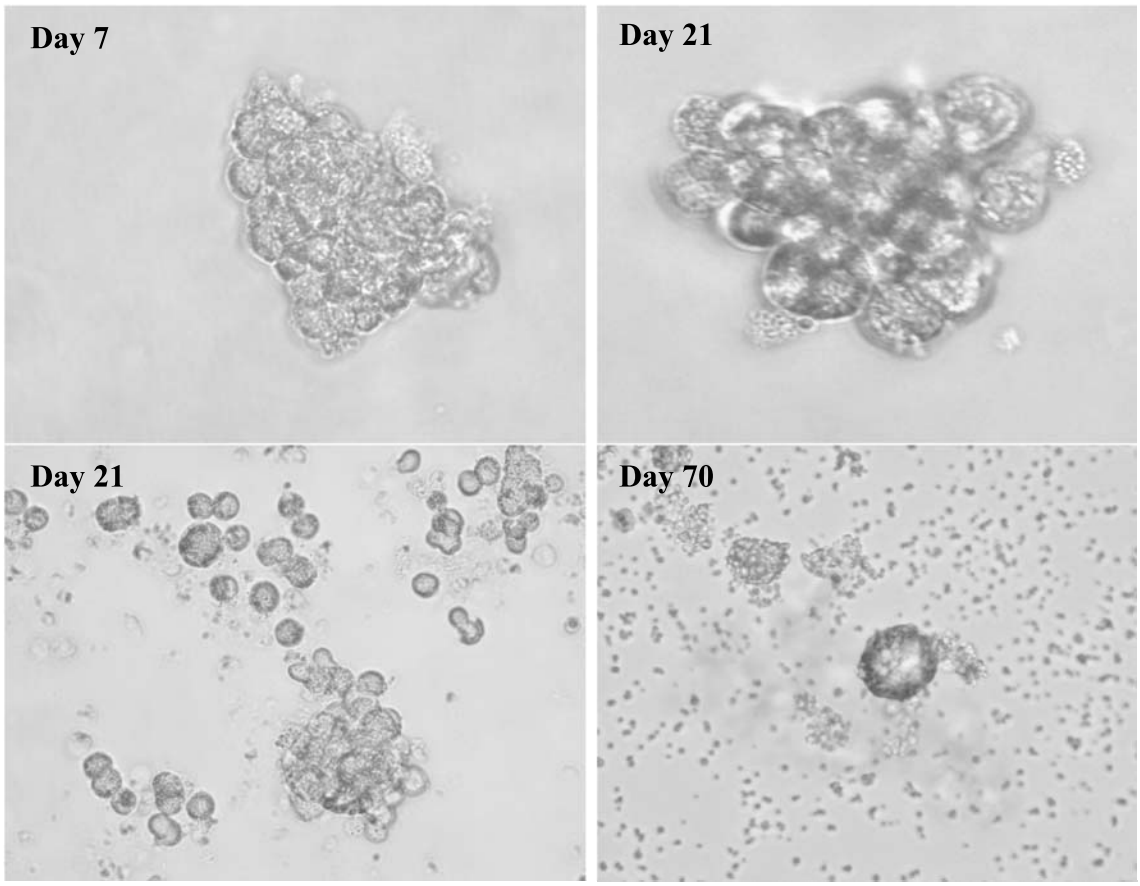

Figure 4.5. Growth of SKOV-3 spheroids under differentiating conditions. SKOV-3 spheroid cells were initially established under stem cell conditions, then transferred to differentiating medium to induce growth of attached and differentiated cells and monitored over a period of 70 days. After 21 days, single cells in suspension were detected; however, it was not possible to identify attached cells at any time point. Cells were detected by light microscopy (Nikon T1-SM inverted microscope; Nikon, Melville, NY).

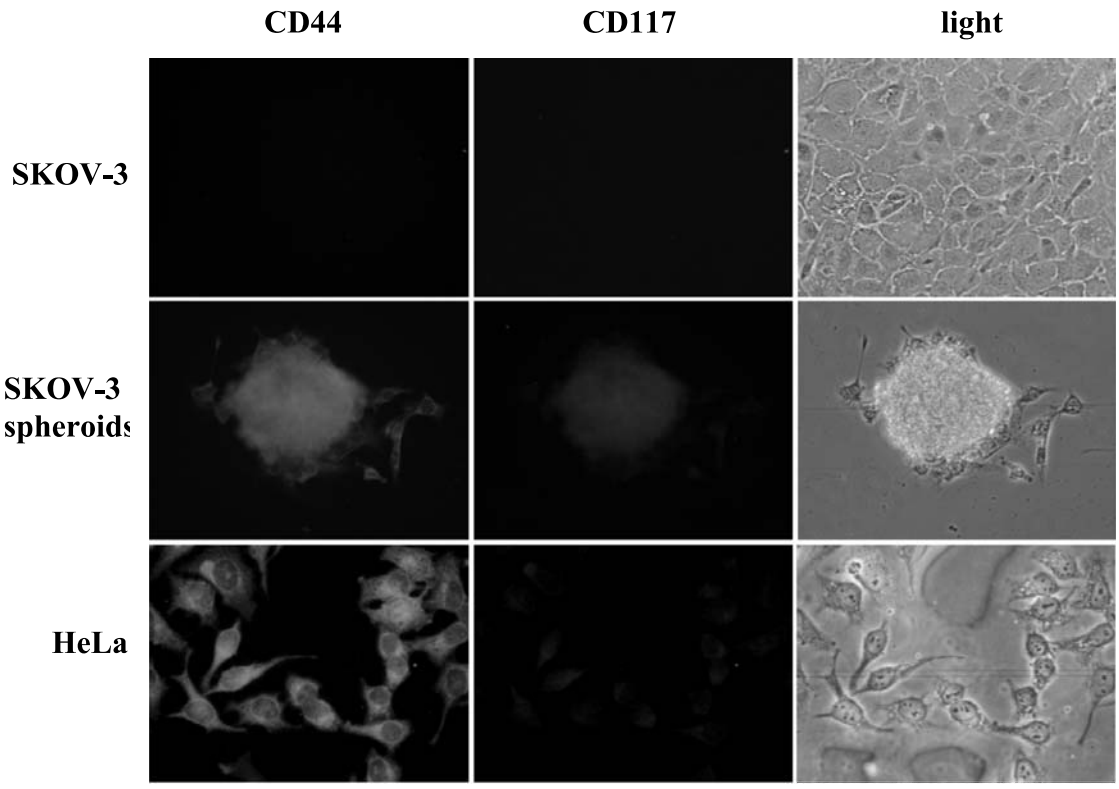

Figure 4.6. CD44 and CD117 expression in SKOV-3, SKOV-3 spheroid and HeLa cells. SKOV-3 and HeLa cells were grown under differentiating conditions, whereas SKOV-3 spheroids were maintained in medium supplemented with stem cell growth factors. Cells were probed with primary chicken anti-human-CD44 and goat anti-human-CD117 antibodies, and fluorescently labeled secondary anti-chicken-FITC and anti-goat-Texas Red antibodies and detected by an epifluorescent Nikon T1-SM inverted microscope (Nikon, Melville, NY).

Phage Display Selections

An initial phage display selection round was performed against SKOV-3 cells grown under differentiating conditions to pre-clear the library from phage clones that bound to these cells. The DNA of both bound and unbound phage clones were sequenced, and the foreign peptide inserts were determined to follow the process of selection and detect potential contamination. In the collections of SKOV-3 bound and unbound phage, 17 (P1-P17) and 18 (N1-N18) individual phage clones were identified (Table 4.1). Of the SKOV-3 bound clones, 47% (8/17), and 39% (7/18) of the unbound phage, were found to contain stop codons in the foreign peptide inserts. As a result these phage clones displayed no foreign inserts and could be described as “pseudo-wild type”.

Unbound phage from the first round of selection were used in a subsequent screening round against SKOV-3 spheroids. Surface bound phage were initially eluted with acid, after which potentially internalized phage were collected by CHAPS elution. Again, random clones were sequenced to determine the foreign peptide inserts and to evaluate the selection process. In the acid and CHAPS elutions, 22 (A1-A22) and 21 (C1-C21) individual phage clones were identified, respectively, of which 55% (12/22) and 52% (11/21) contained stop codons (Table 4.2).

Table 4.1. Negative phage display selection of a f88-cys5 library against SKOV-3 cells.

Negative selection			
SKOV-3 bound phage		Unbound phage	
Phage No.	Sequence	Phage No.	Sequence
P1	PNPACTNTPSCSSPP	N1	RPDTCGWGPPCRPGN
P2	TPQICQAIYTCSISV	N2	NTARCQTNTRCQPVA
P3	S*LTCPF*TSCPKYD	N3	HVPHCAAVESCWHY*
P4	EFPHC*RRLHC*PPQ	N4	KESPCRSPT*CTAPI
P5	PRXSCGTSAPCRPRQ	N5	PTRPCPPTPHCNRSG
P6	HPINCTPRQPCIDPT	N6	HNRSCHPIPSCTAPA
P7	P*PLCALTPICPPHT	N7	PSEGCSTL*VCCTRS
P8	LVAHCPPILGCPRPT	N8	VTLHCHPIMYC*DSC
P9	PNFNCWHRIQCPDRA	N9	NIHACQXPLRCTSPP
P10	PTQCEQSM*CNSPP	N10	HPNKCRISRVCTRTP
P11	RPSHCTPQKVCAQT*	N11	PHSQCVKKFQCPLLM
P12	RLRICPRQNPCV*CD	N12	SPTLCHANKNCPRPS
P13	IASMCVPNLHC*SPE	N13	*TDICPISTFCIDIR
P14	RPRFCETLPACQTPL	N14	TRVDCHPPHNCPKPS
P15	HQPTCNPRQRCTMAS	N15	IDPHC*PRRRGMDTW
P16	QPNTCPSPLMC*LPQ	N16	WRRYCWAAPVCTPSQ
P17	ATPTCLMRQPCLSNP	N17	NTSKCKTTLHCGRSR
		N18	PPAGCVAPAQCPC*C

The phage display library (10^{13} virions) was incubated with 10^{6} SKOV-3 cells grown under differentiating conditions. Bound phage were eluted with 2.5% CHAPS. Unbound phage were collected and used in a subsequent positive selection round. All phage were amplified in *E. coli* and the DNA of random clones were sequenced and the foreign peptide inserts were determined.

*Stop codon.

Table 4.2. Positive phage display selection of a f88-cys5 library against SKOV-3 spheroid cells.

Positive selection			
Acid elution		CHAPS elution	
Phage No.	Sequence	Phage No.	Sequence
A1	IPDCCDPSATC*RVL	C1	YPGSCRRSLPC*VQR
A2	VSPTCTRPSSCTQPP	C2	R*PACMRTPGCRSRV
A3	R*PACMRTPGCRSRV	C3	APAGCQVPTPCRQRS
A4	RRHECPLAAFCDLRR	C4	LSRTCLFKTCPGPL
A5	QNAKCTDARPCPVLR	C5	YPGSCRRSLPC*VQR
A6	TKLNCSP*APCQNPW	C6	LSNTCDTPMTCHKTP
A7	YPGSCRRSLPC*VQR	C7	LSRTCHL*DVCPGPL
A8	YPGSCRRSLPC*VQR	C8	QQQRCYDNAQCTNGTP
A9	PYANCPAKHRCLYLH	C9	PPDKCFAAGTCTNDT
A10	YPGSCRRSLPC*VQR	C10	LRRTCHL**RCPGPL
A11	PRTHCTYITQCSALA	C11	R*PACMRTPGCRSRV
A12	RWRHCHAQHQCPAHY	C12	PSLSCCR*HSCPQWQ
A13	*R*LCPTPQPCARLF	C13	TYASCM*TPLCPPAE
A14	X*RLCSLRPGCCSGC	C14	LSNTCDTPMTCHKTP
A15	QQSVCCVTRGCMQEN	C15	LTILCDTPMTCLPRP
A16	YPGSCRRSLPC*VQR	C16	LSRTCHL*DACPGPL
A17	PPASCQTHPTCSPDT	C17	IPNCCHPSATC*HVL
A18	YPGSCRRSLPC*VQR	C18	E*IMCDLMACT*KS
A19	LFPNCCHPSATC*HVL	C19	PPASCPQHPRCNTQP
A20	LSNTCDTPMTCHKTP	C20	R*PACMRTPGCRSRV
A21	R*PACMRTPGCRSRV	C21	LSNTCDTPMTCHKTP
A22	PLESCGATAACDPAH		

The phage display library (10^{13} virions) was incubated with 10^{6} SKOV-3 spheroid cells grown under stem cell conditions. Bound phage were initially eluted with acid (0.1 M HCl, pH 2) followed by elution with 2.5% CHAPS. Bound phage were collected, amplified in *E. coli* and the DNA of random clones were sequenced and the foreign peptide inserts were determined.

*Stop codon.

Discussion

Previous studies by other groups have shown that cancer stem cell spheroids may be formed by culturing cells under stem cell conditions [14, 19, 21, 291]. To identify peptides with binding affinity for ovarian cancer stem cells, our laboratory established such spheroid cells from the human ovarian carcinoma cell line SKOV-3. These spheroids formed over a period of three days and resembled CSC aggregates reported by others [14, 21]. In order to validate that these cells were in fact cancer stem cell-like, the capability of the spheroids to give rise to differentiated cells was investigated. Single cells were observed after 21 days under differentiating conditions; however, these were floating and morphologically different from attached SKOV-3 cells [292]. The reason for the absence of differentiated cells is unclear. Previous studies have reported development of mature cells by CSC spheroids under similar conditions [20, 21]. One possible explanation may be that the spheroid cells had undergone senescence, and were as a result unresponsive to the conditions in the differentiating medium. In fact, CSC have been shown to constitute the major fraction of quiescent cells in ovarian tumors [293]. Another reason may lie in the fact that FBS contains low levels of FGF as well as other growth factors [294], which may cause the cells to stay in a de-differentiated state. In future experiments, this may be overcome by using other serums or FBS from which growth factors have been removed. Alternatively, the SKOV-3 spheroids may lack some of the properties generally observed for CSC, as the cells are derived from a cultured cell line and have not recently been propagated from a tumor. A change in morphology,

protein expression as well as in growth characteristics are known to change over time in cultured cell lines, and may therefore be vastly different from primary tumor cells [295, 296]. Nevertheless, other research groups have showed that spheroids, that expressed CSC biomarkers and that gave rise to differentiated cells, could be formed from cell lines [17, 292], suggesting that our cells may have changed over time in culture, or that the differentiating medium contained inhibiting factors.

To further investigate the characteristics of the SKOV-3 spheroids, expression of the ovarian CSC markers CD44 and CD117 was evaluated using fluorescent microscopy. Increased levels of both markers were detected in the SKOV-3 spheroids compared to SKOV-3 cells, indicating that the former had undergone transformation to a less mature state and/or had been enriched from the original population of cells. Similar results have previously been observed by others, in which spheroids were found to express elevated levels of several stem cell related proteins including CD44 and CD117 [19-21, 297].

Based on these results, the SKOV-3 spheroids were used in a phage display selection to identify phage clones with binding affinity to ovarian CSC. After two rounds of selection of an f88-cys5 phage library several individual clones were identified. Of these, almost half contained stop codons in the foreign insert, indicating that these clones resembled WT phage and lacked display of non-inherent peptides. Since the foreign peptides are presented at the NH_2-terminus of cpVIII, and are therefore the first part of the protein to be synthesized, a stop codon in this sequence will result in termination of translation [248]. As the DNA in f88 libraries contains two cpVIII genes, one for normal and one for peptide-displayed coat protein, the virion will morphologically be identical to WT [298]. The lack of a foreign displayed peptide may give these ‘pseudo’ WT phage a

growth advantage, and the population of clones with stop codons may therefore become more prevalent in selected pools. Additionally, termination codons may occur by frameshift mutations [298], or from the mere probability of a stop codon occurring in a 15-mer amino acid sequence. In contrast to f88 libraries, the fUSE5 library lacks a copy of wild type cpIII [299], and stop codons in the foreign peptide sequence will as a result render the phage incapable of infecting bacteria. This explains why stop codons are absent in fUSE5, but are observed in the f88-cys5 library. Further, other research groups have reported the presence of termination codons in f88 libraries; although at much lower levels than what was observed in this study [300, 301].

Taking these results together, our laboratory decided that this study should be redone in future experiments using cancer cells derived from excised human ovarian tumors obtained at the University of Missouri Hospital. By doing so, potential spheroids would be more likely to resemble and behave like physiological CSC, and selected peptides would be more probable to target these cells *in vivo*. Further, the phage display selection should be done using a different library without a high percentage of stop codons, such as fUSE5, which has previously been successfully employed in our laboratory.

Conclusion

In conclusion, these experiments demonstrated that it was possible to establish CSC-like SKOV-3 spheroid cells by growing these under stem cell conditions, and that these cells expressed the ovarian CSC biomarkers CD44 and CD117. Nonetheless, the spheroid cells failed to give rise to differentiated cells. To select peptides with binding affinity for ovarian CSC, a phage display selection using a f88-cys5 library was initiated. However, this library was found to contain a high amount of phage clones with termination codons in the foreign peptide inserts.

Acknowledgements

This work was supported by a Merit Review Award from the Veterans Administration (SLD).

REFERENCES

1. Jemal, A, Siegel, R, Ward, E, Hao, Y, Xu, J, Murray, T, and Thun, M J. Cancer statistics, 2008. *CA Cancer J Clin*, 2008. **58**(2): p. 71-96.

2. Brennan, R, Federico, S, and Dyer, M A. The war on cancer: have we won the battle but lost the war? *Oncotarget*, 2010. **1**(2): p. 77-83.

3. Pecorelli, S, Favalli, G, Zigliani, L, and Odicino, F. Cancer in women. *Int J Gynaecol Obstet*, 2003. **82**(3): p. 369-379.

4. Aletti, G D, Gallenberg, M M, Cliby, W A, Jatoi, A, and Hartmann, L C. Current Management Strategies for Ovarian Cancer. *Mayo Clin Proc*, 2007. **82**(6): p. 751-770.

5. Siegel, R, Naishadham, D, and Jemal, A. Cancer statistics, 2013. *CA Cancer J Clin*, 2013. **63**(1): p. 11-30.

6. American Cancer Society, Cancer Facts and Figures. 2014. Accessed 3/26/2014; http://www.cancer.org/acs/groups/content/@research/documents/webcontent/acspc-042151.pdf.

7. Neesham, D. Ovarian cancer screening. *Aust Fam Physician*, 2007. **36**(3): p. 126-128.

8. Bast, R C, Jr., et al. New tumor markers: CA125 and beyond. *Int J Gynecol Cancer*, 2005. **15** (3): p. 274-81.

9. Eltabbakh, G H, Belinson, J L, Kennedy, A W, Gupta, M, Webster, K, and Blumenson, L E. Serum CA-125 measurements > 65 U/mL. Clinical value. *J Reprod Med*, 1997. **42**(10): p. 617-24.

10. Bast, R C, Jr., Hennessy, B, and Mills, G B. The biology of ovarian cancer: new opportunities for translation. *Nat Rev Cancer*, 2009. **9**(6): p. 415-28.

11. Markman, M. Pharmaceutical management of ovarian cancer : current status. *Drugs*, 2008. **68**(6): p. 771-89.

12. Ozols, R F. Treatment goals in ovarian cancer. *Int J Gynecol Cancer*, 2005. **15**: p. 3-11.

13. Hirschmann-Jax, C, Foster, A E, Wulf, G G, Nuchtern, J G, Jax, T W, Gobel, U, Goodell, M A, and Brenner, M K. A distinct "side population" of cells with high drug efflux capacity in human tumor cells. *Proc Natl Acad Sci U S A* 2004. **101**(39): p. 14228-14233.

14. Bapat, S A, Mali, A M, Koppikar, C B, and Kurrey, N K. Stem and Progenitor-Like Cells Contribute to the Aggressive Behavior of Human Epithelial Ovarian Cancer. *Cancer Res*, 2005. **65**(8): p. 3025-3029.

15. Clarke, M F, Dick, J E, Dirks, P B, Eaves, C J, Jamieson, C H, Jones, D L, Visvader, J, Weissman, I L, and Wahl, G M. Cancer stem cells--perspectives on current status and future directions: AACR Workshop on cancer stem cells. *Cancer Res*, 2006. **66**(19): p. 9339-44.

16. Clarke, M F and Fuller, M. Stem cells and cancer: two faces of eve. *Cell*, 2006. **124**(6): p. 1111-5.

17. Szotek, P P, et al. Ovarian cancer side population defines cells with stem cell-like characteristics and Mullerian Inhibiting Substance responsiveness. *PNAS*, 2006. **103**(30): p. 11154-11159.

18. Ponnusamy, M P and Batra, S K. Ovarian cancer: emerging concept on cancer stem cells. *J Ovarian Res*, 2008. **1**(1): p. 4.

19. Zhang, S, Balch, C, Chan, M W, Lai, H-C, Matei, D, Schilder, J M, Yan, P S, Huang, T H-M, and Nephew, K P. Identification and Characterization of Ovarian Cancer-Initiating Cells from Primary Human Tumors. *Cancer Res*, 2008. **68**(11): p. 4311-4320.

20. Alvero AB, C R, Fu HH, Montagna M, Schwartz PE, Rutherford T, Silasi DA, Steffensen KD, Waldstrom M, Visintin I, Mor G. Molecular phenotyping of

human ovarian cancer stem cells unravels the mechanisms for repair and chemoresistance. *Cell Cycle*, 2009. **8**(1): p. 158-166.

21. Shi, M, Jiao, J, Lu, W, Ye, F, Ma, D, Dong, Q, and Xie, X. Identification of cancer stem cell-like cells from human epithelial ovarian carcinoma cell line. *Cell Mol Life Sci*, 2010: p. 1-11.

22. Peletskaya, E N, Glinsky, G, Deutscher, S L, and Quinn, T P. Identification of peptide sequences that bind the Thomsen-Friedenreich cancer-associated glycoantigen from bacteriophage peptide display libraries. *Molec Divers*, 1996. **2**: p. 13-8.

23. Chen, J, Cheng, Z, Hoffman, T J, Jurisson, S S, and Quinn, T P. Melanoma-targeting properties of (99m)technetium-labeled cyclic alpha-melanocyte-stimulating hormone peptide analogues. *Cancer Res*, 2000. **60**(20): p. 5649-58.

24. Chen, J, Cheng, Z, Owen, N K, Hoffman, T J, Miao, Y, Jurisson, S S, and Quinn, T P. Evaluation of an (111)In-DOTA-rhenium cyclized alpha-MSH analog: a novel cyclic-peptide analog with improved tumor-targeting properties. *J Nucl Med*, 2001. **42**(12): p. 1847-55.

25. Chen, J, Cheng, Z, Miao, Y, Jurisson, S S, and Quinn, T P. Alpha-melanocyte-stimulating hormone peptide analogs labeled with technetium-99m and indium-111 for malignant melanoma targeting. *Cancer*, 2002. **94**(4): p. 1196-201.

26. Landon, L A, Peletskaya, E N, Glinsky, V V, Karasseva, N, Quinn, T P, and Deutscher, S L. Combinatorial evolution of high-affinity peptides that bind to the Thomsen-Friedenreich carcinoma antigen. *J Protein Chem*, 2003. **22**(2): p. 193-204.

27. Miao, Y, et al. Melanoma therapy via peptide-targeted {alpha}-radiation. *Clin Cancer Res*, 2005. **11**(15): p. 5616-21.

28. Miao, Y, Owen, N K, Fisher, D R, Hoffman, T J, and Quinn, T P. Therapeutic efficacy of a 188Re-labeled alpha-melanocyte-stimulating hormone peptide analog in murine and human melanoma-bearing mouse models. *J Nucl Med*, 2005. **46**(1): p. 121-9.

29. Zou, J, Glinsky, V V, Landon, L A, Matthews, L, and Deutscher, S L. Peptides specific to the galectin-3 carbohydrate recognition domain inhibit metastasis-associated cancer cell adhesion. *Carcinogenesis*, 2005. **26**(2): p. 309-18.

30. Kumar, D S L. Galectin-3-Targeting Peptides as Novel In Vivo tumor-Imaging and Targeting Agents. *Tumor Microvasculature Environment AACR Meeting. Florence, Italy.*, 2006.

31. Newton, J R, Kelly, K A, Mahmood, U, Weissleder, R, and Deutscher, S L. In vivo selection of phage for the optical imaging of PC-3 human prostate carcinoma in mice. *Neoplasia*, 2006. **8**(9): p. 772-80.

32. Kumar, S R, Quinn, T P, and Deutscher, S L. Evaluation of an 111In-radiolabeled peptide as a targeting and imaging agent for ErbB-2 receptor expressing breast carcinomas. *Clin Cancer Res*, 2007. **13**(20): p. 6070-9.

33. Miao, Y, Shelton, T, and Quinn, T P. Therapeutic efficacy of a 177Lu-labeled DOTA conjugated alpha-melanocyte-stimulating hormone peptide in a murine melanoma-bearing mouse model. *Cancer Biother Radiopharm*, 2007. **22**(3): p. 333-41.

34. Newton, J R, Miao, Y, Deutscher, S L, and Quinn, T P. Melanoma imaging with pretargeted bivalent bacteriophage. *J Nucl Med*, 2007. **48**(3): p. 429-36.

35. Hilderbrand, S A, Kelly, K A, Niedre, M, and Weissleder, R. Near infrared fluorescence-based bacteriophage particles for ratiometric pH imaging. *Bioconjug Chem*, 2008. **19**(8): p. 1635-9.

36. Kumar, S R and Deutscher, S L. 111In-labeled galectin-3-targeting peptide as a SPECT agent for imaging breast tumors. *J Nucl Med*, 2008. **49**(5): p. 796-803.

37. Miao, Y and Quinn, T P. Peptide-targeted radionuclide therapy for melanoma. *Crit Rev Oncol Hematol*, 2008. **67**(3): p. 213-28.

38. Deutscher, S L, Figueroa, S D, and Kumar, S R. Tumor targeting and SPECT imaging properties of an (111)In-labeled galectin-3 binding peptide in prostate carcinoma. *Nucl Med Biol*, 2009. **36**(2): p. 137-46.

39. Newton-Northup, J R, Figueroa, S D, Quinn, T P, and Deutscher, S L. Bifunctional phage-based pretargeted imaging of human prostate carcinoma. *Nucl Med Biol*, 2009. **36**(7): p. 789-800.

40. Kumar, S R, Gallazzi, F A, Ferdani, R, Anderson, C J, Quinn, T P, and Deutscher, S L. In vitro and in vivo evaluation of Cu-radiolabeled KCCYSL peptides for targeting epidermal growth factor receptor-2 in breast carcinomas. *Cancer Biother Radiopharm*, 2010. **25**(6): p. 693-703.

41. Newton-Northup, J R, Figueroa, S D, and Deutscher, S L. Streamlined In Vivo Selection and Screening of Human Prostate Carcinoma Avid Phage Particles for Development of Peptide Based In Vivo Tumor Imaging Agents. *Comb Chem High Throughput Screen*, 2010.

42. Kumar, S R, Gallazzi, F A, Quinn, T P, and Deutscher, S L. (64)Cu-labeled peptide for PET of breast carcinomas expressing the Thomsen-Friedenreich carbohydrate antigen. *J Nucl Med*, 2011. **52**(11): p. 1819-26.

43. Ghosh, D, Lee, Y, Thomas, S, Kohli, A G, Yun, D S, Belcher, A M, and Kelly, K A. M13-templated magnetic nanoparticles for targeted in vivo imaging of prostate cancer. *Nat Nano*, 2012. **7**: p. 677-682.

44. Larimer, B, Thomas, W, Smith, G, and Deutscher, S. Affinity Maturation of an ERBB2-Targeted SPECT Imaging Peptide by In Vivo Phage Display. *Mol Imaging Biol*, 2014: p. 1-10.

45. Behr, T M, et al. Reduction of the renal uptake of radiolabeled monoclonal antibody fragments by cationic amino acids and their derivatives. *Cancer Res*, 1995. **55**(17): p. 3825-34.

46. Behr, T M, Gotthardt, M, Barth, A, and Behe, M. Imaging tumors with peptide-based radioligands. *Q J Nucl Med*, 2001. **45**(2): p. 189-200.

47. Goldenberg, D M. Targeted therapy of cancer with radiolabeled antibodies. *J Nucl Med*, 2002. **43**(5): p. 693-713.

48. Reubi, J C. Peptide receptors as molecular targets for cancer diagnosis and therapy. *Endocr Rev*, 2003. **24**(4): p. 389-427.

49. Rolleman, E J, Valkema, R, de Jong, M, Kooij, P P, and Krenning, E P. Safe and effective inhibition of renal uptake of radiolabelled octreotide by a combination of lysine and arginine. *Eur J Nucl Med Mol Imaging*, 2003. **30**(1): p. 9-15.

50. Deutscher, S L. Phage display in molecular imaging and diagnosis of cancer. *Chem Rev*, 2010. **110**(5): p. 3196-211.

51. Kucharewicz-Krukowska, A and Slopek, S. Immunogenic effect of bacteriophage in patients subjected to phage therapy. *Arch Immunol Ther Exp (Warsz)*, 1987. **35**(5): p. 553-61.

52. Zou, J, Dickerson, M T, Owen, N K, Landon, L A, and Deutscher, S L. Biodistribution of filamentous phage peptide libraries in mice. *Mol. Biol. Rep.*, 2004. **31**(2): p. 121-9.

53. Smith, G P. Filamentous fusion phage: novel expression vectors that display cloned antigens on the virion surface. *Science*, 1985. **228**(4705): p. 1315-7.

54. Smith, G P and Petrenko, V A. Phage Display. *Chem Rev*, 1997. **97**(2): p. 391-410.

55. Marvin, D A. Filamentous phage structure, infection and assembly. *Curr Opin Struct Biol*, 1998. **8**(2): p. 150-8.

56. Godwin, A K, Testa, J R, and Hamilton, T C. The biology of ovarian cancer development. *Cancer*, 1993. **71**(S2): p. 530-536.

57. Ness, R B and Cottreau, C. Possible role of ovarian epithelial inflammation in ovarian cancer. *J Natl Cancer Inst*, 1999. **91**(17): p. 1459-67.

58. Purdie, D M, Bain, C J, Siskind, V, Webb, P M, and Green, A C. Ovulation and risk of epithelial ovarian cancer. *Int J Cancer*, 2003. **104**(2): p. 228-32.

59. Hennessy, B T, Coleman, R L, and Markman, M. Ovarian cancer. *The Lancet*, 2009. **374**(9698): p. 1371-1382.

60. Piek, J M, Verheijen, R H, Kenemans, P, Massuger, L F, Bulten, H, and van Diest, P J. BRCA1/2-related ovarian cancers are of tubal origin: a hypothesis. *Gynecol Oncol*, 2003. **90**(2): p. 491.

61. Kindelberger, D W, et al. Intraepithelial carcinoma of the fimbria and pelvic serous carcinoma: Evidence for a causal relationship. *Am J Surg Pathol*, 2007. **31**(2): p. 161-9.

62. Schildkraut, J M, Schwingl, P J, Bastos, E, Evanoff, A, and Hughes, C. Epithelial ovarian cancer risk among women with polycystic ovary syndrome. *Obstet Gynecol*, 1996. **88**(4 Pt 1): p. 554-9.

63. Alsop, K, et al. BRCA mutation frequency and patterns of treatment response in BRCA mutation-positive women with ovarian cancer: a report from the Australian Ovarian Cancer Study Group. *J Clin Oncol*, 2012. **30**(21): p. 2654-63.

64. Struewing, J P, Hartge, P, Wacholder, S, Baker, S M, Berlin, M, McAdams, M, Timmerman, M M, Brody, L C, and Tucker, M A. The risk of cancer associated with specific mutations of BRCA1 and BRCA2 among Ashkenazi Jews. *N Engl J Med*, 1997. **336**(20): p. 1401-8.

65. Ben David, Y, et al. Effect of BRCA mutations on the length of survival in epithelial ovarian tumors. *J Clin Oncol*, 2002. **20**(2): p. 463-6.

66. King, M C, Marks, J H, and Mandell, J B. Breast and ovarian cancer risks due to inherited mutations in BRCA1 and BRCA2. *Science*, 2003. **302**(5645): p. 643-6.

67. Kolasa, I K, Rembiszewska, A, Janiec-Jankowska, A, Dansonka-Mieszkowska, A, Lewandowska, A M, Konopka, B, and Kupryjanczyk, J. PTEN mutation, expression and LOH at its locus in ovarian carcinomas. Relation to TP53, K-RAS and BRCA1 mutations. *Gynecol Oncol*, 2006. **103**(2): p. 692-697.

68. Ahmed, A A, et al. Driver mutations in TP53 are ubiquitous in high grade serous carcinoma of the ovary. *J Pathol*, 2010. **221**(1): p. 49-56.

69. Roh, M H, et al. High-grade fimbrial-ovarian carcinomas are unified by altered p53, PTEN and PAX2 expression. *Mod Pathol*, 2010. **23**(10): p. 1316-1324.

70. Shih Ie, M and Kurman, R J. Ovarian tumorigenesis: a proposed model based on morphological and molecular genetic analysis. *Am J Pathol*, 2004. **164**(5): p. 1511-8.

71. Fukumoto, M and Nakayama, K. Ovarian epithelial tumors of low malignant potential: are they precursors of ovarian carcinoma? *Pathol Int*, 2006. **56**(5): p. 233-9.

72. Jechlinger, M, et al. Autocrine PDGFR signaling promotes mammary cancer metastasis. *The Journal of clinical investigation*, 2006. **116**(6): p. 1561-70.

73. Massague, J. TGFbeta in Cancer. *Cell*, 2008. **134**(2): p. 215-30.

74. Li, T and Jiang, S. Effect of bFGF on invasion of ovarian cancer cells through the regulation of Ets-1 and urokinase-type plasminogen activator. *Pharm Biol*, 2010. **48**(2): p. 161-5.

75. Huber, M A, Kraut, N, and Beug, H. Molecular requirements for epithelial-mesenchymal transition during tumor progression. *Curr Opin Cell Biol*, 2005. **17**(5): p. 548-58.

76. Guarino, M, Rubino, B, and Ballabio, G. The role of epithelial-mesenchymal transition in cancer pathology. *Pathology*, 2007. **39**(3): p. 305-18.

77. Eltabbakh, G H. Recent advances in the management of women with ovarian cancer. *Minerva Ginecol*, 2004. **56**(1): p. 81-9.

78. Sonoda, Y. Management of early ovarian cancer. *Oncology (Williston Park)*, 2004. **18**(3): p. 343-56.

79. Lapidot, T, et al. A cell initiating human acute myeloid leukaemia after transplantation into SCID mice. *Nature*, 1994. **367**(6464): p. 645-8.

80. Magee, J A, Piskounova, E, and Morrison, S J. Cancer stem cells: impact, heterogeneity, and uncertainty. *Cancer Cell*, 2012. **21**(3): p. 283-96.

81. Foster, R, Buckanovich, R J, and Rueda, B R. Ovarian cancer stem cells: working towards the root of stemness. *Cancer Lett*, 2013. **338**(1): p. 147-57.

82. Shah, M M and Landen, C N. Ovarian cancer stem cells: Are they real and why are they important? *Gynecol Oncol*, 2014. **132**(2): p. 483-489.

83. Bonnet, D and Dick, J E. Human acute myeloid leukemia is organized as a hierarchy that originates from a primitive hematopoietic cell. *Nat Med*, 1997. **3**(7): p. 730-7.

84. Al-Hajj, M, Wicha, M S, Benito-Hernandez, A, Morrison, S J, and Clarke, M F. Prospective identification of tumorigenic breast cancer cells. *Proc Natl Acad Sci U S A*, 2003. **100**(7): p. 3983-8.

85. Fang, D, et al. A tumorigenic subpopulation with stem cell properties in melanomas. *Cancer Res*, 2005. **65**(20): p. 9328-37.

86. Patrawala, L, et al. Highly purified CD44+ prostate cancer cells from xenograft human tumors are enriched in tumorigenic and metastatic progenitor cells. *Oncogene*, 2006. **25**(12): p. 1696-708.

87. Miralles, C, et al. Cancer antigen 125 associated with multiple benign and malignant pathologies. *Ann Surg Oncol*, 2003. **10**(2): p. 150-4.

88. Zurawski, V R, Jr., Orjaseter, H, Andersen, A, and Jellum, E. Elevated serum CA 125 levels prior to diagnosis of ovarian neoplasia: relevance for early detection of ovarian cancer. *Int J Cancer*, 1988. **42**(5): p. 677-80.

89. Bast, R C, Jr. Status of tumor markers in ovarian cancer screening. *J Clin Oncol*, 2003. **21**(10): p. 200s-205s.

90. Ferraro, S, Braga, F, Lanzoni, M, Boracchi, P, Biganzoli, E M, and Panteghini, M. Serum human epididymis protein 4 vs carbohydrate antigen 125 for ovarian cancer diagnosis: a systematic review. *Journal of clinical pathology*, 2013. **66**(4): p. 273-81.

91. Hellstrom, I, Raycraft, J, Hayden-Ledbetter, M, Ledbetter, J A, Schummer, M, McIntosh, M, Drescher, C, Urban, N, and Hellstrom, K E. The HE4 (WFDC2)

protein is a biomarker for ovarian carcinoma. *Cancer Res*, 2003. **63**(13): p. 3695-700.

92. Drapkin, R, von Horsten, H H, Lin, Y, Mok, S C, Crum, C P, Welch, W R, and Hecht, J L. Human epididymis protein 4 (HE4) is a secreted glycoprotein that is overexpressed by serous and endometrioid ovarian carcinomas. *Cancer Res*, 2005. **65**(6): p. 2162-9.

93. Moore, R G, et al. The use of multiple novel tumor biomarkers for the detection of ovarian carcinoma in patients with a pelvic mass. *Gynecol Oncol*, 2008. **108**(2): p. 402-8.

94. Huhtinen, K, et al. Serum HE4 concentration differentiates malignant ovarian tumours from ovarian endometriotic cysts. *Br J Cancer*, 2009. **100**(8): p. 1315-9.

95. Shah, C A, et al. Influence of ovarian cancer risk status on the diagnostic performance of the serum biomarkers mesothelin, HE4, and CA125. *Cancer Epidemiol Biomarkers Prev*, 2009. **18**(5): p. 1365-72.

96. Moore, R G, Miller, M C, Steinhoff, M M, Skates, S J, Lu, K H, Lambert-Messerlian, G, and Bast, R C, Jr. Serum HE4 levels are less frequently elevated than CA125 in women with benign gynecologic disorders. *Am J Obstet Gynecol*, 2012. **206**(4): p. 351 e1-8.

97. Escudero, J M, Auge, J M, Filella, X, Torne, A, Pahisa, J, and Molina, R. Comparison of serum human epididymis protein 4 with cancer antigen 125 as a tumor marker in patients with malignant and nonmalignant diseases. *Clin Chem*, 2011. **57**(11): p. 1534-44.

98. Badgwell, D, et al. Urinary mesothelin provides greater sensitivity for early stage ovarian cancer than serum mesothelin, urinary hCG free beta subunit and urinary hCG beta core fragment. *Gynecol Oncol*, 2007. **106**(3): p. 490-7.

99. Nguyen, L, Cardenas-Goicoechea, S J, Gordon, P, Curtin, C, Momeni, M, Chuang, L, and Fishman, D. Biomarkers for early detection of ovarian cancer. *Women's Health*, 2013. **9**(2): p. 171-187.

100. Slack-Davis, J K, Atkins, K A, Harrer, C, Hershey, E D, and Conaway, M. Vascular cell adhesion molecule-1 is a regulator of ovarian cancer peritoneal metastasis. *Cancer Res*, 2009. **69**(4): p. 1469-76.

101. Urieli-Shoval, S, Finci-Yeheskel, Z, Dishon, S, Galinsky, D, Linke, R P, Ariel, I, Levin, M, Ben-Shachar, I, and Prus, D. Expression of serum amyloid a in human ovarian epithelial tumors: implication for a role in ovarian tumorigenesis. *J Histochem Cytochem*, 2010. **58**(11): p. 1015-23.

102. Scambia, G, et al. Prognostic significance of interleukin 6 serum levels in patients with ovarian cancer. *Br J Cancer*, 1995. **71**(2): p. 354-6.

103. Moshkovskii, S A, Vlasova, M A, Pyatnitskiy, M A, Tikhonova, O V, Safarova, M R, Makarov, O V, and Archakov, A I. Acute phase serum amyloid A in ovarian cancer as an important component of proteome diagnostic profiling. *Proteomics Clin Appl*, 2007. **1**(1): p. 107-17.

104. Edgell, T, Martin-Roussety, G, Barker, G, Autelitano, D J, Allen, D, Grant, P, and Rice, G E. Phase II biomarker trial of a multimarker diagnostic for ovarian cancer. *J Cancer Res Clin Oncol*, 2010. **136**(7): p. 1079-88.

105. Yurkovetsky, Z, et al. Development of a multimarker assay for early detection of ovarian cancer. *J Clin Oncol*, 2010. **28**(13): p. 2159-66.

106. Sharma, A, et al. Risk of epithelial ovarian cancer in asymptomatic women with ultrasound-detected ovarian masses: a prospective cohort study within the UK collaborative trial of ovarian cancer screening (UKCTOCS). *Ultrasound Obstet Gynecol*, 2012. **40**(3): p. 338-44.

107. Mohaghegh, P and Rockall, A G. Imaging strategy for early ovarian cancer: characterization of adnexal masses with conventional and advanced imaging techniques. *Radiographics*, 2012. **32**(6): p. 1751-73.

108. Bharwani, N, Reznek, R H, and Rockall, A G. Ovarian Cancer Management: the role of imaging and diagnostic challenges. *Eur J Radiol*, 2011. **78**(1): p. 41-51.

109. Basu, S, Kwee, T C, Surti, S, Akin, E A, Yoo, D, and Alavi, A. Fundamentals of PET and PET/CT imaging. *Ann N Y Acad Sci*, 2011. **1228**: p. 1-18.

110. Wadas, T J, Wong, E H, Weisman, G R, and Anderson, C J. Coordinating Radiometals of Copper, Gallium, Indium, Yttrium, and Zirconium for PET and SPECT Imaging of Disease. *Chem. Rev.*, 2010. **110**(5): p. 2858-2902.

111. Sandler, M P. Diagnostic nuclear medicine. 4th ed 2003, Philadelphia: *Lippincott/Williams & Wilkins*.

112. Iyer, R B, Balachandran, A, and Devine, C E. PET/CT and cross sectional imaging of gynecologic malignancy. *Cancer Imaging*, 2007. **7**: p. S130-8.

113. Nishizawa, S, Inubushi, M, Ozawa, F, Kido, A, and Okada, H. Physiological FDG uptake in the ovaries after hysterectomy. *Ann Nucl Med*, 2007. **21**(6): p. 345-8.

114. Zhu, Z H, Cheng, W Y, Cheng, X, and Dang, Y H. Characteristics of physiological uptake of uterus and ovaries on 18F-fluorodeoxyglucose positron emission tomography. *Zhongguo Yi Xue Ke Xue Yuan Xue Bao*, 2007. **29**(1): p. 124-9.

115. Nortier, F M, Mills, S J, and Steyn, G F. Excitation functions and production rates of relevance to the production of 111In by proton bombardment of natCd and natIn up to 100 MeV. *Int J Radiat Appl Instrum*, 1990. **41**(12): p. 1201-1208.

116. Vallabhajosula, S. Molecular imaging: radiopharmaceuticals for PET and SPECT 2009, Berlin; New York: *Springer-Verlag*.

117. Heskamp, S, Laverman, P, Rosik, D, Boschetti, F, van der Graaf, W T A, Oyen, W J G, van Laarhoven, H W M, Tolmachev, V, and Boerman, O C. Imaging of Human Epidermal Growth Factor Receptor Type 2 Expression with 18F-Labeled Affibody Molecule ZHER2:2395 in a Mouse Model for Ovarian Cancer. *J Nucl Med*, 2012. **53**(1): p. 146-153.

118. Kelly, K A, Nahrendorf, M, Yu, A M, Reynolds, F, and Weissleder, R. In vivo phage display selection yields atherosclerotic plaque targeted peptides for imaging. *Mol Imaging Biol*, 2006. **8**(4): p. 201-7.

119. Nahrendorf, M, Jaffer, F A, Kelly, K A, Sosnovik, D E, Aikawa, E, Libby, P, and Weissleder, R. Noninvasive vascular cell adhesion molecule-1 imaging identifies

inflammatory activation of cells in atherosclerosis. *Circulation*, 2006. **114**(14): p. 1504-11.

120. Nahrendorf, M, et al. 18F-4V for PET-CT imaging of VCAM-1 expression in atherosclerosis. *JACC. Cardiovascular imaging*, 2009. **2**(10): p. 1213-22.

121. Scalici, J M, et al. Imaging VCAM-1 as an Indicator of Treatment Efficacy in Metastatic Ovarian Cancer. *J Nucl Med*, 2013.

122. Hilderbrand, S A and Weissleder, R. Near-infrared fluorescence: application to in vivo molecular imaging. *Curr Opin Chem Biol*, 2010. **14**(1): p. 71-9.

123. Aina, O H, Marik, J, Gandour-Edwards, R, and Lam, K S. Near-infrared optical imaging of ovarian cancer xenografts with novel alpha 3-integrin binding peptide "OA02". *Mol Imaging*, 2005. **4**(4): p. 439-47.

124. Pysz, M A, Gambhir, S S, and Willmann, J K. Molecular imaging: current status and emerging strategies. *Clinical radiology*, 2010. **65**(7): p. 500-16.

125. Corbin, I R, Ng, K K, Ding, L, Jurisicova, A, and Zheng, G. Near-infrared fluorescent imaging of metastatic ovarian cancer using folate receptor-targeted high-density lipoprotein nanocarriers. *Nanomedicine*, 2012. **8**(6): p. 875-890.

126. Lim, M C, Seo, S-S, Kang, S, Kim, S K, Kim, S H, Yoo, C W, and Park, S-Y. Intraoperative image-guided surgery for ovarian cancer. *Quant Imaging Med Surg*, 2012. **2**(2): p. 114-117.

127. van Dam, G M, et al. Intraoperative tumor-specific fluorescence imaging in ovarian cancer by folate receptor-alpha targeting: first in-human results. *Nat Med*, 2011. **17**(10): p. 1315-9.

128. Heintz, A P, Odicino, F, Maisonneuve, P, Quinn, M A, Benedet, J L, Creasman, W T, Ngan, H Y, Pecorelli, S, and Beller, U. Carcinoma of the ovary. FIGO 26th Annual Report on the Results of Treatment in Gynecological Cancer. *Int J Gynaecol Obstet*, 2006. **95**(1): p. S161-92.

129. Piccart, M J, et al. Randomized intergroup trial of cisplatin-paclitaxel versus cisplatin-cyclophosphamide in women with advanced epithelial ovarian cancer: three-year results. *J Natl Cancer Inst*, 2000. **92**(9): p. 699-708.

130. Bookman, M A, et al. Evaluation of new platinum-based treatment regimens in advanced-stage ovarian cancer: a Phase III Trial of the Gynecologic Cancer Intergroup. *J Clin Oncol*, 2009. **27**(9): p. 1419-25.

131. Kigawa, J. New strategy for overcoming resistance to chemotherapy of ovarian cancer. *Yonago Acta Med*, 2013. **56**(2): p. 43-50.

132. Eric Pujade-Lauraine, F H, Béatrice Weber, Alexander Reuss, Andres Poveda, Gunnar Kristensen, Roberto Sorio, Ignace B. Vergote, Petronella Witteveen, Aristotelis Bamias, Deolinda Pereira, Pauline Wimberger, Ana Oaknin, Mansoor Raza Mirza, Philippe Follana, David T. Bollag, Isabelle Ray-Coquard. AURELIA: A randomized phase III trial evaluating bevacizumab (BEV) plus chemotherapy (CT) for platinum (PT)-resistant recurrent ovarian cancer (OC). in *J Clin Oncol 30*2012.

133. Romero, I and Bast, R C, Jr. Minireview: human ovarian cancer: biology, current management, and paths to personalizing therapy. *Endocrinology*, 2012. **153**(4): p. 1593-602.

134. Audeh, M W, et al. Oral poly(ADP-ribose) polymerase inhibitor olaparib in patients with BRCA1 or BRCA2 mutations and recurrent ovarian cancer: a proof-of-concept trial. *The Lancet*. **376**(9737): p. 245-251.

135. Naumann, R W, et al. PRECEDENT: a randomized phase II trial comparing vintafolide (EC145) and pegylated liposomal doxorubicin (PLD) in combination versus PLD alone in patients with platinum-resistant ovarian cancer. *J Clin Oncol*, 2013. **31**(35): p. 4400-6.

136. Zalutsky, M R and Bigner, D D. Radioimmunotherapy with alpha-particle emitting radioimmunoconjugates. *Acta Oncol*, 1996. **35**(3): p. 373-9.

137. McDevitt, M R, Sgouros, G, Finn, R D, Humm, J L, Jurcic, J G, Larson, S M, and Scheinberg, D A. Radioimmunotherapy with alpha-emitting nuclides. *Eur J Nucl Med*, 1998. **25**(9): p. 1341-51.

138. Larsen, R H, Akabani, G, Welsh, P, and Zalutsky, M R. The cytotoxicity and microdosimetry of astatine-211-labeled chimeric monoclonal antibodies in human glioma and melanoma cells in vitro. *Radiat Res*, 1998. **149**(2): p. 155-62.

139. Friesen, C, Glatting, G, Koop, B, Schwarz, K, Morgenstern, A, Apostolidis, C, Debatin, K M, and Reske, S N. Breaking chemoresistance and radioresistance with [213Bi]anti-CD45 antibodies in leukemia cells. *Cancer Res*, 2007. **67**(5): p. 1950-8.

140. Kassis, A I. Radiotargeting agents for cancer therapy. *Expert Opin Drug Deliv*, 2005. **2**(6): p. 981-91.

141. Wild, D, Frischknecht, M, Zhang, H, Morgenstern, A, Bruchertseifer, F, Boisclair, J, Provencher-Bolliger, A, Reubi, J-C, and Maecke, H R. Alpha- versus Beta-Particle Radiopeptide Therapy in a Human Prostate Cancer Model (213Bi-DOTA-PESIN and 213Bi-AMBA versus177Lu-DOTA-PESIN). *Cancer Res*, 2011. **71**(3): p. 1009-1018.

142. O'Donoghue, J A and Wheldon, T E. Targeted radiotherapy using Auger electron emitters. *Phys Med Biol*, 1996. **41**(10): p. 1973-92.

143. Boswell, C A and Brechbiel, M W. Auger electrons: lethal, low energy, and coming soon to a tumor cell nucleus near you. *J Nucl Med*, 2005. **46**(12): p. 1946-7.

144. Heyerdahl, H, Abbas, N, Sponheim, K, Mollatt, C, Bruland, O, and Dahle, J. Targeted alpha therapy with 227Th-trastuzumab of intraperitoneal ovarian cancer in nude mice. *Curr Radiopharm*, 2013. **6**(2): p. 106-16.

145. Alvarez, R D, et al. A Phase I study of combined modality (90)Yttrium-CC49 intraperitoneal radioimmunotherapy for ovarian cancer. *Clin Cancer Res*, 2002. **8**(9): p. 2806-11.

146. Mamede, M, Saga, T, Kobayashi, H, Ishimori, T, Higashi, T, Sato, N, Brechbiel, M W, and Konishi, J. Radiolabeling of avidin with very high specific activity for internal radiation therapy of intraperitoneally disseminated tumors. *Clin Cancer Res*, 2003. **9**(10 Pt 1): p. 3756-62.

147. Newton, J R and Deutscher, S L. In vivo bacteriophage display for the discovery of novel peptide-based tumor-targeting agents. *Methods Mol Biol*, 2009. **504**: p. 275-90.

148. Armstrong, J, Perham, R N, and Walker, J E. Domain structure of bacteriophage fd adsorption protein. *FEBS Lett*, 1981. **135**(1): p. 167-72.

149. Gray, C W, Brown, R S, and Marvin, D A. Adsorption complex of filamentous fd virus. *J Mol Biol*, 1981. **146**(4): p. 621-7.

150. Crissman, J W and Smith, G P. Gene-III protein of filamentous phages: evidence for a carboxyl-terminal domain with a role in morphogenesis. *Virology*, 1984. **132**(2): p. 445-55.

151. Karasseva, N G, Glinsky, V V, Chen, N X, Komatireddy, R, and Quinn, T P. Identification and characterization of peptides that bind human ErbB-2 selected from a bacteriophage display library. *J Protein Chem*, 2002. **21**(4): p. 287-96.

152. Arap, W, Pasqualini, R, and Ruoslahti, E. Cancer treatment by targeted drug delivery to tumor vasculature in a mouse model. *Science*, 1998. **279**(5349): p. 377-80.

153. Chen, X, Sievers, E, Hou, Y, Park, R, Tohme, M, Bart, R, Bremner, R, Bading, J R, and Conti, P S. Integrin alpha v beta 3-targeted imaging of lung cancer. *Neoplasia*, 2005. **7**(3): p. 271-9.

154. Ploug, M, Ostergaard, S, Gardsvoll, H, Kovalski, K, Holst-Hansen, C, Holm, A, Ossowski, L, and Dano, K. Peptide-derived antagonists of the urokinase receptor. affinity maturation by combinatorial chemistry, identification of functional epitopes, and inhibitory effect on cancer cell intravasation. *Biochemistry*, 2001. **40**(40): p. 12157-68.

155. Carter, P, et al. Humanization of an anti-p185HER2 antibody for human cancer therapy. *Proc Natl Acad Sci U S A*, 1992. **89**(10): p. 4285-9.

156. Frederick, P J, Straughn Jr, J M, Alvarez, R D, and Buchsbaum, D J. Preclinical studies and clinical utilization of monoclonal antibodies in epithelial ovarian cancer. *Gynecologic Oncology*, 2009. **113**(3): p. 384-390.

157. Lub-de Hooge, M N, et al. Preclinical characterisation of 111In-DTPA-trastuzumab. *Br J Pharmacol*, 2004. **143**(1): p. 99-106.

158. Klastersky, J. Adverse effects of the humanized antibodies used as cancer therapeutics. *Curr Opin Oncol*, 2006. **18**(4): p. 316-20.

159. Bakker, W H, et al. In vivo application of [111In-DTPA-D-Phe1]-octreotide for detection of somatostatin receptor-positive tumors in rats. *Life Sci*, 1991. **49**(22): p. 1593-601.

160. Miao, Y, Benwell, K, and Quinn, T P. 99mTc- and 111In-labeled alpha-melanocyte-stimulating hormone peptides as imaging probes for primary and pulmonary metastatic melanoma detection. *J Nucl Med*, 2007. **48**(1): p. 73-80.

161. McQuade, P, Miao, Y, Yoo, J, Quinn, T P, Welch, M J, and Lewis, J S. Imaging of melanoma using 64Cu- and 86Y-DOTA-ReCCMSH(Arg11), a cyclized peptide analogue of alpha-MSH. *J Med Chem*, 2005. **48**(8): p. 2985-92.

162. Wei, L, Miao, Y, Gallazzi, F, Quinn, T P, Welch, M J, Vavere, A L, and Lewis, J S. Gallium-68-labeled DOTA-rhenium-cyclized alpha-melanocyte-stimulating hormone analog for imaging of malignant melanoma. *Nucl Med Biol*, 2007. **34**(8): p. 945-53.

163. Deutscher, S L, Figueroa, S D, and Kumar, S R. In-labeled KCCYSL peptide as an imaging probe for ErbB-2-expressing ovarian carcinomas. *J Labelled Comp Radiopharm*, 2009. **52**(14): p. 583-590.

164. Haisma, H J, Moseley, K R, Battaile, A I, Griffiths, T C, Zurawski, V R, and Knapp, R C. Biodistribution, pharmacokinetics and imaging of 131I-labelled OC125 in ovarian cancer. *Int J Cancer*, 1988. **41**(S2): p. 109-113.

165. Lam, K S, Aina, O, Peng, L, Liu, R, Marik, J, Cherry, S, and Sutcliffe-Goulden, J. Highly specific targeting peptides for imaging and therapy of lymphoma and ovarian cancer, in *AACR Meeting Abstracts*2005. p. 1244.

166. Dijkgraaf, I, Kruijtzer, J A, Frielink, C, Corstens, F H, Oyen, W J, Liskamp, R M, and Boerman, O C. Alpha v beta 3 integrin-targeting of intraperitoneally growing tumors with a radiolabeled RGD peptide. *Int J Cancer*, 2007. **120**(3): p. 605-10.

167. Society, A C. Cancer Facts and Figures 2014. 2014. Accessed Accessed February 24th, **2014**; http://www.cancer.org/acs/groups/content/@research/documents/document/acspc-041770.pdf.

168. Bast, R C, Jr. Early detection of ovarian cancer: new technologies in pursuit of a disease that is neither common nor rare. *Trans Am Clin Climatol Assoc*, 2004. **115**: p. 233-47.

169. Peletskaya, E N, Glinsky, V V, Glinsky, G V, Deutscher, S L, and Quinn, T P. Characterization of peptides that bind the tumor-associated Thomsen-Friedenreich antigen selected from bacteriophage display libraries. *J Mol Biol*, 1997. **270**: p. 374-84.

170. Leinonen, J, Wu, P, Koivunen, E, Narvanen, A, and Stenman, U H. Development of novel peptide ligands modulating the enzyme activity of prostate-specific antigen. *Scand J Clin Lab Invest Suppl*, 2000. **233**: p. 59-64.

171. Hao, J, Serohijos, A W, Newton, G, Tassone, G, Wang, Z, Sgroi, D C, Dokholyan, N V, and Basilion, J P. Identification and rational redesign of peptide ligands to CRIP1, a novel biomarker for cancers. *PLoS Comput Biol*, 2008. **4**(8): p. e1000138.

172. Koistinen, H, Narvanen, A, Pakkala, M, Hekim, C, Mattsson, J M, Zhu, L, Laakkonen, P, and Stenman, U H. Development of peptides specifically modulating the activity of KLK2 and KLK3. *Biol Chem*, 2008. **389**(6): p. 633-42.

173. Landon, L A, Zou, J, and Deutscher, S L. Is phage display technology on target for developing peptide-based cancer drugs? *Curr Drug Discov Technol*, 2004. **1**(2): p. 113-32.

174. Newton, J R and Deutscher, S L. Molecular targets and biomarkers for imaging cancer: Phage peptide display. Vol. Molecular Imaging. 2006: *Springer-Verlag: Berlin*.

175. Arap, W, et al. Steps toward mapping the human vasculature by phage display. *Nat Med*, 2002. **8**(2): p. 121-7.

176. Essler, M and Ruoslahti, E. Molecular specialization of breast vasculature: a breast-homing phage-displayed peptide binds to aminopeptidase P in breast vasculature. *Proc Natl Acad Sci*, 2002. **99**(4): p. 2252-7.

177. Yao, V J, Ozawa, M G, Trepel, M, Arap, W, McDonald, D M, and Pasqualini, R. Targeting pancreatic islets with phage display assisted by laser pressure catapult microdissection. *Am J Pathol*, 2005. **166**(2): p. 625-36.

178. Smith, G P. G. P. Smith Lab Homepage. 2006. Accessed 2/26/2014; http://www.biosci.missouri.edu/smithGP/PhageDisplayWebsite/PhageDisplayWebsiteIndex.html.

179. Bast Jr, R C, Siegal, F P, Runowicz, C, Klug, T L, Zurawski Jr, V R, Schonholz, D, Cohen, C J, and Knapp, R C. Elevation of serum CA 125 prior to diagnosis of an epithelial ovarian carcinoma. *Gynecol Oncol*, 1985. **22**(1): p. 115-120.

180. Hung, M C, Zhang, X, Yan, D H, Zhang, H Z, He, G P, Zhang, T Q, and Shi, D R. Aberrant expression of the c-erbB-2/neu protooncogene in ovarian cancer. *Cancer Lett*, 1992. **61**(2): p. 95-103.

181. Went, P T, Lugli, A, Meier, S, Bundi, M, Mirlacher, M, Sauter, G, and Dirnhofer, S. Frequent EpCam protein expression in human carcinomas. *Hum Pathol*, 2004. **35**(1): p. 122-8.

182. Abramoff, M D, Magalhaes, P.J., Ram, S.J. . Image Processing with ImageJ. *Biophotonics Int.*, 2004. **11**(7): p. 36-42.

183. Vegt, E, de Jong, M, Wetzels, J F M, Masereeuw, R, Melis, M, Oyen, W J G, Gotthardt, M, and Boerman, O C. Renal Toxicity of Radiolabeled Peptides and Antibody Fragments: Mechanisms, Impact on Radionuclide Therapy, and Strategies for Prevention. *J Nucl Med*, 2010. **51**(7): p. 1049-1058.

184. Cannistra, S A. Cancer of the ovary. *N Engl J Med*, 2004. **351**(24): p. 2519-29.

185. Moss, E L, Hollingworth, J, and Reynolds, T M. The role of CA125 in clinical practice. *Journal of clinical pathology*, 2005. **58**(3): p. 308-12.

186. Gorelik, E, Landsittel, D P, Marrangoni, A M, Modugno, F, Velikokhatnaya, L, Winans, M T, Bigbee, W L, Herberman, R B, and Lokshin, A E. Multiplexed immunobead-based cytokine profiling for early detection of ovarian cancer. *Cancer Epidemiol Biomarkers Prev*, 2005. **14**(4): p. 981-7.

187. Fujiwaki, R, Hata, T, Miyazaki, K, Kawamura, T, and Inada, K. Elevation of serum interleukin-1 receptor antagonist levels in women with gynaecological cancers. *British journal of obstetrics and gynaecology*, 1997. **104**(12): p. 1407-8.

188. Su, Z, Graybill, W S, and Zhu, Y. Detection and monitoring of ovarian cancer. *Clin Chim Acta*, 2013. **415**: p. 341-5.

189. Peletskaya, E N, Glinsky, G, Deutscher, S L, and Quinn, T P. Identification of peptide sequences that bind the Thomsen-Friedenreich cancer-associated glycoantigen from bacteriophage peptide display libraries. *Mol Divers*, 1996. **2**(1-2): p. 13-8.

190. Houimel, M, Schneider, P, Terskikh, A, and Mach, J P. Selection of peptides and synthesis of pentameric peptabody molecules reacting specifically with ErbB-2 receptor. *Int J Cancer*, 2001. **92**(5): p. 748-55.

191. Urbanelli, L, Ronchini, C, Fontana, L, Menard, S, Orlandi, R, and Monaci, P. Targeted gene transduction of mammalian cells expressing the HER2/neu receptor by filamentous phage. *J Mol Biol*, 2001. **313**(5): p. 965-76.

192. Pakkala, M, Jylhasalmi, A, Wu, P, Leinonen, J, Stenman, U H, Santa, H, Vepsalainen, J, Perakyla, M, and Narvanen, A. Conformational and biochemical analysis of the cyclic peptides which modulate serine protease activity. *J Pept Sci*, 2004. **10**(7): p. 439-47.

193. Kelly, K A, Waterman, P, and Weissleder, R. In vivo imaging of molecularly targeted phage. *Neoplasia*, 2006. **8**(12): p. 1011-8.

194. Witt, H, Hajdin, K, Iljin, K, Greiner, O, Niggli, F K, Schafer, B W, and Bernasconi, M. Identification of a rhabdomyosarcoma targeting peptide by phage display with sequence similarities to the tumour lymphatic-homing peptide LyP-1. *Int J Cancer*, 2009. **124**(9): p. 2026-32.

195. Koolpe, M, Dail, M, and Pasquale, E B. An ephrin mimetic peptide that selectively targets the EphA2 receptor. *J Biol Chem*, 2002. **277**(49): p. 46974-9.

196. Pasqualini, R and Ruoslahti, E. Organ targeting in vivo using phage display peptide libraries. *Nature*, 1996. **380**(6572): p. 364-6.

197. Rajotte, D, Arap, W, Hagedorn, M, Koivunen, E, Pasqualini, R, and Ruoslahti, E. Molecular heterogeneity of the vascular endothelium revealed by in vivo phage display. *The Journal of clinical investigation*, 1998. **102**(2): p. 430-7.

198. Ludtke, J J, Sololoff, A V, Wong, S C, Zhang, G, and Wolff, J A. In vivo selection and validation of liver-specific ligands using a new T7 phage peptide display system. *Drug delivery*, 2007. **14**(6): p. 357-69.

199. Chen, X, Park, R, Tohme, M, Shahinian, A H, Bading, J R, and Conti, P S. MicroPET and autoradiographic imaging of breast cancer alpha v-integrin expression using 18F- and 64Cu-labeled RGD peptide. *Bioconjug Chem*, 2004. **15**(1): p. 41-9.

200. Liu, S, Hsieh, W Y, Jiang, Y, Kim, Y S, Sreerama, S G, Chen, X, Jia, B, and Wang, F. Evaluation of a (99m)Tc-labeled cyclic RGD tetramer for noninvasive imaging integrin alpha(v)beta3-positive breast cancer. *Bioconjug Chem*, 2007. **18**(2): p. 438-46.

201. Ma, C, Yin, G, Yan, D, He, X, Zhang, L, Wei, Y, and Huang, Z. A novel peptide specifically targeting ovarian cancer identified by in vivo phage display. *J Pept Sci*, 2013: p. 730-736.

202. Choi, J H, Choi, K C, Auersperg, N, and Leung, P C. Gonadotropins upregulate the epidermal growth factor receptor through activation of mitogen-activated protein kinases and phosphatidyl-inositol-3-kinase in human ovarian surface epithelial cells. *Endocr Relat Cancer*, 2005. **12**(2): p. 407-21.

203. Holliger, P, Riechmann, L, and Williams, R L. Crystal structure of the two N-terminal domains of g3p from filamentous phage fd at 1.9 A: evidence for conformational lability. *J Mol Biol*, 1999. **288**(4): p. 649-57.

204. Kommareddy, S and Amiji, M. Biodistribution and pharmacokinetic analysis of long-circulating thiolated gelatin nanoparticles following systemic administration in breast cancer-bearing mice. *Journal of pharmaceutical sciences*, 2007. **96**(2): p. 397-407.

205. Alexis, F, Pridgen, E, Molnar, L K, and Farokhzad, O C. Factors affecting the clearance and biodistribution of polymeric nanoparticles. *Mol Pharm*, 2008. **5**(4): p. 505-15.

206. Yip, Y L, Hawkins, N J, Smith, G, and Ward, R L. Biodistribution of filamentous phage-Fab in nude mice. *J Immunol Methods*, 1999. **225**(1-2): p. 171-8.

207. Zou, J, Dickerson, M T, Owen, N K, Landon, L A, and Deutscher, S L. Biodistribution of filamentous phage peptide libraries in mice. *Mol Biol Rep*, 2004. **31**(2): p. 121-9.

208. Smith, M W, Al-Jayyoussi, G, and Gumbleton, M. Peptide sequences mediating tropism to intact blood-brain barrier: an in vivo biodistribution study using phage display. *Peptides*, 2012. **38**(1): p. 172-80.

209. Pardridge, W M. The blood-brain barrier: bottleneck in brain drug development. *NeuroRx.*, 2005. **2**(1): p. 3-14.

210. Jain, R K. Delivery of molecular and cellular medicine to solid tumors. *J Control Release*, 1998. **53**(1-3): p. 49-67.

211. Ross, J F, Chaudhuri, P K, and Ratnam, M. Differential regulation of folate receptor isoforms in normal and malignant tissues in vivo and in established cell lines. Physiologic and clinical implications. *Cancer*, 1994. **73**(9): p. 2432-2443.

212. Went, P T H, Lugli, A, Meier, S, Bundi, M, Mirlacher, M, Sauter, G, and Dirnhofer, S. Frequent EpCam protein expression in human carcinomas. *Human Pathol*, 2004. **35**(1): p. 122-128.

213. Woods, A S. The Mighty Arginine, the Stable Quaternary Amines, the Powerful Aromatics, and the Aggressive Phosphate: Their Role in the Noncovalent Minuet. *J Proteome Res*, 2004. **3**(3): p. 478-484.

214. Gallivan, J P and Dougherty, D A. Cation-pi interactions in structural biology. *Proc Natl Acad Sci U S A*, 1999. **96**(17): p. 9459-64.

215. Zhu, W-L, Tan, X-J, Puah, C M, Gu, J-D, Jiang, H-L, Chen, K-X, Felder, C E, Silman, I, and Sussman, J L. How Does Ammonium Interact with Aromatic Groups? A Density Functional Theory (DFT/B3LYP) Investigation. *J Phys Chem A*, 2000. **104**(42): p. 9573-9580.

216. Rensing, S, Arendt, M, Springer, A, Grawe, T, and Schrader, T. Optimization of a synthetic arginine receptor. Systematic tuning of noncovalent interactions. *The Journal of organic chemistry*, 2001. **66**(17): p. 5814-21.

217. Sereda, T J, Mant, C T, Sönnichsen, F D, and Hodges, R S. Reversed-phase chromatography of synthetic amphipathic α-helical peptides as a model for ligand/receptor interactions Effect of changing hydrophobic environment on the relative hydrophilicity/hydrophobicity of amino acid side-chains. *J Chromatogr A*, 1994. **676**(1): p. 139-153.

218. Mant, C T, Kovacs, J M, Kim, H M, Pollock, D D, and Hodges, R S. Intrinsic amino acid side-chain hydrophilicity/hydrophobicity coefficients determined by reversed-phase high-performance liquid chromatography of model peptides: comparison with other hydrophilicity/hydrophobicity scales. *Biopolymers*, 2009. **92**(6): p. 573-595.

219. Kerr, P G. Brenner and Rector's The Kidney (in 2 volumes). *Nephrology*, 2008. **13**(3): p. 267-267.

220. Wessels, B W, et al. MIRD pamphlet No. 20: the effect of model assumptions on kidney dosimetry and response--implications for radionuclide therapy. *J Nucl Med*, 2008. **49**(11): p. 1884-99.

221. Behr, T M, Goldenberg, D M, and Becker, W. Reducing the renal uptake of radiolabeled antibody fragments and peptides for diagnosis and therapy: present status, future prospects and limitations. *Eur J Nucl Med*, 1998. **25**(2): p. 201-12.

222. Bakker, W H, et al. [111In-DTPA-D-Phe1]-octreotide, a potential radiopharmaceutical for imaging of somatostatin receptor-positive tumors: synthesis, radiolabeling and in vitro validation. *Life Sci*, 1991. **49**(22): p. 1583-91.

223. Krenning, E P, et al. Somatostatin receptor scintigraphy with [111In-DTPA-D-Phe1]- and [123I-Tyr3]-octreotide: the Rotterdam experience with more than 1000 patients. *Eur J Nucl Med*, 1993. **20**(8): p. 716-31.

224. Hosseinimehr, S J, Tolmachev, V, and Orlova, A. Liver uptake of radiolabeled targeting proteins and peptides: considerations for targeting peptide conjugate design. *Drug Discov Today*, 2012. **17**(21–22): p. 1224-1232.

225. Bahmani, B, Guerrero, Y, Vullev, V, Singh, S P, Kundra, V, and Anvari, B. ICG-loaded polymeric nanocapsules functionalized with anti-HER2 for targeted fluorescence imaging and photodestruction of ovarian cancer cells, in *SPIE Proceedings Reporters, Markers, Dyes, Nanoparticles, and Molecular Probes for Biomedical Applications*2013. p. 859602-859602-5.

226. Granowska, M, Britton, K E, Shepherd, J H, Nimmon, C C, Mather, S, Ward, B, Osborne, R J, and Slevin, M L. A prospective study of 123I-labeled monoclonal antibody imaging in ovarian cancer. *J Clin Oncol*, 1986. **4**(5): p. 730-6.

227. Kranenburg, D L, Kroonenburgh, M J P G, Trimbos, J B, Fleuren, G J, and Pauwels, E K J. Imaging of ovarian cancer with radiolabelled monoclonal antibodies. *Arch Gynecol Obstet*, 1990. **247**(3): p. 107-116.

228. Peltier, P, et al. Usefulness of imaging ovarian cancer recurrence with In-111-labeled monoclonal antibody (OC125) specific for CA125 antigen. *Annals of Oncology*, 1993. **4**(4): p. 307-311.

229. Orlova, A, et al. Tumor Imaging Using a Picomolar Affinity HER2 Binding Affibody Molecule. *Cancer Res*, 2006. **66**(8): p. 4339-4348.

230. Shahbazi-Gahrouei, D and Abdolahi, M. Detection of MUC1-Expressing Ovarian Cancer by C595 Monoclonal Antibody-Conjugated SPIONs Using MR Imaging. *The Scientific World J*, 2013. **2013**: p. 7.

231. Hama, Y, Urano, Y, Koyama, Y, Gunn, A J, Choyke, P L, and Kobayashi, H. A Self-Quenched Galactosamine-Serum Albumin-RhodamineX Conjugate: A "Smart" Fluorescent Molecular Imaging Probe Synthesized with Clinically Applicable Material for Detecting Peritoneal Ovarian Cancer Metastases. *Clinical Cancer Research*, 2007. **13**(21): p. 6335-6343.

232. Kosaka, N, Ogawa, M, Longmire, M R, Choyke, P L, and Kobayashi, H. Multi-targeted multi-color in vivo optical imaging in a model of disseminated peritoneal ovarian cancer. *BIOMEDO*, 2009. **14**(1): p. 014023-014023-8.

233. Alexander, V M, Sano, K, Yu, Z, Nakajima, T, Choyke, P L, Ptaszek, M, and Kobayashi, H. Galactosyl Human Serum Albumin-NMP1 Conjugate: A Near Infrared (NIR)-Activatable Fluorescence Imaging Agent to Detect Peritoneal Ovarian Cancer Metastases. *Bioconjugate Chem*, 2012. **23**(8): p. 1671-1679.

234. Zavaleta, C L, Goins, B A, Bao, A, McManus, L M, McMahan, C A, and Phillips, W T. Imaging of 186Re-liposome therapy in ovarian cancer xenograft model of peritoneal carcinomatosis. *J Drug Target*, 2008. **16**(7): p. 626-37.

235. Kumar, S R and Deutscher, S L. Galectin-3-Targeting Peptides as Novel In Vivo tumor-Imaging and Targeting Agents., in *Tumor Microvasculature Environment AACR Meeting*2006, AACR: Florence, Italy.

236. Ding, H, Prodinger, W M, and Kopecek, J. Identification of CD21-binding peptides with phage display and investigation of binding properties of HPMA copolymer-peptide conjugates. *Bioconjug Chem*, 2006. **17**(2): p. 514-23.

237. Du, B, Qian, M, Zhou, Z, Wang, P, Wang, L, Zhang, X, Wu, M, Zhang, P, and Mei, B. In vitro panning of a targeting peptide to hepatocarcinoma from a phage display peptide library. *Biochem Biophys Res Commun*, 2006. **342**(3): p. 956-62.

238. Zang, L, Shi, L, Guo, J, Pan, Q, Wu, W, Pan, X, and Wang, J. Screening and identification of a peptide specifically targeted to NCI-H1299 from a phage display peptide library. *Cancer Lett*, 2009. **281**(1): p. 64-70.

239. Abbineni, G, Modali, S, Safiejko-Mroczka, B, Petrenko, V A, and Mao, C. Evolutionary Selection of New Breast Cancer Cell-Targeting Peptides and Phages with the Cell-Targeting Peptides Fully Displayed on the Major Coat and Their Effects on Actin Dynamics during Cell Internalization. *Mol Pharm*, 2010.

240. Segers, J, Laumonier, C, Burtea, C, Laurent, S, Elst, L V, and Muller, R N. From phage display to magnetophage, a new tool for magnetic resonance molecular imaging. *Bioconjug Chem*, 2007. **18**(4): p. 1251-8.

241. Li, Z, et al. Trackable and Targeted Phage as Positron Emission Tomography (PET) Agent for Cancer Imaging. *Theranostics*, 2011. **1**: p. 371-80.

242. Yacoby, I, Shamis, M, Bar, H, Shabat, D, and Benhar, I. Targeting antibacterial agents by using drug-carrying filamentous bacteriophages. *Antimicrob Agents Chemother*, 2006. **50**(6): p. 2087-97.

243. Ghosh, D, Kohli, A G, Moser, F, Endy, D, and Belcher, A M. Refactored M13 Bacteriophage as a Platform for Tumor Cell Imaging and Drug Delivery. *ACS Synth Biol*, 2012. **1**(12): p. 576-582.

244. Mount, J D, Samoylova, T I, Morrison, N E, Cox, N R, Baker, H J, and Petrenko, V A. Cell targeted phagemid rescued by preselected landscape phage. *Gene*, 2004. **341**: p. 59-65.

245. Staquicini, F I, Sidman, R L, Arap, W, and Pasqualini, R. Phage display technology for stem cell delivery and systemic therapy. *Adv Drug Deliv Rev*, 2010. **62**(12): p. 1213-6.

246. Altschul, S F, Madden, T L, Schaffer, A A, Zhang, J, Zhang, Z, Miller, W, and Lipman, D J. Gapped BLAST and PSI-BLAST: a new generation of protein database search programs. *Nucleic Acids Res.*, 1997. **25**(17): p. 3389-402.

247. Shtatland, T, Guettler, D, Kossodo, M, Pivovarov, M, and Weissleder, R. PepBank - a database of peptides based on sequence text mining and public peptide data sources. *BMC Bioinformatics*, 2007. **8**(1): p. 280.

248. Rakonjac, J, Bennett, N J, Spagnuolo, J, Gagic, D, and Russel, M. Filamentous bacteriophage: biology, phage display and nanotechnology applications. *Curr Issues Mol Biol*, 2011. **13**(2): p. 51-76.

249. Spear, M A, Breakefield, X O, Beltzer, J, Schuback, D, Weissleder, R, Pardo, F S, and Ladner, R. Isolation, characterization, and recovery of small peptide phage display epitopes selected against viable malignant glioma cells. *Cancer gene therapy*, 2001. **8**(7): p. 506-11.

250. Adey, N B, Mataragnon, A H, Rider, J E, Carter, J M, and Kay, B K. Characterization of phage that bind plastic from phage-displayed random peptide libraries. *Gene*, 1995. **156**(1): p. 27-31.

251. Tavassoli, F A D P. Pathology and Genetics. Tumours of the Breast and female Genital Organs. 4th ed 2003: *International Agency for Research on Cancer and World Health Organization.*

252. Baron, A T, et al. Soluble epidermal growth factor receptor (sEGFR/sErbB1) as a potential risk, screening, and diagnostic serum biomarker of epithelial ovarian cancer. *Cancer Epidemiol Biomarkers Prev*, 2003. **12**(2): p. 103-13.

253. Baron, A T, Boardman, C H, Lafky, J M, Rademaker, A, Liu, D, Fishman, D A, Podratz, K C, and Maihle, N J. Soluble epidermal growth factor receptor (sEGFR) [corrected] and cancer antigen 125 (CA125) as screening and diagnostic tests for epithelial ovarian cancer. *Cancer Epidemiol Biomarkers Prev*, 2005. **14**(2): p. 306-18.

254. Gadducci, A, Ferdeghini, M, Cosio, S, Fanucchi, A, Cristofani, R, and Genazzani, A R. The clinical relevance of serum CYFRA 21-1 assay in patients with ovarian cancer. *Int J Gynecol Cancer*, 2001. **11**(4): p. 277-82.

255. Borgono, C A, Grass, L, Soosaipillai, A, Yousef, G M, Petraki, C D, Howarth, D H, Fracchioli, S, Katsaros, D, and Diamandis, E P. Human kallikrein 14: a new potential biomarker for ovarian and breast cancer. *Cancer Res*, 2003. **63**(24): p. 9032-41.

256. Luo, L Y, et al. The serum concentration of human kallikrein 10 represents a novel biomarker for ovarian cancer diagnosis and prognosis. *Cancer Res*, 2003. **63**(4): p. 807-11.

257. Yousef, G M, et al. Human kallikrein 5: a potential novel serum biomarker for breast and ovarian cancer. *Cancer Res*, 2003. **63**(14): p. 3958-65.

258. Shan, S J, Scorilas, A, Katsaros, D, Rigault de la Longrais, I, Massobrio, M, and Diamandis, E P. Unfavorable prognostic value of human kallikrein 7 quantified by ELISA in ovarian cancer cytosols. *Clin Chem*, 2006. **52**(10): p. 1879-86.

259. Cooper, B C, Ritchie, J M, Broghammer, C L, Coffin, J, Sorosky, J I, Buller, R E, Hendrix, M J, and Sood, A K. Preoperative serum vascular endothelial growth factor levels: significance in ovarian cancer. *Clin Cancer Res*, 2002. **8**(10): p. 3193-7.

260. Hefler, L A, Zeillinger, R, Grimm, C, Sood, A K, Cheng, W F, Gadducci, A, Tempfer, C B, and Reinthaller, A. Preoperative serum vascular endothelial growth factor as a prognostic parameter in ovarian cancer. *Gynecol Oncol*, 2006. **103**(2): p. 512-7.

261. Dean, M, Fojo, T, and Bates, S. Tumour stem cells and drug resistance. *Nat Rev Cancer*, 2005. **5**(4): p. 275-84.

262. Diehn, M and Clarke, M F. Cancer stem cells and radiotherapy: new insights into tumor radioresistance. *J Natl Cancer Inst*, 2006. **98**(24): p. 1755-7.

263. Baba, T, et al. Epigenetic regulation of CD133 and tumorigenicity of CD133+ ovarian cancer cells. *Oncogene*, 2009. **28**(2): p. 209-18.

264. Kryczek, I, et al. Expression of aldehyde dehydrogenase and CD133 defines ovarian cancer stem cells. *Int J Cancer*, 2011.

265. Vescovi, A L, Reynolds, B A, Fraser, D D, and Weiss, S. bFGF regulates the proliferative fate of unipotent (neuronal) and bipotent (neuronal/astroglial) EGF-generated CNS progenitor cells. *Neuron*, 1993. **11**(5): p. 951-66.

266. Locke, M, Heywood, M, Fawell, S, and Mackenzie, I C. Retention of intrinsic stem cell hierarchies in carcinoma-derived cell lines. *Cancer Res*, 2005. **65**(19): p. 8944-50.

267. Sharom, F J. ABC multidrug transporters: structure, function and role in chemoresistance. *Pharmacogenomics*, 2008. **9**(1): p. 105-27.

268. Derda, R, Tang, S K, Li, S C, Ng, S, Matochko, W, and Jafari, M R. Diversity of phage-displayed libraries of peptides during panning and amplification. *Molecules*, 2011. **16**(2): p. 1776-803.

269. Hombach-Klonisch, S, et al. Cancer stem cells as targets for cancer therapy: selected cancers as examples. *Arch Immunol Ther Exp (Warsz)*, 2008. **56**(3): p. 165-80.

270. Sidhu, S S. Phage display in biotechnology and drug discovery. Drug discovery series 2005, Boca Raton: *CRC Press/Taylor & Francis*. xviii, 748 p.

271. Hui, X, et al. Specific targeting of the vasculature of gastric cancer by a new tumor-homing peptide CGNSNPKSC. *J Control Release*, 2008. **131**(2): p. 86-93.

272. Beerli, R R, Graus-Porta, D, Woods-Cook, K, Chen, X, Yarden, Y, and Hynes, N E. Neu differentiation factor activation of ErbB-3 and ErbB-4 is cell specific and displays a differential requirement for ErbB-2. *Mol Cell Biol*, 1995. **15**(12): p. 6496-505.

273. Hartmann, F, Horak, E M, Cho, C, Lupu, R, Bolen, J B, Stetler-Stevenson, M A, Pfreundschuh, M, Waldmann, T A, and Horak, I D. Effects of the tyrosine-kinase inhibitor geldanamycin on ligand-induced Her-2/neu activation, receptor expression and proliferation of Her-2-positive malignant cell lines. *Int J Cancer*, 1997. **70**(2): p. 221-9.

274. Matarrese, P, Fusco, O, Tinari, N, Natoli, C, Liu, F T, Semeraro, M L, Malorni, W, and Iacobelli, S. Galectin-3 overexpression protects from apoptosis by improving cell adhesion properties. *Int J Cancer*, 2000. **85**(4): p. 545-54.

275. Glinsky, V V, Glinsky, G V, Rittenhouse-Olson, K, Huflejt, M E, Glinskii, O V, Deutscher, S L, and Quinn, T P. The role of Thomsen-Friedenreich antigen in adhesion of human breast and prostate cancer cells to the endothelium. *Cancer Res*, 2001. **61**(12): p. 4851-7.

276. Kim, J H, et al. Identification of epithelial cell adhesion molecule autoantibody in patients with ovarian cancer. *Clin Cancer Res*, 2003. **9**(13): p. 4782-91.

277. Smith, G P and Scott, J K. Libraries of peptides and proteins displayed on filamentous phage. *Methods Enzymol*, 1993. **217**: p. 228-57.

278. Miao, Y, Hoffman, T J, and Quinn, T P. Tumor-targeting properties of 90Y- and 177Lu-labeled alpha-melanocyte stimulating hormone peptide analogues in a murine melanoma model. *Nucl Med Biol*, 2005. **32**(5): p. 485-93.

279. Garvalov, B K and Acker, T. Cancer stem cells: a new framework for the design of tumor therapies. *J Mol Med*, 2011. **89**(2): p. 95-107.

280. Garcia Garayoa, E, et al. Chemical and biological characterization of new Re(CO)3/[99mTc](CO)3 bombesin analogues. *Nucl Med Biol*, 2007. **34**(1): p. 17-28.

281. Racusen, L C, Whelton, A, and Solez, K. Effects of lysine and other amino acids on kidney structure and function in the rat. *Am J Pathol*, 1985. **120**(3): p. 436-42.

282. Anderson, C J and Welch, M J. Radiometal-labeled agents (non-technetium) for diagnostic imaging. *Chem Rev*, 1999. **99**(9): p. 2219-34.

283. Quon, A and Gambhir, S S. FDG-PET and beyond: molecular breast cancer imaging. *J Clin Oncol*, 2005. **23**(8): p. 1664-73.

284. Kumar, R. PET/PET/CT in ovarian cancer. *Ind J Med Paed Oncol*, 2007. **27**(1).

285. Wei, L, et al. Melanoma imaging using (111)In-, (86)Y- and (68)Ga-labeled CHX-A"-Re(Arg11)CCMSH. *Nucl Med Biol*, 2009. **36**(4): p. 345-54.

286. Newton-Northup, J R, Figueroa, S D, and Deutscher, S L. Streamlined in vivo selection and screening of human prostate carcinoma avid phage particles for development of peptide based in vivo tumor imaging agents. *Comb Chem High Throughput Screen*, 2011. **14**(1): p. 9-21.

287. Kwekkeboom, D J, et al. Overview of results of peptide receptor radionuclide therapy with 3 radiolabeled somatostatin analogs. *J Nucl Med*, 2005. **46 Suppl 1**: p. 62S-6S.

288. Garkavij, M, Nickel, M, Sjogreen-Gleisner, K, Ljungberg, M, Ohlsson, T, Wingardh, K, Strand, S E, and Tennvall, J. 177Lu-[DOTA0,Tyr3] octreotate therapy in patients with disseminated neuroendocrine tumors: Analysis of

dosimetry with impact on future therapeutic strategy. *Cancer*, 2010. **116**(4 Suppl): p. 1084-92.

289. Kelly, K A, Bardeesy, N, Anbazhagan, R, Gurumurthy, S, Berger, J, Alencar, H, Depinho, R A, Mahmood, U, and Weissleder, R. Targeted nanoparticles for imaging incipient pancreatic ductal adenocarcinoma. *PLoS Med*, 2008. **5**(4): p. e85.

290. Gomes, A F and Gozzo, F C. Chemical cross-linking with a diazirine photoactivatable cross-linker investigated by MALDI- and ESI-MS/MS. *J Mass Spectrom*, 2010. **45**(8): p. 892-9.

291. Silva, I A, et al. Aldehyde dehydrogenase and CD133 define angiogenic ovarian cancer stem cells that portend poor patient survival. *Cancer Res*, 2011.

292. Ma, L, Lai, D, Liu, T, Cheng, W, and Guo, L. Cancer stem-like cells can be isolated with drug selection in human ovarian cancer cell line SKOV3. *Acta Biochim Biophys Sin (Shanghai)*, 2010. **42**(9): p. 593-602.

293. Kusumbe, A P and Bapat, S A. Cancer stem cells and aneuploid populations within developing tumors are the major determinants of tumor dormancy. *Cancer Res*, 2009. **69**(24): p. 9245-53.

294. Scientific, T. Growth Factors in Cell Culture Serum. 2014. Accessed 3/19/2014; http://www.thermoscientific.com/en/about-us/general-landing-page/growth-factors-in-cell-culture-serum.html.

295. Briske-Anderson, M J, Finley, J W, and Newman, S M. The influence of culture time and passage number on the morphological and physiological development of Caco-2 cells. *Proc Soc Exp Biol Med*, 1997. **214**(3): p. 248-57.

296. Esquenet, M, Swinnen, J V, Heyns, W, and Verhoeven, G. LNCaP prostatic adenocarcinoma cells derived from low and high passage numbers display divergent responses not only to androgens but also to retinoids. *J Steroid Biochem Mol Biol*, 1997. **62**(5-6): p. 391-9.

297. Parrott, J A, Kim, G, and Skinner, M K. Expression and action of kit ligand/stem cell factor in normal human and bovine ovarian surface epithelium and ovarian cancer. *Biol Reprod*, 2000. **62**(6): p. 1600-9.

298. Smith, G P. Phage-Display Vectors and Libraries Based on Filamentous Phage Strain fd-tet. 2006. Accessed 3/19/2014; http://www.biosci.missouri.edu/smithgp/PhageDisplayWebsite/PhageDisplayWebsiteIndex.html.

299. Scott, J K and Smith, G P. Searching for peptide ligands with an epitope library. *Science*, 1990. **249**(4967): p. 386-90.

300. Horwacik, I, Czaplicki, D, Talarek, K, Kowalczyk, A, Bolesta, E, Kozbor, D, and Rokita, H. Selection of novel peptide mimics of the GD2 ganglioside from a constrained phage-displayed peptide library. *Int J Mol Med*, 2007. **19**(5): p. 829-39.

301. Sparks, W O, Rohlfing, A, and Bonning, B C. A peptide with similarity to baculovirus ODV-E66 binds the gut epithelium of Heliothis virescens and impedes infection with Autographa californica multiple nucleopolyhedrovirus. *J Gen Virol*, 2011. **92**(Pt 5): p. 1051-60.

Addendum

The *in vivo* phage display selections described in Chapter 2 were performed by Jessica Newton-Northup prior to the Mette Soendergaard joining the laboratory in 2009. The remaining selections, as well as all other experiments, were carried out by Mette Soendergaard under initial technical guidance of Jessica Newton-Northup.

Chapter 2 and Chapter 3 of this dissertation have been submitted to the Journal of Nuclear Medicine (JNM) and Combinatorial Chemistry and High-Throughput Screening, respectively, as research manuscripts for publication. The Chapter 4 introduction has been published in the Journal of Molecular Biomarkers and Diagnosis as a review paper.

VITA

Mette Soendergaard was born March 28th, 1980, in Gentofte, Denmark. She received her Bachelor of Science degree in February 2007, and her Master or Science degree in April 2009, both in Biology-Biotechnology from the University of Copenhagen. She received her Ph.D. in Biochemistry in May 2014 from the University of Missouri-Columbia.